# University of Alberta

High Order Corrections to Fundamental Constants

by

Matthew Dowling

A thesis submitted to the Faculty of Graduate Studies and Research
in partial fulfillment of the requirements for the degree of

Doctor of Philosophy

Department of Physics


Fall 2012
Edmonton, Alberta

This is dedicated to my wife and best friend who has always been there with words of encouragement, advice and support whenever I needed them.

**Abstract**

This thesis explores the determination of a few of the fundamental constants of the standard model by employing different methods than those historically used. Modern field theory techniques are applied to the calculation of the $\alpha^2(Z\alpha)^5$ corrections to the Lamb shift leading to an increase in the precision of the current value. It is then shown how these same techniques can be used to compute the $\alpha(Z\alpha)^5$ corrections to the bound electron $g$-factor. Next, the beyond the standard model decay of a muon into an electron and a particle called a Majoron is considered. This calculation provides the theory that underlies a new method of searching for the Majoron that does not require any modification of currently planned muon to electron conversion experiments. Finally, the two related decays of a $b$-quark decaying to a $c$-quark and leptons and a muon decaying to an electron and neutrinos are considered in a new kinematic configuration. This new approach provides the $\mathcal{O}(\alpha_s^2)$ corrections to the semileptonic $b$-quark decay rate and is currently the only method that gives access to the $\mathcal{O}(\alpha^3)$ corrections to the muon decay rate. All of these corrections are used in determining fundamental properties of the standard model as well as the ongoing search for new physics.

# Contents

# List of Tables

# List of Figures

# Chapter 1

# Introduction

In particle physics one of the 'holy grails' is to find a single theory that successfully describes the building blocks of matter and their interactions. As of today, the theory providing the closest approximation to this is called the standard model of particle physics (SM). The SM describes interactions of spin 1/2 matter particles: the quarks,

$$\begin{pmatrix} u \\ d \end{pmatrix} \begin{pmatrix} c \\ s \end{pmatrix} \begin{pmatrix} t \\ b \end{pmatrix},$$

and the leptons,

$$\begin{pmatrix} \nu_e \\ e \end{pmatrix} \begin{pmatrix} \nu_\mu \\ \mu \end{pmatrix} \begin{pmatrix} \nu_\tau \\ \tau \end{pmatrix},$$

mediated by bosons,

$$\gamma,\ W^{\pm},\ Z^0,\ g,\ H.$$

The quarks and leptons also have a related partner called an anti-particle. Anti-particles have the same properties as their partner particle except their quantum numbers are reversed. For example, the anti-electron (positron) has the same mass as an electron but its charge is positive instead of negative. All of these particles have been observed except for the Higgs boson, $H$. The two main Large Hadron Collider (LHC) experiments ATLAS and CMS recently announced the discovery of a new particle that is so far consistent with the SM Higgs [1, 2]. It will take much more data and effort to conclusively determine if this is the SM Higgs or something more exotic.

Apart from having yet to conclusively discover the Higgs boson, the SM has been tested with an amazing degree of precision. The electromagnetic coupling constant $\alpha$, for example, has been determined to be [3]

$$\alpha^{-1} = 137.035\,999\,074(44). \tag{1.1}$$

This value agrees well with the next best determination using a different method, such as electron-electron scattering, and makes quantum electrodynamics (QED), a component of the SM, one of the most precisely tested theories to date. In fact, in the roughly 40 years since the SM was formulated, every test that has been used to check its validity has shown it to be accurate, almost. Even with this success it is expected that the SM is not a complete theory. One of the major reasons for believing this is that astronomical measurements show there is very likely some

other kind of matter out there. It has been named dark matter because it does not interact electromagnetically (i.e. it does not give off any light). As well, there are a few experimental measurements possibly showing signs of some new kind of physics not included in the SM. The most significant of these results is the determination of the charge radius of the proton. A recent measurement [4] showed that the radius of the proton should be

$$r_p = 0.84184(67)\text{fm}. \tag{1.2}$$

The current CODATA recommended value [3],

$$r_p = 0.8775(51)\text{fm}, \tag{1.3}$$

does not take this measurement into account because it differs so widely from previous measurements [5, 6]. The difference between these two values is at the $7\sigma$ level (they differ by roughly seven times the error) making it one of the most significant discrepancies in the SM today. In the two years since the new value for the charge radius of the proton was published, no explanation has been found that can explain the difference.

There are typically two approaches used in the search for new physics. The first involves colliding particles at higher and higher energies to see if anything new is created. This is the method employed by accelerators like the Tevatron and the LHC. By colliding protons at very high energy, the LHC hopes to produce new particles, like the Higgs, if they exist. The second approach comes in at the other end of the energy spectrum: precision measurements. These experiments are typically low energy, but control of the parameters in the experiment is so good that extremely precise measurements can be made. These measurements can be sensitive to new forces or particles through "virtual corrections". A simple example shows how this can happen and what is meant by virtual corrections. It also helps introduce some of the main concepts from particle physics that will be used in this thesis.

### Virtual Corrections

Consider a process like the decay of the muon ($\mu$). In the SM, the muon is able to decay into a muon neutrino ($\nu_\mu$), an electron anti-neutrino ($\overline{\nu}_e$) and an electron ($e$) through the weak force ($W^\pm, Z^0$). This decay process can be represented by a diagram such as the one in Figure 1.1. These kinds of diagrams are referred to as

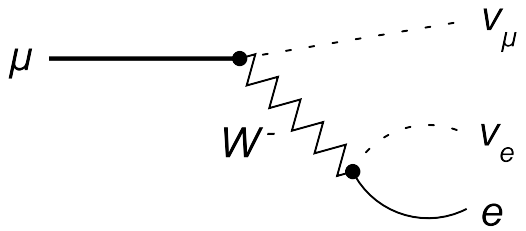


**Figure 1.1:** A representation of the tree level decay of a muon. The wavy line represents the $W^-$ that is responsible for this kind of decay being possible.

Feynman diagrams and actually represent a mathematical expression that gives the

amplitude for such a process to occur. The magnitude of the total amplitude can then be used to compute a physical quantity, such as the decay rate.

This is not the only Feynman diagram that takes a muon and produces the neutrinos and electron. Another example is illustrated in Figure 1.2. This time, the

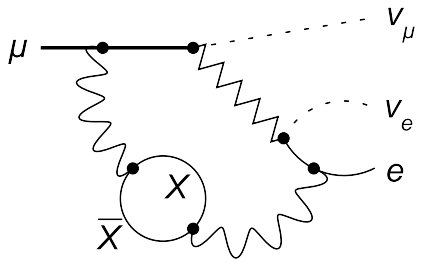


**Figure 1.2:** Another Feynman diagram that also contributes to muon decay. The loop can be any particle anti-particle pair that interact electromagnetically.

diagram has an extra part with two photons ($\gamma$), the wavy lines, and a loop where one line is a particle ($X$) and the other is its anti-particle ($\overline{X}$). The (anti-)particle in this loop can be any kind of particle that interacts electromagnetically. This diagram starts with a muon and produces the same kinds of particles in the final state as the diagram in Figure 1.1, but in a more complicated way. Its contribution is suppressed by powers of the QED coupling constant, $\alpha$, so it is called a correction. When a process like muon decay is measured in an experiment, it is only possible to see the initial muon and the final electron and neutrinos. All of the other particles in the diagrams are known as virtual particles. They are not physically created but are able to contribute to the process anyway. One way of thinking about these particles is that they borrow an amount of energy $\Delta E$ from the vacuum and are able to "exist" for a short period of time $\Delta t$ such that the uncertainty relation

$$\Delta E \Delta t \leq \frac{\hbar}{2} \tag{1.4}$$

is satisfied. The photons and particle anti-particle loop make up the virtual correction.

If there is a new particle that has not been detected yet, and it interacts electromagnetically, it would contribute to muon decay via diagrams like those in Figure 1.2. The decay rate must be measured very precisely in order to measure the effects of a new particle in this way, as the contribution from the loop diagram in Figure 1.2 is proportional to $\alpha^2 \left(\frac{m_\mu}{m_X}\right)^2$, which is very small for $m_X \gg m_\mu$.

This brings us to the main topic in this thesis: high order corrections. In addition to searching for new physics, precision experiments are used to measure the many fundamental parameters in the SM. This means that in order to obtain useful predictions from theory, the values of all free parameters need to be known. Typically, these parameters are found by comparing a measurement with the related theoretical prediction and then assuming the two should be equal. It is then possible to extract the value of the parameter of interest. Since the assumption that the measurement and theory should be equal may not be true, it is necessary to have more than one

method of determining these parameters. In addition, to properly compare the experimental and theoretical values, both should have similar error, otherwise the one with the larger error limits the precision of the final result. To this end, theorists are continually computing higher and higher order corrections to various processes.

### Perturbation Theory

The term higher order corrections has been used a few times without a real explanation for what it means. The fact is, calculations in quantum field theory (QFT) are rather difficult. They are so difficult that no full calculation of a physically realizable process has ever been carried out. It is, however, possible to carry out an asymptotic expansion in some small parameter in the theory. This procedure was created by both Feynman [7] and Schwinger [8, 9] independently. During a long bus ride in 1948 Dyson realized that the two theories by Feynman and Schwinger were identical. His derivation of this [10] has become the standard method of introducing perturbation theory.

In carrying out this expansion, a standard set of rules can be inferred that hold at any order in the expansion. It has been found that there are only a few different rules that need to be followed in order to build up any amplitude required. In addition, each of these terms can intuitively and conveniently be represented by a picture called a Feynman diagram. For QED, the coupling constant $\alpha \approx 1/137$ provides an ideal parameter for this expansion. In quantum chromodynamics (QCD), the situation is not as simple because the coupling constant, $\alpha_s$, is relatively large at energies below the $b$-quark mass. In that theory, the perturbative expansion should be augmented by an estimate of non-perturbative effects.

Feynman diagrams are a convenient tool to organize and keep track of the different contributions to the process being considered. The rules for constructing the diagrams are known as the Feynman rules and are (partially) shown in Figure 1.3. These are the propagators and vertices that make up the SM. Note that if the fermions in the W-Fermion vertex are leptons, one must be an $e, \mu$, or $\tau$ and the other must be a neutrino. As well, this lepton neutrino pair must be of the same flavour $(e, \mu, \tau)$. Only the vertices that will be relevant for this thesis have been included. In addition to the vertices listed in Figure 1.3 there are vertices for:

$$gggg,\ Z^0ff,\ \gamma W^+W^-,\ Z^0W^+W^-,\ \gamma\gamma W^+W^-,\ \gamma Z^0W^+W^-,\ Z^0Z^0W^+W^-,$$
$$W^+W^-W^+W^-,\ W^+W^-H,\ Z^0Z^0H,\ Hff,\ HHH,\ HHW^+W^-,$$
$$HHZ^0Z^0,\ HHHH.$$

Finally, rules are also required for how to include the external particles.

| | |
|---|---|
| **Incoming Fermions**: $u(p,s)$ | **Incoming anti-Fermions**: $v(p,s)$ |
| **Outgoing Fermions**: $\overline{u}(p,s)$ | **Outgoing anti-Fermions**: $\overline{v}(p,s)$ |
| **Incoming Photons,Bosons**: $\epsilon(k,\lambda)$ | **Outgoing Photons,Bosons**: $\epsilon^*(k,\lambda)$ |
| **Incoming Gluons**: $\epsilon(k,\lambda)a^c$ | **Outgoing Gluons**: $\epsilon^*(k,\lambda)a^{c*}$ |

The $u(v)$'s are the positive(negative) energy wave function solutions of the free Dirac equation and the $\epsilon$'s are polarization vectors. In addition, the $a^c$'s are the colour wave functions of the gluons with $c = 1, \ldots, 8$.

**Propagators**

Fermions



$$i\frac{\not{p}+m}{p^2-m^2}$$

Photons

$$\frac{i}{k^2}\left(-g^{\mu\nu}+(1-\xi)\frac{k^\mu k^\nu}{k^2}\right)$$

Gluons

$$\frac{i}{k^2}\left(-g^{\mu\nu}+(1-\xi)\frac{k^\mu k^\nu}{k^2}\right)\delta^{ab}$$

Vector Bosons ($V = W^\pm, Z^0$)

$$\frac{i}{k^2-m_V^2}\left(-g^{\mu\nu}+\frac{k^\mu k^\nu}{m_V^2}\right)$$

Higgs



$$\frac{i}{k^2-m_H^2}$$

**Vertices**

Photon-Fermion

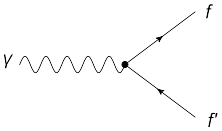


$$-ig\gamma_\mu$$

Gluon-Fermion

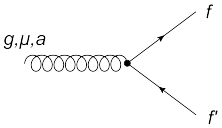


$$-ig_s\frac{\lambda^a}{2}\gamma_\mu$$

3-Gluon

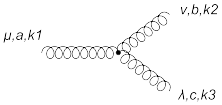


$$-g_s f_{abc}[g_{\mu\nu}(k_1-k_2)_\lambda + g_{\nu\lambda}(k_2-k_3)_\mu + g_{\lambda\mu}(k_3-k_1)_\nu]$$

W-Fermion

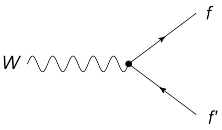


$$-i\frac{g}{\sqrt{2}}\gamma_\mu\frac{(1-\gamma^5)}{2}V_{ff'}$$

**Figure 1.3:** A sample of the Feynman rules for the standard model. Note that the photon and massive vector bosons are denoted by the same type of line. Unless specified, this type of line always refers to a photon instead of the $Z^0$ and it should be clear from the vertices if the particle is a $W$.

As an example of how to apply these rules, let's look at how to compute the decay rate of a $b$-quark into a $c$-quark and leptons. This is one of the dominant decay modes of the $b$-quark and can be measured accurately in experiments. It will be considered in much more detail in Chapter 6. To start, the interaction that converts a $b$-quark into a $c$-quark comes in the form of the weak interaction. The resulting $W$ boson can then decay into two leptons: an electron, muon or tau, and the associated neutrino. When the process is drawn out, the result is the diagram in Figure 1.4, which represents the amplitude for the process to occur. To convert

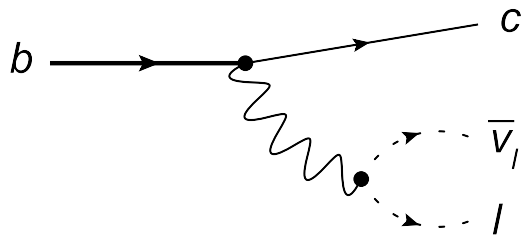


**Figure 1.4:** The Feynman diagram for semileptonic $b$-quark decay. Each line and vertex represents a factor that contributes to the decay rate.

from the diagram form to an equation, the fermion lines are followed from finish to start applying the Feynman rules as the different propagators and vertices are encountered. Starting with the outgoing $c$-quark gives

$$i\mathcal{M} = \left[\overline{u}(p_c)\frac{igV_{cb}}{2\sqrt{2}}(1-\gamma^5)u(p_b)\right]\left[\overline{u}(p_\ell)\frac{ig}{2\sqrt{2}}(1-\gamma^5)\overline{v}(p_\nu)\right], \tag{1.5}$$

where the spin indices have been ignored in the wave functions. Note that the factors $V_{ff'}$ for leptons are zero unless the flavour of $f$ and $f'$ is the same, in which case it is one. This indicates that the weak force is unable to change the flavour of lepton and has led to a rule called lepton flavour conservation. Until recently, lepton flavour conservation was considered to be an exactly conserved symmetry of the SM. Chapter 5 will explore a model that allows lepton flavour to be violated.

Figure 1.4 is just the leading order contribution to the decay rate. To take into account higher order corrections a way of including more interactions must be found. In the case of the $b$-quark decay rate gluons can be added through interactions with the quarks. As shown in Figure 1.5, there are three ways that a single gluon can be added in this example. The number of gluon lines indicates the order of the correction. To see this, consider the vertex contribution from gluon-fermion interactions:

$$-ig_s\frac{\lambda^a}{2}\gamma_\mu. \tag{1.6}$$

For each gluon-fermion vertex, an extra factor of $g_s$ is included. The amplitude of the process in terms of powers of $g_s$ is then

$$i\mathcal{M} \propto 1 + g_s + g_s^2 + \ldots, \tag{1.7}$$

where the dots indicate higher order contributions. In order to compute the decay rate, the square of the amplitude is taken. When this is done, the terms proportional to $g_s$ will give zero so that the first order correction is proportional to $g_s^2$. Each of

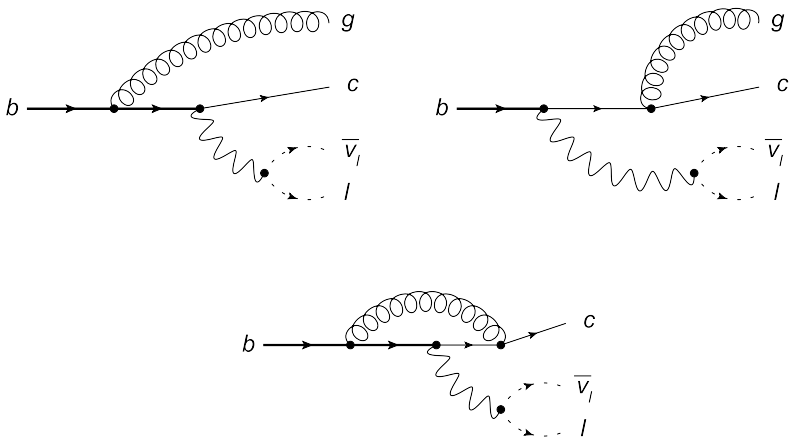


**Figure 1.5:** The first order diagrams contributing to semileptonic $b$-quark decay.

these diagrams has a single gluon and it is found that a single gluon added to a diagram increases the power of the coupling constant by two. Using the relation

$$\alpha_s = 4\pi g_s^2, \tag{1.8}$$

it is seen that the number of gluons determines the power of $\alpha_s$ and thus the order of the correction.

With perturbation theory being one of the very few methods of calculation in QED, the past 60 years have been very fruitful in developing methods and algorithms to compute the integrals associated with Feynman diagrams. It has become possible, with the help of computers, to do the lengthy and highly complex calculations needed to match experimental precision and extract extremely precise values for different physical constants. For example, the current value of the fine structure constant relies on the calculation of 12672 "tenth-order" Feynman diagrams [11] (tenth-order is in quotes as they are technically the fifth-order terms in the expansion. The ten comes from counting factors of $g$ instead of $\alpha$). This determination of $\alpha$ comes from comparing the calculations and measurements of the electron $g$-factor [12].

## 1.1 Experiments

This section takes a look at some of the experiments that are able to produce the precise measurements needed to extract fundamental constants in the SM. The meaning of the constants will only be briefly discussed leaving more detailed descriptions to the chapters that consider each one respectively.

### Lamb Shift

The Lamb shift is a spin-independent correction to atomic energy levels due to quantum loops. It has been an important quantity in the history of the development of QED. Its theoretical calculation showed the importance of perturbation theory and renormalization. There are a few different ways of measuring the Lamb shift. The Lamb shift that splits the $2S_{1/2}$ and $2P_{1/2}$ levels in hydrogen will be the focus of this section. Using a direct measurement, the most precise value of the $2S_{1/2}$ -

$2P_{1/2}$ splitting was done by Lundeen and Pipkin in 1981 (1057.845(9) MHz) [13]. In 1994 Hagley and Pipkin made an indirect measurement of the $2S_{1/2}$ - $2P_{1/2}$ splitting by measuring the $2S_{1/2}$ - $2P_{3/2}$ splitting and subtracting the theoretical value for the $2P_{1/2}$ - $2P_{3/2}$ splitting (1057.842(12) MHz) [14]. These two experiments relied on a technique of measuring the relevant transition frequency called the separated oscillatory field (SOC) method.

The SOC method was first introduced by Norman Ramsey in 1956 in his book 'Molecular Beams' [15]. The idea of this method is to prepare the two level system of interest in its ground state. For the $2S_{1/2}$ - $2P_{1/2}$ Lamb shift, a beam of hydrogen atoms is prepared in the $2S_{1/2}$ state. The beam is then sent through two regions that have an oscillating electromagnetic field and are separated by some distance much larger than the length of the regions with the oscillating fields. The oscillating fields induce transitions between the two states of the system. Measurements of the number of atoms that have a final state of $2P_{1/2}$ are made as the frequency of the oscillating fields is changed. This measurement is done by counting the Lyman-$\alpha$ photons emitted in the decay from the $2P_{1/2}$ state. When the frequency of the oscillating field matches the frequency of the transition, a maximum is found in the number of atoms that have transitioned. The change in energy of this transition is related to the frequency, $\omega$, by $\Delta E = \hbar\omega$. This can also be done with just a single oscillating field region. The benefit of using two regions is the interference effect created with the separation of the regions.

Consider a single atom proceeding through the fields. Amplitudes can be assigned to the different processes that are classically thought of taking place. First, let $C_{iif}$ be the amplitude for the atom to go through the first region with no change and then transition as it proceeds through the second region. Similarly, let $C_{iff}$ be the amplitude for the atom to transition in the first region and remain in the excited state as it goes through the second region. The cross term $C_{iff}C^*_{iif}$ produces an interference effect that ends up narrowing the peak observed at the transition frequency. This narrowing is what allows a much more precise measurement of the frequency as shown in Figure 1.6. The Lamb shift is used to measure either the Rydberg constant $R_\infty$ or the charge radius of the proton.

### Electron $g$-Factor

The electron $g$-factor is another historically important quantity. It is a proportionality factor between the spin and magnetic moments expressed in units of $\frac{e}{2m_e}$. Dirac's equation in relativistic quantum mechanics shows that it should be exactly two. Furthermore, QED corrections show that the $g$-factor should actually be slightly larger than two. Today, the ability to measure the value of the $g$-factor precisely gives the best determination of the fine structure constant $\alpha$. In addition, the bound electron $g$-factor (which is considered in Chapter 4) is used to determine the mass of the electron to a precision of 14 digits [16].

As with the Lamb shift, there are a few different ways of measuring the electron $g$-factor. Here, the method that currently provides the most precise measurement of both the free and bound electron $g$-factors will be described: by use of a Penning trap. The Penning trap is a device first built and named by Hans Dehmelt in 1959 based on ideas from Frans Penning. It uses a combination of a non-uniform electric field and a uniform magnetic field to confine charged particles in a small area. The motion

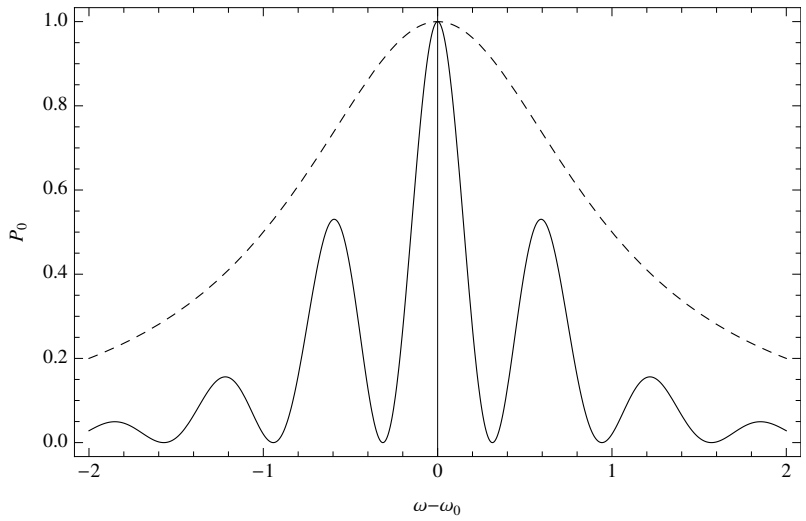


**Figure 1.6:** The interference effect of the SOC method narrows the peak that occurs at the transition frequency. The frequency $\omega_0$ corresponds to the energy difference between the two levels. Here, the dashed line corresponds to having a single region with an oscillating field while the solid line corresponds to having two regions with the field. Both are normalized so that the maximum is $P_0$.

of the charged particles in the trap is shown in Figure 1.7. The three frequencies of

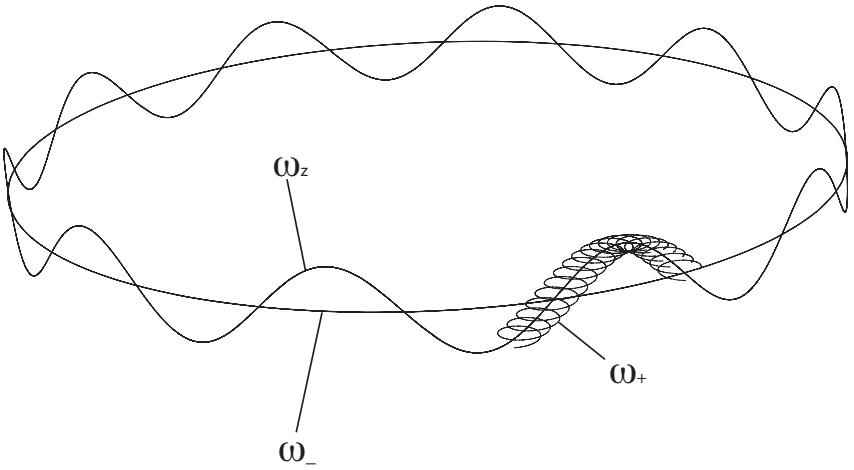


**Figure 1.7:** The motion of an electron in a Penning trap. The different frequencies $\omega_-, \omega_+$ and $\omega_z$ are all separately measurable.

the motion of the particle can be measured, and it is then possible to calculate the cyclotron frequency, $\omega_c$ of the particle using the relation,

$$\omega_c^2 = \omega_+^2 + \omega_-^2 + \omega_z^2. \tag{1.9}$$

The cyclotron frequency is also related to the the magnetic field that the particle is moving in,

$$\omega_c = \frac{e}{m_e}|\vec{B}|. \tag{1.10}$$

Taking a look at the Larmor precession frequency of the particle, it is seen that it is related it to the magnetic moment of the particle,

$$-\vec{\mu}\cdot\vec{B} = g\frac{e}{m_e}\vec{S}\cdot\vec{B} = \hbar\omega_L. \tag{1.11}$$

When the spin and magnetic field are aligned it is possible to solve for the Larmor frequency,

$$\omega_L = g\frac{e}{2m_e}|\vec{B}|. \tag{1.12}$$

Dividing the two frequencies gives a very simple expression for the free electron $g$-factor,

$$g = 2\frac{\omega_L}{\omega_c}. \tag{1.13}$$

The bound electron can be treated similarly. This time, the motion of the atom comes into play. The Larmor frequency of the electron is the same as before and the cyclotron frequency now refers to the atom (it must be an ion). This changes the equation for the cyclotron frequency to,

$$\omega_c = \frac{Q}{m_{\text{ion}}}B, \tag{1.14}$$

where $Q$ is the total charge of the ion and $m_{ion}$ is the mass of the ion. Again, taking the quotient of the two frequencies gives a formula for the bound electron $g$-factor,

$$g_b = 2\frac{\omega_L}{\omega_c}\frac{m_e}{m_{\text{ion}}}\frac{Q}{e}. \tag{1.15}$$

Thus, if the ion mass is well known, the mass of the electron can be extracted by comparing Equation 1.15 with a theoretical calculation of $g_b$. Note that here $\omega_c$ is different from the one for a free electron, so that the value $2\frac{\omega_L}{\omega_c}$ does not correspond to the free electron $g$-factor.

### Muon Lifetime

The muon lifetime has become an important tool in particle physics. Recently, the MuLan collaboration was able to measure the lifetime with a precision of one part-per-million [17]. This value is used to determine a constant called the Fermi constant, $G_F$ which, along with $\alpha$ and $m_Z$ is one of the most precisely known parameters of the electroweak theory (a combination of QED and the theory of weak interactions). The value of $G_F$ is important in processes involving the weak interaction and is defined by

$$\frac{G_F}{(\hbar c)^3} = \frac{\sqrt{2}}{8}\frac{g^2}{m_W^2}. \tag{1.16}$$

Through this relation it is seen that $G_F$ is related to the weak coupling constant and the mass of the $W$ boson and can be interpreted as an effective coupling constant when the relevant measurement is not sensitive to the full effects of the weak interaction. The experiments that measure the muon lifetime are conceptually simple and can be done in high school laboratories. In [17] the setup consisted of a beam of muons that could be turned on and off. The muons were then collected in a target of either AK-3 (an alloy of 30% Cr, 10% Co and 60% Fe) or a $SiO_2$ quartz disk for

a period of $5\mu$s. The measurements were performed with a period of $22\mu$s where the muons were allowed to decay. This setup was surrounded by a layer of plastic scintillators and then a layer of photomultiplier tubes. The detections were binned into a histogram for the final lifetime measurement. This process was repeated 170 times in order to obtain a large number of events. To extract the muon lifetime from this data, the experiment had to account for other effects such as spin precession, pileup, timing stability, etc. Apart from these sources of error, the measurement comes down to fitting the sum of the histograms with the function

$$F(t) = Ae^{-t/\tau_\mu} + B, \tag{1.17}$$

where $B$ accounts for a flat background and $A$ accounts for polarization. In the case of an AK-3 target, $A$ also takes into account spin precession as AK-3 is a ferromagnetic material.

With the increasing precision that the previously described experiments are able to achieve, it is important for the theory community to make sure the accuracy of the theory is at least matching that of the experiments. Improving the theoretical description of the processes used to determine some of the fundamental constants in the SM will the main focus of this thesis.

This thesis will proceed as follows. In Chapter 2 a few of the theoretical tools that were used in obtaining the results will be introduced with explicit examples showing how they are used. Chapter 3 focuses on a new calculation of the $\alpha^2(Z\alpha)^5$ corrections to the Lamb shift. The problem is approached using the loop integration tools developed in Chapter 2. This is in contrast to the work in [18, 19] where the corrections are calculated using atomic physics methods. In Chapter 4 it will be shown how the methods of Chapter 3 will be used to compute the $\alpha(Z\alpha)^5$ corrections to the bound electron $g$-factor for the first time.

In Chapter 5 one of the main results of this thesis is presented. A beyond the standard model process is considered that allows for a new type of muon decay. One of the daughter particles of this new decay is a, so far unseen, massless boson called the Majoron. The results provide the theoretical background for a new method of searching for this kind of decay. Future bound muon decay experiments will be able to use the results without requiring a special setup or cuts as opposed to current searches.

Chapter 6 will present the $\alpha_s^2$ corrections to the semileptonic $b$-quark decay rate discussed above. As with the Lamb shift and $g$-factor, the calculation is approached in a slightly different way from previous calculations. It is found that the approach has properties making the computation much easier as compared to the previous determinations. These simplifications provide the method that will allow the calculation of the $\alpha^3$ corrections to the standard model muon decay rate. The formulation of this and some initial results will be presented in Chapter 7.

# Chapter 2

# Tools for Loop Integrals

Before corrections to different processes can be presented, some of the methods used to compute high order corrections need to be introduced. Perturbation theory is one of only a few ways used to carry out calculations in quantum field theory and as a result there are a large number of methods that have been developed to deal with the integrals that appear. In this chapter the focus will be on the techniques used in the calculations presented later in this thesis.

To start, a method of converting phase space integrals into loop integrals will be discussed. This has the benefit of making most calculations in this thesis loop calculations. As a result, the tools for loop integrals that will be built up over the course of this chapter will be be useful for all problems. After this, the basic one loop integral will be discussed. The evaluation of this integral introduces some important techniques and also provides the basis for many of the other methods that will be used.

From here, a method of rewriting loop integrals in terms of a set of integrals that is considered to be easier to evaluate will be introduced. The technique is based on integration by parts identities and is useful if a large number of integrals need to be evaluated. Following this, an identity known as Mellin-Barnes will be used to evaluate one of the integrals appearing in the Lamb shift calculation from Chapter 3. This method allows for both numerical and analytic evaluation of loop integrals.

Finally, a method called sector decomposition will be described that allows an algorithmic extraction of infinities that are commonly found in the evaluation of loop integrals. The extraction of these poles allows numerical calculations to be done without having to characterize the poles of each integral separately and carry out subtractions: a method that is commonly used. Furthermore, the algorithmic nature of the method has allowed computer programs to be developed that will carry out the integral with minimal input from the user.

## 2.1 The Optical Theorem

One thing that all higher order corrections have in common is the loop integral. These integrals appear when there are closed loops in the diagram being considered. The momentum flowing through this loop is unconstrained by momentum conservation rules so the loop momentum must be integrated over all possible values. The techniques for evaluating loop integrals have become quite advanced. For decay pro-

cesses, like muon decay and $b$-quark decay, an identity known as the optical theorem can be used. This theorem provides a way for the decay rate to be re-written in terms of self-energy diagrams: diagrams where only one particle enters the diagram and the same kind of particle leaves. The exact formulation of the optical theorem is

$$\mathrm{Im}\mathcal{M}(p \to p) = \frac{1}{2}\sum_f \int d\Pi_f |\mathcal{M}(p \to f)|^2. \tag{2.1}$$

What this says is that the imaginary part of the amplitude for the process $p \to p$ is equal to the sum of the square of the amplitude for the process $p \to f$ over all final states $f$ as long as $f$ exists as an intermediate state in the $p \to p$ process. Instead of presenting a formal proof of this theorem, a more intuitive description using Feynman diagrams will be shown. Remember, a Feynman diagram gives the amplitude for a process. In order to actually compute the property of interest (i.e. a decay rate) the amplitude is typically squared. An example of this is shown in Figure 2.1 for $b$-quark decay, and has been drawn in a suggestive form. Connecting the lines of the $c, \nu_\ell$

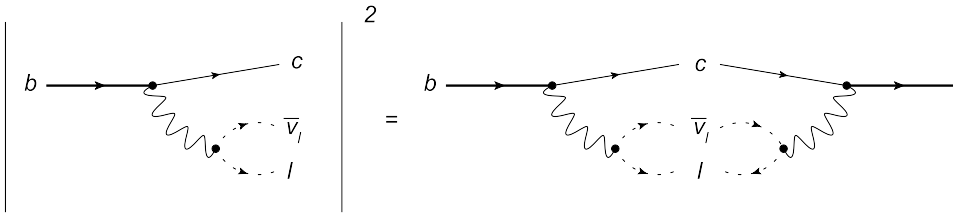


**Figure 2.1:** A diagrammatic representation of squaring the amplitude for the process $b \to c\ell\nu_\ell$.

and $\ell$ pairs would produce a self-energy diagram almost equivalent to the square of the amplitude. The optical theorem formalizes this equivalence and says that the imaginary part of the self-energy diagram is equal to the square of the amplitude. With this method of converting decay processes into self-energy diagrams, tools are needed to carry out the required loop integrals.

## 2.2 One Loop Integral

The basis for almost all of the methods encountered in this thesis is the ability to compute the one loop integral shown in Figure 2.2. This diagram is not a Feynman

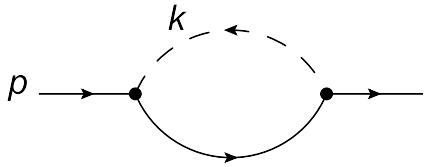


**Figure 2.2:** The basic one loop integral often called the one loop on-shell integral.

diagram, but instead is a representation of the denominators (also known as propagators) that appear. This kind of diagram will be used frequently. The relevant information comes from the internal lines. A dashed (or sometimes dotted) line will

denote a massless propagator $1/(k^2)$ and a solid line will denote a massive propagator $1/[k^2+m^2]$, unless otherwise stated. Four momentum conservation rules still apply at the vertices, but the vertices themselves do not contribute any factors. In the case of Figure 2.2 the integral is

$$\text{on-shell}(a,b) = \int \frac{d^D k}{(2\pi)^D} \frac{1}{(k^2)^a[(k+p)^2+M^2]^b}, \tag{2.2}$$

where the integral is carried out in $D = 4-2\epsilon$ dimensions and $M^2 = -p^2$. Note that a procedure by the name of Wick rotation has been used here that rotates the 4-vectors to Euclidean space with the replacement $x^0 \to ix^0$. This has the effect of changing the sign of the mass in the propagators. As well, by doing the integral in $D$ dimensions instead of four, the divergences commonly encountered appear explicitly. In single diagrams they will appear as powers of $1/\epsilon$ after an expansion in $\epsilon$. All such terms should cancel when the contributing diagrams are summed. This procedure is known as dimensional regularization. Also notice that the propagators have been given general powers $a$ and $b$. Frequently the same type of integral will appear differing only in the powers of the propagators. If possible, the best way to take this into account is to compute the integrals with general powers so the result can be applied to all cases instead of carrying out each integral separately. A family of integrals, differing only in the powers of the propagates, is referred to as a topology.

To compute this integral, an identity called Feynman parameters is used. This technique is based on an identity that allows factors in the denominators to be combined.

$$\frac{1}{A^a B^b} = \frac{\Gamma(a+b)}{\Gamma(a)\Gamma(b)} \int_0^1 dx \frac{x^{a-1}(1-x)^{b-1}}{[Ax+B(1-x)]^{a+b}} \tag{2.3}$$

If needed, this can be applied multiple times to combine as many propagators as required. A more general form of this identity exists that allows the combination of more than two denominators in one shot.

$$\frac{1}{A_1 \dots A_n} = \Gamma(n) \int_0^1 dx_1 \dots dx_n \frac{\delta\left(\sum x_i - 1\right)}{\left[\sum x_i A_i\right]^n} \tag{2.4}$$

Although the two methods are based on the same identity, it is possible that one will give a slightly nicer representation of the integral allowing one to carry out the resulting integrals more easily.

Applying Equation 2.3 to the on-shell integral of Equation 2.2 gives

$$\text{on-shell}(a,b) = \frac{\Gamma(a+b)}{\Gamma(a)\Gamma(b)(2\pi)^D} \int_0^1 dx \int d^D k \frac{x^{b-1}(1-x)^{a-1}}{[k^2+2k\cdot px]^{a+b}}. \tag{2.5}$$

Next, the square for $k$ is completed and $k$ is shifted $k \to k' - p$. The momentum $k$ is unconstrained so the shift only changes the integrand.

$$\text{on-shell}(a,b) = \frac{\Gamma(a+b)}{\Gamma(a)\Gamma(b)(2\pi)^D} \int_0^1 dx \int d^D k' \frac{x^{b-1}(1-x)^{a-1}}{[k'^2+M^2x^2]^{a+b}} \tag{2.6}$$

The $k'$ integral can be carried out by moving to hyper-spherical coordinates. This involves an integral over $D-1$ angles which is given by

$$\int \Omega_D = \frac{2\pi^{D/2}}{\Gamma(\frac{D}{2})}, \tag{2.7}$$

where $\Omega_D$ indicates the angular part of a $D$-dimensional integral. The radial, $K$, integral is then

$$\int_0^\infty dK \frac{K^{D-1}}{[K^2+M^2x^2]^{a+b}}. \tag{2.8}$$

Making the change of variables $K = \sqrt{y}Mx$ produces an integral giving a beta function.

$$\int_0^\infty dy \frac{[M^2x^2]^{D/2-a-b}}{2} \frac{y^{D/2-1}}{[y+1]^{a+b}} = \frac{[M^2x^2]^{D/2-a-b}}{2} \frac{\Gamma\left(\frac{D}{2}\right)\Gamma\left(a+b-\frac{D}{2}\right)}{\Gamma(a+b)}. \tag{2.9}$$

This leaves just the $x$ integral to carry out, which is, again, in the form of a beta function as is common when using Feynman parameters.

$$\begin{aligned}
\text{on-shell}(a,b) &= (M^2)^{\frac{D}{2}-a-b} \frac{2\pi^{\frac{D}{2}}}{2(2\pi)^D\Gamma\left(\frac{D}{2}\right)} \frac{\Gamma\left(\frac{D}{2}\right)\Gamma\left(a+b-\frac{D}{2}\right)}{\Gamma(a)\Gamma(b)} && (2.10)\\
&\quad \int_0^1 dx x^{D-2a-b-1}(1-x)^{a-1} \\
&= \frac{(M^2)^{\frac{D}{2}-a-b}}{(4\pi)^{\frac{D}{2}}} \frac{\Gamma\left(a+b-\frac{D}{2}\right)}{\Gamma(a)\Gamma(b)} \frac{\Gamma(a)\,\Gamma(D-2a-b)}{\Gamma(D-a-b)} && (2.11)\\
&= \frac{(M^2)^{\frac{D}{2}-a-b}}{(4\pi)^{\frac{D}{2}}} \frac{\Gamma\left(a+b-\frac{D}{2}\right)\Gamma(D-2a-b)}{\Gamma(b)\Gamma(D-a-b)}. && (2.12)
\end{aligned}$$

Note that if the integral is carried out when $b$ is a negative integer or zero, the result is zero. This an example of something called a scaleless integral. In dimensional regularization, all scaleless integrals are zero. If it is possible to identify them before carrying out any integral this can simplify the expression – sometimes considerably.

This method of computing loop integrals is common. The result for the $k'$ integral in Equation 2.6 will be of particular use;

$$\int \frac{d^Dk}{(2\pi)^D} \frac{1}{[k^2+M^2]^a} = \frac{\Gamma\left(a-\frac{D}{2}\right)}{(4\pi)^{\frac{D}{2}}\Gamma(a)} \left(\frac{1}{M^2}\right)^{a-\frac{D}{2}} \tag{2.13}$$

## 2.3 Integration By Parts

The next method that will be considered is called integration by parts (IBP). This procedure is useful when topologies cannot be solved with general powers as done in the previous section. The basis for the method is the identity

$$\int d^Dk \frac{\partial}{\partial k^\mu} q^\mu I(k,q,\ldots) = 0, \tag{2.14}$$

where $I$ is the integral to be evaluated, $k$ is any of the loop momenta in $I$, and $q$ can also include the external momenta. Note that $q = k$ is a valid choice. If this identity is applied using all possible combinations of $q$ and $k$, a system of equations is formed that can then be used to rewrite the original integral in terms of integrals that are, hopefully, easier to calculate.

To see how this method works, the on-shell integral from Equation 2.2 will be used as a simple example. Although the result of this integral for a general form has

already been worked out, it provides a good demonstration of the IBP method. The integral depends on two momenta, $k$ and $p$. For simplicity

$$I(a,b) = \frac{1}{(k^2)^a[k^2+2p\cdot k]^b}, \tag{2.15}$$

is defined. This creates two identities that can be applied. Multiplying by $p^\mu$ and taking the derivative with respect to $k_\mu$ gives

$$\begin{aligned}
\frac{\partial}{\partial k^\mu} p^\mu I(a,b) &= \left[-a\frac{2k\cdot p}{(k^2)} - b\frac{2k\cdot p + 2p\cdot p}{[k^2+2k\cdot p]}\right] I(a,b) && (2.16)\\
&= \left[-a\left(\frac{[k^2+2k\cdot p]}{(k^2)} - 1\right)\right. \\
&\quad \left. -b\left(1 - \frac{(k^2)-2M^2}{[k^2+2k\cdot p]}\right)\right] I(a,b) && (2.17)\\
&= (a-b)I(a,b) - aI(a+1,b-1) \\
&\quad + bI(a-1,b+1) - 2M^2 bI(a,b+1). && (2.18)
\end{aligned}$$

For a second relation, $k^\mu$ can be multiplied instead of $p^\mu$ giving

$$\frac{\partial}{\partial k^\mu} k^\mu I(a,b) = (D-2a-b)I(a,b) - bI(a-1,b+1). \tag{2.19}$$

When integrated, the expressions in Equations 2.18 and 2.19 should give zero.

The next step is to try to use these relations to reduce the integral to a form that is easy to integrate. In this example, the first simplification is easy to find. Looking at Equation 2.19, $a$ can be reduced to zero by repeatedly applying

$$\int d^D k I(a,b) = \frac{b}{D-2a-b}\int d^D k I(a-1,b+1). \tag{2.20}$$

Of course, this also increases $b$ by one each time it is used, but the number of propagators to deal with is reduced by one and it may be possible to reduce $b$ as well.

For the second relation, consider the sum of Equations 2.18 and 2.19;

$$\int d^D k \left[(D-a-2b)I(a,b) - aI(a+1,b-1) - 2M^2 bI(a,b+1)\right] = 0. \tag{2.21}$$

As is, this doesn't look like it will help much because this produces one term that increases $b$ and another that decreases $b$. The powers $a$ and $b$ are arbitrary though, so $b$ can be shifted to $b-1$. This gives the identity

$$\begin{aligned}
\int d^D k I(a,b) &= \frac{1}{2M^2(b-1)}\int d^D k \left[(D-a-2(b-1))\, I(a,b-1)\right. \\
&\quad \left. -aI(a+1,b-2)\right]. && (2.22)
\end{aligned}$$

Notice here that because of the denominator, this relation cannot be applied when $b=1$. Thus the integral is reduced to $I(a,1)$ with this relation alone. If, however the relation in Equation 2.20 is applied first and then the relation in Equation 2.22 is used, any integral can be reduced to the case

$$\int \frac{d^D k}{[k^2+2p\cdot k]}. \tag{2.23}$$

Equation 2.23 is known as a master integral because any on-shell type integral can be reduced to this one. In the end then, only the integral in Equation 2.23 is needed instead of the full general result in Equation 2.12.

This method is very useful for calculations of high order corrections when the number of integrals becomes large. It allows one to reduce all of the integrals to a small set of master integrals that are easier to compute than the full set. The technique of reduction and selection of the "simplest" integrals is not a trivial task but has been automated in a few ways [20, 21]. Even with these routines, it may be convenient to change the set of master integrals to a set where the user is able to obtain more accurate results. Such was the case for the Lamb shift calculation in Chapter 3.

## 2.4 Mellin-Barnes

Now that a problem of interest can be reduced to a set of master integrals, there needs to be a way of computing them. The first approach that is typically used is applying Feynman parameters to see if the resulting integrals can be carried out. If this is possible, then the calculations are done. Quite often, though, more complex methods are required.

Mellin-Barnes (MB) integrals are integrals resulting from an identity that splits denominators instead of combining them like Feynman parameters. The identity is

$$\frac{1}{[A+B]^a} = \frac{1}{\Gamma(a)}\frac{1}{2\pi i}\int_{c-i\infty}^{c+i\infty} d\omega \frac{A^\omega}{B^{\omega+a}}\Gamma(-\omega)\Gamma(\omega+a), \tag{2.24}$$

where $c$ is a real number used for the contour integration. To see how this relation is useful, consider, as an example, the master integral $I_{21}$ from the Lamb shift calculation and shown Figure A.1. For convenience, this is reproduced in Figure 2.3.

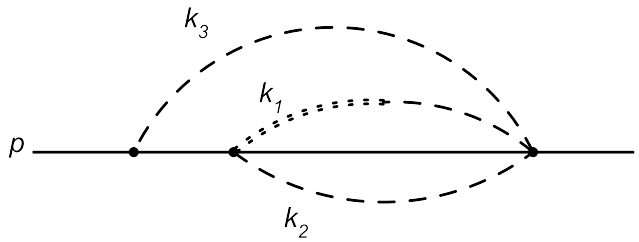


**Figure 2.3:** Master integral $I_{21}$. The double dotted line indicates a delta function.

Before starting, note one important aspect of the Lamb shift calculation. When dealing with the interactions between the electron and neucleus a new propagator is defined that, for current purposes, reduces to a massless propagator and a delta function of the scalar product between the loop momentum flowing through the nucleus and external momentum. For example, if $k$ is the loop momentum flowing through the nucleus and $p$ is the external momentum then the propagator is proportional to

$$\frac{\delta(p\cdot k)}{k^2}. \tag{2.25}$$

In Figure 2.3 this is shown by the double dashed line.

The integral that needs to be calculated is

$$I_{21} = \int \frac{[d^D k_1][d^D k_2][d^D k_3]\delta(2p\cdot k_1)}{(k_1^2)(k_2^2)(k_3^2)[k_3^2+2p\cdot k_3][(k_1+k_2+k_3)^2+2p\cdot(k_2+k_3)]}, \tag{2.26}$$

where the scalar product $p\cdot k_1$ has been set to zero because of the delta function. This is consistent with waiting until after the $k_1$ integral is carried out. For simplicity, the notation $[d^D k] = \frac{d^D k}{(2\pi)^D}$ is also used.

The $k_2$ part of the integral is considered first.

$$I_{k_2} = \int \frac{[d^D k_2]}{(k_2^2)[(k_1+k_2+k_3)^2+2p\cdot(k_2+k_3)]} \tag{2.27}$$

The denominators can be combined using Feynman parameters with $(1-x)$ multiplying the $k_2^2$ term.

$$I_{k_2} = \int_0^1 dx \int \frac{[d^D k_2]}{[k_2^2+2k_2\cdot(p+k_1+k_3)x+(k_1+k_3)^2x+2p\cdot k_3 x]^2} \tag{2.28}$$

Completing the square for $k_2$ and shifting $k_2 \to k_2-(p+k_1+k_3)x$ so that the integration over $k_2$ can be completed gives

$$\begin{aligned} I_{k_2} &= \int_0^1 dx \int \frac{[d^D k_2]}{[k_2^2+(k_1+k_3)^2x(1-x)+2p\cdot k_3 x(1-x)+x^2]^2} && (2.29)\\ &= \frac{\Gamma(\epsilon)}{(4\pi)^{D/2}}\int_0^1 dx \frac{[x(1-x)]^{-\epsilon}}{\left[(k_1+k_3)^2+2p\cdot k_3+\frac{x}{(1-x)}\right]^{\epsilon}}. && (2.30)\end{aligned}$$

In this final expression, if the $\frac{x}{(1-x)}$ term was not present, there would simply be a massive propagator. Fortunately the denominator can be split using the MB identity. This leaves a beta function from the $x$ integral.

$$\begin{aligned} I_{k_2} &= \frac{1}{2\pi i}\frac{\Gamma(\epsilon)}{(4\pi)^{D/2}}\int_{c-i\infty}^{c+i\infty}\frac{dw}{[(k_1+k_3)^2+2p\cdot k_3]^{-w}}\frac{\Gamma(-w)\Gamma(w+\epsilon)}{\Gamma(\epsilon)} \\ &\quad \times\int_0^1 dx x^{-w-2\epsilon}(1-x)^w && (2.31)\\ &= \frac{1}{2\pi i}\frac{1}{(4\pi)^{D/2}}\int_{c-i\infty}^{c+i\infty}\frac{dw}{[(k_1+k_3)^2+2p\cdot k_3]^{-w}} \\ &\quad \frac{\Gamma(-w)\Gamma(w+\epsilon)\Gamma(1-w-2\epsilon)\Gamma(1+w)}{\Gamma(2-2\epsilon)} && (2.32)\end{aligned}$$

With the $k_2$ integral done and a nice propagator in the result, the $k_3$ integral can now be considered. For now, the gamma functions and MB integral is left out in order to concentrate only on the $k_3$ part.

$$I_{k_3} = \int \frac{[d^D k_3]}{(k_3^2)[k_3^2+2p\cdot k_3][(k_1+k_3)^2+2p\cdot k_3]^{-w}} \tag{2.33}$$

Again, Feynman parameters are introduced, but notice that there are two options here: combine all three denominators at once or combine two of them and then the

resulting two. Either way the expression has two Feynman parameters. Combining all three at once allows the integrations to be computed without needing to introduce more MB integrals. The choice of parameters used here is $k_3^2 x$ and $[(k_1+k_3)^2+2p\cdot k_3]y$.

$$I_{k_3} = \frac{\Gamma(2-w)}{\Gamma(-w)}\int_0^1 dy\int_0^{1-y} dx\int \frac{[d^Dk_3]y^{-w-1}}{[k_3^2+2k_3\cdot(p(1-x)+k_1y)+k_1^2y]^{2-w}} \tag{2.34}$$

Completing the square for $k_3$ and shifting $k_3 \to k_3-(p(1-x)+k_1y)$ gives

$$\begin{aligned} I_{k_3} &= \frac{\Gamma(2-w)}{\Gamma(-w)}\int_0^1 dy\int_0^{1-y} dx\int \frac{[d^Dk_3]y^{-w-1}}{[k_3^2+k_1^2y(1-y)+(1-x)^2]^{2-w}} &(2.35)\\ &= \frac{\Gamma(\epsilon-w)}{\Gamma(-w)(4\pi)^{D/2}}\int_0^1 dy\int_0^{1-y} dx\frac{y^{-w-1}[y(1-y)]^{w-\epsilon}}{\left[k_1^2+\frac{(1-x)^2}{y(1-y)}\right]^{\epsilon-w}}. &(2.36)\end{aligned}$$

The only thing left (momentum wise) is the $k_1$ integral. This can be separated into the radial and angular part after taking into account the delta function and making the change of variables $k_1^2 \to z$.

$$I_{k_3} = \frac{\sqrt{\pi}}{(4\pi)^D}\frac{\Gamma(\epsilon-w)}{\Gamma(-w)\Gamma(3/2-\epsilon)}\int_0^\infty dz\int_0^1 dy\int_0^{1-y} dx\frac{y^{-1-\epsilon}(1-y)^{w-\epsilon}z^{-1/2-\epsilon}}{\left[z+\frac{(1-x)^2}{y(1-y)}\right]^{\epsilon-w}} \tag{2.37}$$

Next, a change variables is made again with $z \to t\frac{(1-x)^2}{y(1-y)}$ leaving a beta function in the $t$ integral and a sum of beta functions in the $x$ and $y$ integrals. Again, the gamma functions are dropped here for convenience.

$$\begin{aligned} I_{k_3} &= \frac{\sqrt{\pi}}{(4\pi)^D}\int_0^\infty dt\frac{t^{1/2-\epsilon-1}}{(t+1)^{\epsilon-w}}\int_0^1 dy y^{-1/2-w+\epsilon-1}(1-y)^{1/2+\epsilon-1} &(2.38)\\ &\times\int_0^{1-y} dx(1-x)^{1+2w-4\epsilon} &(2.39)\end{aligned}$$

After integrating over $t$,$x$ and $y$, the result is (in full)

$$\begin{aligned} I_{21} &= \frac{\sqrt{\pi}}{(4\pi)^{3D/2}}\frac{1}{2\pi i}\int_{c-i\infty}^{c+i\infty} dw\frac{\Gamma(1/2-\epsilon)\Gamma(1/2+\epsilon)}{\Gamma(2-2\epsilon)\Gamma(3/2-\epsilon)}\\ &\left(\frac{\Gamma(3/2+w-3\epsilon)}{\Gamma(2+w-2\epsilon)}-\frac{\Gamma(-1/2-w+\epsilon)}{\Gamma(-w+2\epsilon)}\right)\Gamma(1+w)\Gamma(w+\epsilon)\\ &\frac{\Gamma(1-w-2\epsilon)\Gamma(-1/2-w+2\epsilon)\Gamma(-2-2w+4\epsilon)}{\Gamma(-1-2w+4\epsilon)}. \end{aligned} \tag{2.40}$$

The final step, is to carry out the contour integration. In some cases, this can be done analytically by closing the contour on either the right or left of $c$ and summing the poles from the gamma functions. More complicated integrals will involve more than one MB integral that needs to be computed. In these cases, it is likely that the only way to obtain a result is to use a numerical method of integration or to sum the poles numerically.

The integral in our example is one of the cases that can be computed analytically. Before integrating, Equation 2.40 is expanded in $\epsilon$. This allows the poles of the gamma function to be found and makes it possible to choose an appropriate contour for the integration. The final result to order $\epsilon^0$ is

$$I_{21} = \pi^2 \left(1 - \frac{2\pi^2}{3}\right). \tag{2.41}$$

The factor of two difference between this result and the result in Appendix A comes from using $\delta(2p \cdot k)$ as opposed to $\delta(p \cdot k)$.

This method can be very powerful and is the only way to obtain analytic results for some of the Lamb shift master integrals in Chapter 3.

## 2.5 Sector Decomposition

In the event that the resulting Mellin-Barnes integrals are too complicated, another method can be used to compute master integrals numerically while keeping the dependence on $\epsilon$ analytic. Keeping the explicit powers of $\epsilon$ is important as it is likely that the integral of interest will have $\epsilon$ poles.

Sector decomposition is a systematic method of breaking up the integral into regions, each of which are integrable either numerically or analytically. This method is much more complex than the previously described methods. Fortunately, there are programs written that will automatically carry out the operations to be described. A formal description of the method will be followed with an example in order to elucidate some steps involved in the process.

### 2.5.1 The Idea

Sector decomposition is a method that was developed formally only a few years ago [22] to provide a systematic way of evaluating higher order Feynman integrals when the typical analytic methods proved intractable. It is normal for a loop integral to have divergences; both infrared (IR) and ultraviolet (UV). This makes a numerical approach to evaluating these integrals difficult. One must be able to treat these singularities in a systematic way.

One way of dealing with the IR poles is via a subtraction method. This involves finding the form of the poles and subtracting them from the integral so that what is left is a finite integral that can be evaluated numerically (or if it simple enough analytically). This requires a systematic way of finding the poles of a given integral. Sector decomposition provides a general method of finding and extracting the poles of an integral so that it can be evaluated numerically.

The idea is to take the region of integration and break it up in such a way that each pole lies in a different sector. Using Feynman parameters, this can be done in a systematic way. The poles appear explicitly and can be extracted so the resulting integral is finite and can be numerically integrated.

### 2.5.2 Primary Sectors

The first step is to take the Feynman integral of interest and write it in a way that will allow the pole structure to be determined. Consider a general Feynman loop

integral with $\{k_1, \ldots, k_L\}$ the loop momenta, $\{p_1, \ldots, p_N\}$ the external momenta and $\{m_1, \ldots, m_M\}$ the masses of the propagators. A general scalar Feynman integral can be written as

$$I = \int \prod_{l=1}^{L} [d^D k_l] \prod_{m=1}^{M} D_m(\{k\}, \{p\}, m_m^2), \tag{2.42}$$

where, again $[d^D k] = \frac{d^D k}{(2\pi)^D}$ and $D_m$ denotes a propagator. This procedure can be generalized for propagators of varying power, however it will not be considered here for simplicity. For a good review with general powers, see [23].

The first step is to combine the propagators using the more general form of Feynman parameters from Equation 2.4. The result can always be written in the form,

$$\begin{aligned} I &= \Gamma(n) \int \prod_{l=1}^{L} \left[d^D k_l\right] \int_0^1 dx_1 \ldots dx_n \delta\left(\sum x_i - 1\right) \\ &\times \left[\sum_{j,k=1}^{L} k_j \cdot k_k M_{jk} - 2 \sum_{j=1}^{L} k_j \cdot Q_j + J\right]^{-n}, \end{aligned} \tag{2.43}$$

where $M$ is a matrix of Feynman parameters and $Q$ is a vector of external momenta and Feynman parameters. It is then possible to shift the loop momenta to absorb the linear term and integrate. The result is of the form

$$I = (-1)^n \Gamma(n - LD/2) \int_0^1 d^n x \delta\left(1 - \sum x_i\right) \frac{U^{n-(L+1)D/2}}{F^{n-LD/2}}, \tag{2.44}$$

where $d^n x$ is short for $dx_1 \ldots dx_n$, and

$$F = det(M) \left[J - \sum_{j,k=1}^{L} Q_j \cdot Q_k (M^{-1})_{jk}\right], \tag{2.45}$$

$$U = det(M). \tag{2.46}$$

The integral is now in a form that allows divergences to be found. To disentangle the poles in the integral $I$ the integral is decomposed into what are called primary sectors. The integral is separated into $n$ parts using

$$\int_0^1 d^n x = \int_0^1 d^n x \prod_{j=1}^{n} \theta(x_j \geq 0) = \sum_{l=1}^{n} \int_0^1 \prod_{\substack{j=1 \\ j \neq l}}^{n} \theta(x_l \geq x_j \geq 0), \tag{2.47}$$

where the $\theta$-function is defined by

$$\theta(x \geq y) = \begin{cases} 1 & \text{if } x \geq y \\ 0 & \text{otherwise.} \end{cases} \tag{2.48}$$

Now, an odd but useful transformation of variables is made. This transformation allows one of the $x_i$ integrals to be carried out using the delta function. The change

$$x_j = \begin{cases} x_l t_j & j < l, \\ x_l & j = l, \\ x_l t_{j-1} & j > l. \end{cases} \tag{2.49}$$

is made. It turns out that with this transformation $x_l$ factors completely from both functions $F$ and $U$. In fact, the $x_l$ integral will always be of the form

$$\int \frac{dx_l}{x_l}\delta\left(1 - x_l\left(1 + \sum_{k=1}^{n-1} t_k\right)\right) = 1. \tag{2.50}$$

What is left is $n$ integrals of the form

$$I_l = (-1)^n\Gamma(n - LD/2)\int_0^1 d^{n-1}t\frac{U_l^{n-(L+1)D/2}}{F_l^{N-LD/2}}. \tag{2.51}$$

For simplicity, the overall factor of $(-1)^n\Gamma(n - LD/2)$ is left out as it is a common factor. The integrals $I_l$ define what are referred to as the primary sectors. The poles of the $t$ integrals are still entangled within $U$ and $F$, but it is seen that they occur when the functions $U$ and/or $F$ go to zero.

### 2.5.3 Iterated Decomposition

The integral is now separated into different sectors. This does not guarantee, however, that the poles in each sector do not overlap. To disentangle the poles, an iterative method of sector decomposition is applied that removes the poles from the functions $U$ and $F$ and makes them explicit in the integral.

To start, the functions $U$ and $F$ are considered and the minimal set of parameters $t_s$ such that when set to zero $U$ and/or $F$ goes to zero is determined. For each of these parameters $t_{s_1}, \ldots, t_{s_r}$, the integral is decomposed into sub-integrals using,

$$\prod_{j=1}^{r}\theta(1 \geq t_{s_j} \geq 0) = \sum_{k=1}^{r}\prod_{\substack{j=1\\ j\neq k}}^{r}\theta(t_{s_k} \geq t_{s_j} \geq 0). \tag{2.52}$$

As with the primary sectors, a change of variables is made in each new sector corresponding to

$$t_{s_j} = \begin{cases} t_{s_k}t_{s_j} & j \neq k, \\ t_{s_k} & j = k. \end{cases} \tag{2.53}$$

Again $t_{s_k}$ factorizes from $U$ and $F$, and the integral becomes

$$I_{l_k} = \int_0^1 d^{n-1}t\left(\prod_{j=1}^{n-1} t_j^{A_j - B_j\epsilon}\right)\frac{U_{l_k}^{n-(L+1)D/2}}{F_{l_k}^{n-LD/2}}. \tag{2.54}$$

This procedure should be repeated until the functions $U$ and $F$ contain constant terms and all of the pole structure is contained in the $\left(\prod_{j=1}^{n-1} t_j^{A_j - B_j\epsilon}\right)$ term. The poles can then be read straight from the $A_j$ terms.

It should be noted that it is possible for certain integrals to lead to an infinitely iterative scheme. Other schemes have been outlined that are guaranteed to iterate a finite number of times, but will not be discussed here.

### 2.5.4 Extracting the Poles

With the poles now appearing explicitly in the integral, a simple subtraction routine can be applied to separate the poles from the integral. The integrand is separated into two parts.

$$I_l = \int_0^1 dt_l t_l^{A_l - B_l\epsilon} T(t_l, \epsilon) \tag{2.55}$$

If $A_l < 0$ then there are poles. To deal with them, $T$ is expanded in a Taylor series about $t_l = 0$ to order $|A_l| - 1$. The part with the pole can then be analytically integrated for $t_l$ giving

$$T(t_l, \epsilon) = \sum_{p=0}^{|A_l|-1} T_l^{(p)}(0, \epsilon) \frac{t_l^p}{p!} + R(t_l, \epsilon), \tag{2.56}$$

where $R$ is the remainder of the series. Solving this for $R$ gives the original integrand $T$ less the pole part $T^{(p)}$. By construction, this quantity has no poles and can be integrated either analytically or numerically. Note that $R$ can also be expanded in terms of $\epsilon$ so that in the end, the result is a series in $\epsilon$ just like most other dimensionally regularized results.

### 2.5.5 Example

In order to make these ideas more concrete, a simple but non-trivial example will be considered in the form of the sunset integral in Figure 2.4. The integral is

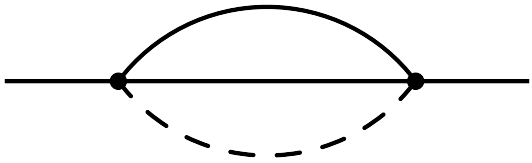

**Figure 2.4:** A two loop integral that can be computed analytically but also provides a non-trivial example of sector decomposition. The dotted line in this case indicates what is known as an eikonal propagator $2p \cdot k_2$ instead of a massless propagator.

$$M_2 = \int \frac{[d^D k_1][d^D k_2]}{[k_1^2 + 2p \cdot k_1][(k_1 + k_2)^2 + 2p \cdot (k_1 + k_2)][2p \cdot k_2]}. \tag{2.57}$$

With three propagators, three Feynman parameters are introduced.

$$\begin{aligned} M_2 &= -\frac{1}{\Gamma(3)} \int [d^D k_1][d^D k_2] \\ &\int_0^1 \frac{\delta(1 - x_1 - x_2 - x_3) d^3x}{[k_1^2(x_1 + x_2) + 2p \cdot k_1(x_1 + x_2) + 2k_1 \cdot k_2 x_2 + k_2^2 x_2 + 2p \cdot k_2(x_2 + x_3)]^3} \end{aligned} \tag{2.58}$$

If the denominator is compared with the expression in Equation 2.43, the $2 \times 2$ matrix $M$ and a 2 component vector $Q$ are apparent. Technically, a scalar component $J$

would also be present, however in this case it is zero. Thus $M$, $Q$, and $J$ are given by

$$M = \begin{bmatrix} x_1+x_2 & x_2 \\ x_2 & x_2 \end{bmatrix}, \quad Q = \begin{bmatrix} -p(x_1+x_2) \\ -p(x_2+x_3) \end{bmatrix}, \quad J = 0. \tag{2.59}$$

Completing the square for $k_1$ allows the change of variables $k_1 \to k_1' - p - k_2\frac{x_2}{x_1+x_2}$ and the integral over $k_1'$ to be carried out.

$$M_2 = -\frac{\Gamma(3-D/2)}{(4\pi)^{D/2}} \int\int_0^1 \frac{\delta(1-x_1-x_2-x_3)[d^Dk_2]d^3x}{(x_1+x_2)^3\left[k_2^2\frac{x_1x_2}{(x_1+x_2)^2} + 2p\cdot k_2\frac{x_3}{x_1+x_2} - p^2\right]^{3-D/2}} \tag{2.60}$$

The same process can be repeated for $k_2$. After a bit of re-arranging, it is possible to get this in the form,

$$M_2 = -\frac{\Gamma(3-D)}{(4\pi)^D}\int_0^1 d^3x \frac{(x_1x_2)^{3-3D/2}\delta(1-x_1-x_2-x_3)}{\left[-p^2x_1x_2\left(x_1+x_2+\frac{x_3^2}{x_2}+\frac{x_3^2}{x_1}\right)\right]^{3-D}} \tag{2.61}$$

Note that this is exactly what would have been obtained if the expression in Equation 2.44 had been naïvely used.

The integral is ready to be decomposed into primary sectors. With three Feynman parameters, there are three integrals. Using the identity in Equation 2.50 and simplifying gives

$$M_2 = -\frac{\Gamma(3-D)(-p^2)^{1-2\epsilon}}{(4\pi)^D}(I_1+I_2+I_3), \tag{2.62}$$

where

$$I_1 = \int_0^1 d^2t \frac{t_1^{3-3D/2}}{\left[(1+t_1)(t_1+t_2^2)\right]^{3-D}}, \tag{2.63}$$

$$I_2 = \int_0^1 d^2t \frac{t_1^{3-3D/2}}{\left[(1+t_1)(t_1+t_2^2)\right]^{3-D}}, \tag{2.64}$$

$$I_3 = \int_0^1 d^2t \frac{(t_1t_2)^{3-3D/2}}{\left[(t_1+t_2)(t_1t_2+1)\right]^{3-D}}. \tag{2.65}$$

$I_1$ and $I_2$ are the same so only two integrals need to be considered. Starting with $I_1$ it is seen that $F$ has a pole and the minimal set of parameters needed is $S_1 = \{t_1, t_2\}$. Making the appropriate change of variables leads to the integrals

$$I_1 = I_{1_1} + I_{1_2}, \tag{2.66}$$

where

$$I_{1_1} = \int_0^1 d^2t \frac{t_1^{-1+\epsilon}}{\left[(1+t_1)(1+t_1t_2^2)\right]^{-1+2\epsilon}}, \tag{2.67}$$

$$I_{1_2} = \int_0^1 d^2t \frac{t_2^{-1+\epsilon}t_1^{-3+3\epsilon}}{\left[(1+t_1t_2)(t_1+t_2)\right]^{-1+2\epsilon}}. \tag{2.68}$$

The integral $I_{1_1}$ is now in the form of Equation 2.55 and shows that there is a first order pole in $t_1$. For the second term however, the procedure must be repeated as there are still poles in the denominator. Starting with $I_{1_1}$ an expansion is done to leading order in $t_1$ so that the pole can be integrated. This gives the expression

$$\begin{aligned} I_{1_1} &= \int_0^1 d^2t t_1^{-1+\epsilon} + \int_0^1 d^2t t_1^{-1+\epsilon} R(t_1, t_2, \epsilon) && (2.69) \\ &= \frac{1}{\epsilon} + \int_0^1 d^2t t_1^{-1+\epsilon} \left( \frac{1}{\left[(1+t_1)(1+t_1t_2^2)\right]^{-1+2\epsilon}} - 1 \right). && (2.70) \end{aligned}$$

From here, the remaining term may be able to be computed analytically. It is usually easiest however, to expand in $\epsilon$ to the desired order and integrate term by term. Doing so to $\mathcal{O}(\epsilon)$ gives,

$$\begin{aligned} I_{1_1} &= \frac{1}{\epsilon} + \int_0^1 d^2t (1 + t_2^2 + t_1t_2^2) \\ &\quad + \frac{\epsilon}{t_1} \left[ \left( -1 + (1+t_1)(1+t_1t_2^2) \right) \ln(t_1) \right. \\ &\quad \left. -2(1+t_1)(1+t_1t_2^2) \ln\left( (1+t_1)(1+t_1t_2^2) \right) \right] + \mathcal{O}(\epsilon^2), && (2.71) \\ &= \frac{1}{\epsilon} + \frac{3}{2} + \epsilon \left( \frac{19}{12} - \frac{\pi^2}{3} - \frac{16\ln(2)}{3} \right) + \mathcal{O}(\epsilon^2). && (2.72) \end{aligned}$$

For $I_{1_2}$ the result is

$$I_{1_2} = -\frac{2}{3\epsilon} - \frac{25}{9} + \epsilon \left( \frac{179}{27} - \frac{23}{6}\pi + \frac{\pi^2}{3} + \frac{7}{3}\ln(2) \right) + \mathcal{O}(\epsilon^2). \quad (2.73)$$

This integral was accomplished by applying the iterated decomposition once more. The procedure is somewhat tedious so only the $I_3$ integral is shown here. Starting with $S = \{t_1, t_2\}$ the integral is

$$I_3 = I_{3_1} + I_{3_2}, \quad (2.74)$$

where

$$\begin{aligned} I_{3_1} &= \int_0^1 d^2t_2 t_{2_1} \frac{(t_{2_1}^2 t_{2_2})^{-3+3\epsilon}}{\left[(t_{2_1} + t_{2_1}t_{2_2})(t_{2_1}^2 t_{2_2} + 1)\right]^{-1+2\epsilon}}, && (2.75) \\ I_{3_2} &= \int_0^1 d^2t_2 t_{2_2} \frac{(t_{2_1} t_{2_2}^2)^{-3+3\epsilon}}{\left[(t_{2_1}t_{2_2} + t_{2_2})(t_{2_1} t_{2_2}^2 + 1)\right]^{-1+2\epsilon}}. && (2.76) \end{aligned}$$

These are the same integrals only differing by the exchange of $t_{2_1}$ and $t_{2_2}$. This leaves

$$I_3 = \int_0^1 d^2t t_1^{-4+4\epsilon} t_2^{-3+3\epsilon} \frac{2}{\left[(1+t_2)(1+t_1^2t_2)\right]^{-1+2\epsilon}}, \quad (2.77)$$

where $t_1$ and $t_2$ are used instead of $t_{2_1}$ and $t_{2_2}$. For simplicity, only a schematic of how this integral should be done is shown. The Taylor expansions in $t_1, t_2$ are denoted by $T_1, T_2$, the remainders by $R_1, R_2$ respectively and the full denominator term by $D$. Expanding first in $t_1$ gives

$$\frac{I_3}{2} = \int_0^1 t_1^{-4+4\epsilon} t_2^{-3+3\epsilon} T_1 + \int_0^1 t_1^{-4+4\epsilon} t_2^{-3+3\epsilon} R_1. \quad (2.78)$$

Next, both $T_1$ and $R_1$ need to be expanded in terms of $t_2$. First, the $T_1$ term. Again, there is the expanded part and a remainder.

$$\int_0^1 t_1^{-4+4\epsilon} t_2^{-3+3\epsilon} T_1 = \int_0^1 t_1^{-4+4\epsilon} t_2^{-3+3\epsilon} (T_{1,2} + R_2), \tag{2.79}$$

where the expansion in $t_1$ then $t_2$ is denoted by $T_{1,2}$. Remember, the expansions are only carried out to high enough order so the remainder term contains no poles. Similarly, expanding $R_1$ gives,

$$\int_0^1 t_1^{-4+4\epsilon} t_2^{-3+3\epsilon} R_1 = \int_0^1 t_1^{-4+4\epsilon} t_2^{-3+3\epsilon} (R_{1,2} + R_3). \tag{2.80}$$

Now the remainder terms need to be replaced with the known expressions.

$$\begin{aligned} R_1 &= D - T_1, && (2.81)\\ R_2 &= T_1 - T_{1,2}, && (2.82)\\ R_3 &= R_1 - R_{1,2}. && (2.83) \end{aligned}$$

Remember that each of these terms should be integrated as is, so that the poles are avoided. This process produces the four integrals

$$\begin{aligned} \frac{I_3}{2} &= \int_0^1 t_1^{-4+4\epsilon} t_2^{-3+3\epsilon} T_{1,2} \\ &+ \int_0^1 t_1^{-4+4\epsilon} t_2^{-3+3\epsilon} R_2 \\ &+ \int_0^1 t_1^{-4+4\epsilon} t_2^{-3+3\epsilon} R_{1,2} \\ &+ \int_0^1 t_1^{-4+4\epsilon} t_2^{-3+3\epsilon} R_3. \end{aligned} \tag{2.84}$$

Integrating and expanding each of these in terms of $\epsilon$ gives

$$\begin{aligned} \frac{I_3}{2} &= -\frac{1}{3\epsilon} + \frac{29}{18} + \frac{523}{108}\epsilon \\ &+ \left(\frac{17}{6} + \frac{\pi^2}{6} - \frac{16}{3}\ln(2)\right)\epsilon \\ &- \frac{1}{3} + 2\epsilon \\ &+ \left(\frac{\pi^2}{6} - \frac{5}{2}\right)\epsilon. \end{aligned} \tag{2.85}$$

The results can now be summed for the final answer. The full expression is

$$\begin{aligned} M_2 &= -\frac{\Gamma(-1+2\epsilon)(-p^2)^{1-2\epsilon}}{(4\pi)^D}(2I_1 + I_3) && (2.86)\\ &= 0. && (2.87) \end{aligned}$$

As it turns out, the result actually starts at $\mathcal{O}(\epsilon)$. It is possible to compute all of the $\mathcal{O}(\epsilon^2)$ terms analytically except for two that must be done numerically with the result

$$M_2 \approx -52.637887\epsilon \tag{2.88}$$

as compared to the analytic result,

$$M_2 = -\frac{16\pi^2}{3}\epsilon \approx -52.637890\epsilon. \tag{2.89}$$

Note, that the reason it is difficult for this method to obtain an analytic result is because of the pre-factor $\Gamma(-1+2\epsilon)$ which has an $\epsilon$ pole. This means the expansions must be computed to $\mathcal{O}(\epsilon^2)$ to obtain the $\mathcal{O}(\epsilon)$ term.

Typically, sector decomposition is used for integrals that are much more difficult than this example. Fortunately programs are available that will automatically compute the integrals given a set of propagators. When needed in this thesis the Mathematica package `FIESTA` [24] is used.

This chapter has introduced a few of the commonly used methods in computing higher order corrections. Starting with a basic one loop integral, it was shown how Feynman parameters can be used to carry out the loop integrals needed. In an effort to make calculations easier, a method of reducing the list of integrals required was introduced. Integration by parts allows a large list of integrals to be rewritten in terms of a small set of master integrals.

With the ability to reduce a problem to a set of master integrals, two methods of carrying out the integrals were then introduced. The first method relied on the Mellin-Barnes identity and allows a separation of terms in denominators while introducing a complex integral. These integrals can then be carried out analytically or numerically using contour integration or by summing poles after closing the contour. The second method provides an algorithm for extracting the poles of an integral so that numerical calculations can be done. This method is useful when the other methods that were introduced are not tractable. It is also a good tool for checking analytic results numerically.

Now that a set of methods for approaching problems is in hand, they can be applied to the problems that will be considered in this thesis. All chapters with the exception of Chapter 5 will use the techniques described above. In some cases, it will be necessary to use additional techniques that have not been discussed here, but will be outlined when they are used.

# Chapter 3

# The Lamb Shift

One of the most important historical tests for QED and its perturbation theory came in the form of what is known as the Lamb shift. In June of 1947, Willis Lamb announced a definitive measurement of the splitting between the energy levels of the $2S_{1/2}$ and $2P^{1/2}$ states in hydrogen at a conference held on Shelter Island in New York. The results of these measurements are typically expressed in terms of a frequency through the relation $\Delta E = \hbar\nu$, where $h$ is Planck's constant and $\nu$ is a frequency. Lamb measured the splitting to be approximately $\nu = 1000$ MHz [25]. Before this announcement, theorists attempted to calculate the difference between these two states and consistently ended up with a divergent result. This caused them to believe that the effect should be unphysical and not show up in any experiment. At this time, the formalism of QED was still being developed. In particular, theorists were just beginning to understand and develop the theory of renormalization. At the same conference, Hendrik Kramers described his work on mass renormalization in a classical non-relativistic theory. Fortunately Hans Bethe realized the connection between these two talks, and used this idea of mass renormalization to calculate the Lamb shift on his way home. He found the value should be 1040 MHz [26], which agrees very well with the value found by Lamb and Robert Retherford. This agreement gave a huge boost to the theory of renormalization which is an integral part of QFT today.

In this chapter a calculation of the $\alpha^2(Z\alpha)^5$ contribution to the Lamb shift is described. The problem is approached in a somewhat different way as compared to previous calculations. This leads to an improvement in precision of approximately an order of magnitude, as well as some new analytic results for individual diagrams.

## 3.1 Perturbation Theory

The corrections to the energy levels due to the Lamb shift can be grouped into four categories,

$$\Delta E = \Delta E_{\text{non-recoil}} + \Delta E_{\text{recoil}} + \Delta E_{\text{vp}} + \Delta E_{\text{proton}}. \tag{3.1}$$

The non-recoil term comes from interactions between the electron and nucleus, as well as self-energy interactions of the electron, and can be calculated assuming an infinitely heavy nucleus. The recoil term comes from the finite mass and non-zero motion of the nucleus. The vp term is the contribution from vacuum polarization effects due to muons and hadrons, while the similar contributions from electrons is

included in the non-recoil term. Finally, the proton term comes from considering the charge radius of the proton to be non-zero. Currently this term introduces the largest uncertainty to the theoretical prediction of the Lamb shift. For a review of the current state of the art calculations in each of these, see [27].

The calculation of the recoil, vp and non-recoil corrections can be built up perturbatively in four expansions. The first is the usual expansion in $\alpha$ and comes from the self-energy of the electron. The second expansion is in the quantity $Z\alpha$, where $Z$ is the atomic number of the nucleus. These terms come from the electron's interactions with the nucleus. By including the factor $Z$, the calculation can be performed for a general nucleus. Note that this expansion will only work in the region where $Z\alpha \ll 1$. The third expansion is in terms of a mass ratio. For the recoil corrections it is the mass ratio of the electron to the nucleus, $\frac{m}{M}$, where $m$ is the mass of the electron and $M$ is the mass of the nucleus. The vp corrections depend on the mass ratio of the electron to a heavier particle (e.g. muon or pion). The mass in the vp corrections comes from loops in the diagrams. Since the electron is much lighter than any of the heavier masses in this problem, these corrections are small and will not be considered here. Finally, the proton term is expressed as an expansion in $m_e r_p$, where $r_p$ is the charge radius of the proton. There is currently some disagreement surrounding the charge radius of the proton. A recent measurement, using the Lamb shift in muonic hydrogen, shows a $7\sigma$ disagreement with previous measurements [4]. It is therefore timely to scrutinize the theory of the Lamb shift.

In this thesis, the calculation of the Lamb shift is centred around the contribution of order $\alpha^2(Z\alpha)^2$ in the non-recoil part of the energy corrections. A sample of the contributing diagrams is given in Figure 3.1. This order of the correction is commonly

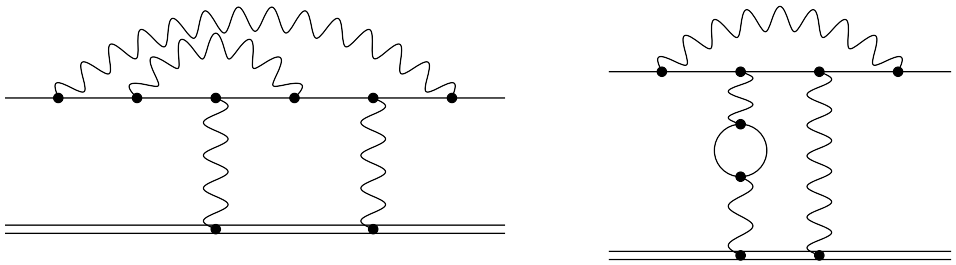

**Figure 3.1:** Two of the 60 diagrams that contribute to the $\alpha^2(Z\alpha)^5$ corrections to the Lamb shift. The double line indicates the nucleus.

quoted as $\alpha^2(Z\alpha)^5$. The extra three factors of $Z\alpha$ come from the amplitude of the hydrogen wave function squared evaluated at the center: $|\psi(0)|^2 = \frac{(Z\alpha\mu)^3}{\pi n^3}$, with $\mu$ the reduced mass of the system. The terms in the expansion can be broken up as shown in Equation 3.2.

$$\begin{aligned}\Delta E_{\text{non-recoil}} = \tfrac{m(Z\alpha)^4}{\pi n^3}\left(\tfrac{\mu}{m}\right)^3 \quad & \left[\alpha\left(A_{40} + (Z\alpha)A_{50} + (Z\alpha)^2 A_{60}\ldots\right)\right. \\ & +\alpha^2\left(B_{40} + (Z\alpha)B_{50} + \ldots\right) \\ & +\alpha^3\left(C_{40} + \ldots\right) \\ & \left.+\ldots\right] \end{aligned} \tag{3.2}$$

In this expansion, the coefficients are organized as follows: $A, B, C$ denote the power of $\alpha$, the first index denotes the power of $Z\alpha$ and the second index denotes the power

of $\ln(Z\alpha)$. The coefficient $A_{61}$ would then be the coefficient of the $\alpha(Z\alpha)^6 \ln(Z\alpha)$ term. The $\alpha^2(Z\alpha)^5$ term, described in this section, corresponds to $B_{50}$. This calculation has actually been done before [18, 19]. The purpose of the present calculation is to apply a new method to the problem and improve the precision. As well, the same method and set of master integrals can be used in the calculation of the bound electron $g$-factor, which will be discussed in Chapter 4. Comparison with [18, 19] provides a very good check of the method and the values of the master integrals.

## 3.2 Method

In order to describe some of the important methods in the calculation, the leading order diagrams that contribute to the $(Z\alpha)^5$ correction are considered and shown in Figure 3.2.

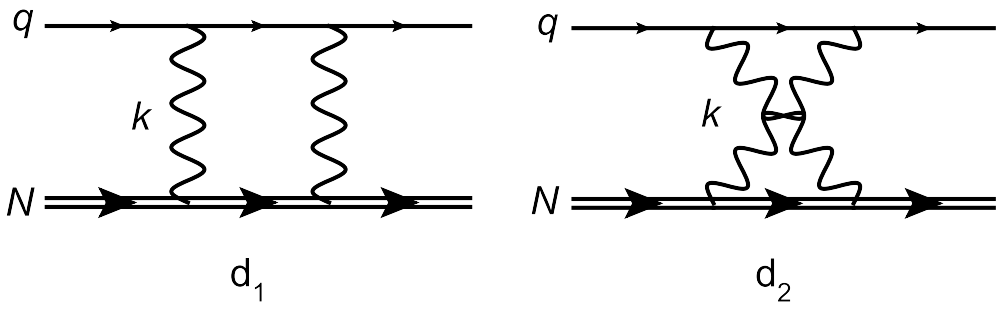


**Figure 3.2:** Tree level contributions to the Lamb shift. The double solid lines indicate a nucleon whereas the single solid lines indicate an electron.

If the expressions for these two diagrams are written out, it is seen that they differ only slightly.

$$\mathrm{d}_1 = \frac{e^4}{(k^2)^2} \frac{\left[\overline{u}(N)\gamma_\alpha(\not{N} - \not{k} + M)\gamma_\beta u(N)\right]}{[(N-k)^2 - M^2 + i0]} \frac{\left[\overline{u}(q)\gamma^\alpha(\not{q} + \not{k} - m)\gamma^\beta u(q)\right]}{[(q+k)^2 - m^2 + i0]}, \tag{3.3}$$

$$\mathrm{d}_2 = \frac{e^4}{(k^2)^2} \frac{\left[\overline{u}(N)\gamma_\beta(\not{N} + \not{k} + M)\gamma_\alpha u(N)\right]}{[(N+k)^2 - M^2 + i0]} \frac{\left[\overline{u}(q)\gamma^\alpha(\not{q} + \not{k} - m)\gamma^\beta u(q)\right]}{[(q+k)^2 - m^2 + i0]}, \tag{3.4}$$

where $\not{k} = k^\mu \gamma_\mu$. Namely, only the nucleon line parts differ in the sign of $k$ and the indices of the $\gamma$ matrices are switched. If only this part of each diagram is considered, a few simplifications can be made. First, notice that because an infinitely heavy nucleus is being considered, $k \ll N$, the denominators can be expanded in a Taylor series. The leading order of this series is the only term required when considering an infinitely heavy nucleus. Higher order terms belong with the recoil corrections. This gives

$$\mathrm{d}_1 + \mathrm{d}_2 \propto \overline{u}(N) \left[\frac{\gamma_\alpha(\not{N} + M)\gamma_\beta}{-2N\cdot k + i0} + \frac{\gamma_\beta(\not{N} + M)\gamma_\alpha}{2N\cdot k + i0}\right] u(N). \tag{3.5}$$

Finally, the $\gamma_\alpha$ and $\not{N}$ terms can be reordered and the Dirac equation can be used to rewrite this as

$$\mathrm{d}_1 + \mathrm{d}_2 \propto \overline{u}(N) N_\alpha \gamma_\beta \left[\frac{1}{N\cdot k + i0} - \frac{1}{N\cdot k - i0}\right] u(N). \tag{3.6}$$

This difference is a delta function ($-2\pi i\delta(N\cdot k)$), and hence a single expression for the sum of the two diagrams in Figure 3.2 is obtained and given in Equation 3.7 ,

$$\mathrm{d}_1+\mathrm{d}_2=-2\pi ie^4\frac{[\overline{u}(N)N_\alpha\gamma_\beta u(N)]}{(k^2)^2}\frac{\left[\overline{u}(q)\gamma^\alpha(\not{q}+\not{k}-m)\gamma^\beta u(q)\right]}{[(q+k)^2-m^2+i0]}\delta(N\cdot k) \tag{3.7}$$

This sum is general and does not depend on possible self interactions on the electron line. Therefore, a new effective propagator can be defined allowing a single diagram to be considered instead of the sum of two. This propagator is given by

$$\mathrm{ph3D}=-2\pi ie^2\frac{\overline{u}(N)N_\alpha\gamma_\beta u(N)}{(k^2)^2}\delta(N\cdot k). \tag{3.8}$$

This propagator is named ph3D because the delta function sets the time-like component of the photon to zero. This is actually a consequence of assuming the nucleus is infinitely heavy. Working in the centre of mass frame of the nucleus means the only non-zero component of the nucleus four-momentum is the time component. The only diagram required is shown in Figure 3.3. The leading order calculation can now be

**Figure 3.3:** The effective diagram, where the dotted line denotes the new propagator ph3D.

considered, and simplifies to

$$\begin{aligned} i\mathcal{M}^{(0)} &= -2\pi ie^4\int\frac{d^4k}{(2\pi)^4}\frac{[\overline{u}(N)N_\alpha\gamma_\beta u(N)]}{(k^2)^2} \\ &\quad\times\frac{\left[\overline{u}(q)\gamma^\alpha(\not{q}+\not{k}-m)\gamma^\beta u(q)\right]}{[(q+k)^2-m^2+i0]}\delta(N\cdot k). \end{aligned} \tag{3.9}$$

Summing over final spins and averaging over initial, gives

$$\begin{aligned} i\mathcal{M}^{(0)} &= -\frac{\pi ie^4}{2Mm}\int\frac{d^4k}{(2\pi)^4}\frac{\mathrm{Tr}\left[(\not{N}+M)N_\alpha\gamma_\beta\right]}{(k^2)^2} \\ &\quad\times\frac{\mathrm{Tr}\left[(\not{q}+m)\gamma^\alpha(\not{q}+\not{k}-m)\gamma^\beta\right]}{[(q+k)^2-m^2+i0]}\delta(N\cdot k). \end{aligned} \tag{3.10}$$

It is then straightforward to work out the traces and rearrange to give

$$\begin{aligned} i\mathcal{M}^{(0)} &= \frac{2^3\pi ie^4}{Mm}\int\frac{d^Dk}{(2\pi)^D}\left[\frac{M^2}{(k^2)^2}-\frac{M^2}{(k^2)[k^2+2q\cdot k]}\right. \\ &\quad\left.-\frac{4M^2m^2}{(k^2)^2[k^2+2q\cdot k]}\right]\delta(N\cdot k). \end{aligned} \tag{3.11}$$

An important aspect of this calculation is that recoil effects are not being considered. Effectively, the electron is treated as being at rest so that $q=(m\ \vec{0})$ while $N=(M\ \vec{0})$. This implies that the electron momentum and the nucleon momentum are parallel

and related by $N = \frac{M}{m}q$. The delta function then becomes $\delta(q \cdot k)\frac{m}{M}$ and the scalar products of $q$ and $k$ in the denominator can immediately be set to zero. Finally, the leading order contribution is

$$i\mathcal{M}^{(0)} = -2^6\pi i e^4 \int \frac{d^D k}{(2\pi)^D} \frac{\delta(k^0)}{(k^2)^2} = 0. \tag{3.12}$$

There is no additional shift to the energies. The reason for this is only the Coulomb photons have been considered whose effects are already included in the solution of the Schrödinger equation.

Contrary to most calculations where the amplitude needs to be squared to obtain a decay rate or cross section, the amplitudes of these diagrams are proportional to the energy shifts. It can be seen how computing these types of diagrams gives the energy splitting of the Lamb shift by taking a close look at the electron propagator. The propagator of the electron has poles at the allowed energy levels as shown in Equation 3.13.

$$\frac{i}{\not{k} - m - E_n} = \frac{i}{\not{k} - m(1 + \tilde{E}_n)} \tag{3.13}$$

The amplitude of a diagram is proportional to the energy. This can be seen by considering the most basic diagram that has just an incoming and outgoing electron. In the centre of momentum frame of the electron, the amplitude is

$$i\mathcal{M} = \overline{u}(p)u(p) = \mathrm{Tr}[\not{p} + m] = 4m. \tag{3.14}$$

The self-energy and interactions with the nucleus are simply higher order corrections to this amplitude and contribute to a change in energy that can be grouped with the mass in the same way as occurs in the propagator. What actually ends up being calculated in this chapter is

$$i\mathcal{M}^{(m)} = 4\delta E_n^{(m)}, \tag{3.15}$$

where $\delta E_n^{(m)}$ is the $m$th order correction to the $n$th energy level.

## 3.3 First Order Corrections

The procedure for transforming the nucleon propagator into a delta function is completely general so this also works at higher orders when electron self interactions are included. At the two loop level six diagrams contribute as shown in Figure 3.4 (diagrams $a$ and $d$ also have mirror images that need to be included).

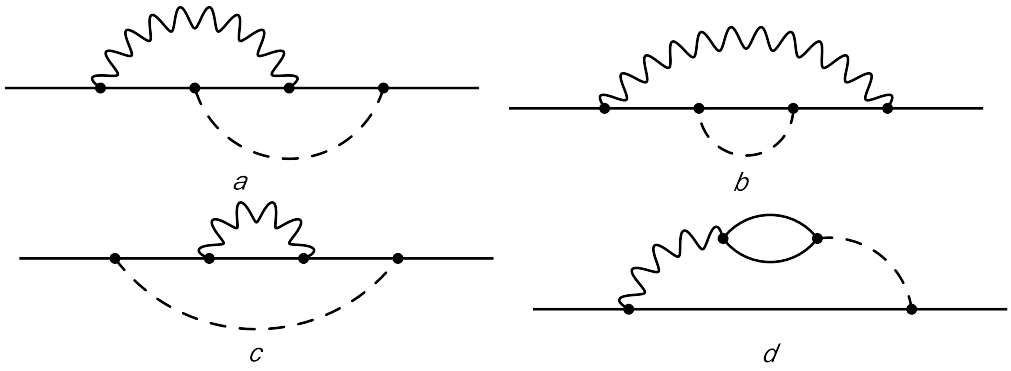


**Figure 3.4:** First order contributions to the Lamb shift. The solid lines indicate the electron line, while the wavy lines indicate photons and the dotted lines indicate the new ph3D propagator. This convention will be used for all diagrams in this calculation.

Fortunately, because the leading order contribution is zero, these diagrams don't have any renormalization terms and should be finite when summed. All of these diagrams also belong to a single topology, named N53d, and shown in Figure 3.5.

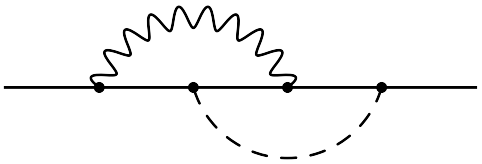

**Figure 3.5:** The single topology (N53d) required for the $\alpha(Z\alpha)^5$ contribution to the Lamb shift.

A similar topology called N5 is considered in [28]. The difference here is that one of the photons is replaced by the three dimensional exotic propagator ph3D. This integral can be solved for general powers of the propagators as a ${}_3F_2$ hypergeometric function, or Laporta reduction [20] can be used to reduce the list of integrals to two simpler master integrals. Using the Laporta reduction program `FIRE` [29], the two master integrals shown in Figure 3.6 are found, both of which can be solved analytically using Feynman parameters.

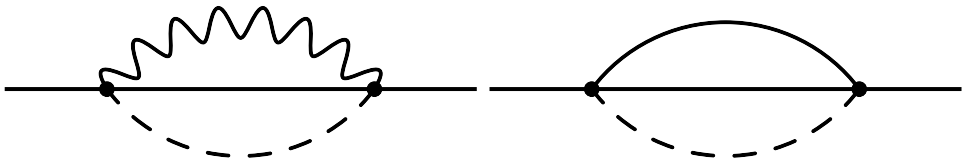

**Figure 3.6:** Two master integrals used in the two loop Lamb shift.

Note that in `FIRE`, the propagator $2p \cdot k$ is used in place of the delta function. This works well for the reduction and does not change the final result as the sign of the propagator does not change the reduction. Remember also, that if the delta function propagator does not appear in the final integral, the total contribution is zero. This is evident if the two contributing diagrams are considered separately

instead of using the delta function. The only difference between the two diagrams is this propagator $\frac{1}{2p\cdot k}$ (see Equation 3.6). If it disappears in the reduction, then the difference between the two diagrams is zero and no calculation needs to be done.

The diagrams in Figure 3.4 have been calculated in order to check the methods used here. The results are

$$a = \frac{\alpha(Z\alpha)^5 m}{8}\left(\frac{425}{32} + 7\xi\right), \tag{3.16}$$

$$b = -\frac{\alpha(Z\alpha)^5 m}{8}\left(\frac{55}{16} + 2\ln(2) + \frac{7}{2}\xi\right), \tag{3.17}$$

$$c = -\frac{\alpha(Z\alpha)^5 m}{8}\left(\frac{11}{2} + \frac{7}{2}\xi\right), \tag{3.18}$$

$$d = \frac{\alpha(Z\alpha)^5 m}{8}\left(\frac{5}{48}\right), \tag{3.19}$$

in perfect agreement with known results [30, 31]. As an extra check of the results, this and subsequent calculations are performed in a general gauge that is denoted with the parameter $\xi$. When summed, the contributions at a given order should not depend on this gauge parameter.

## 3.4 Second Order

The main purpose of this chapter is to compute the second order corrections to the Lamb shift using the loop integral technology that has been developed over the past few decades. These corrections are known and were originally calculated in [18, 19], with the more accurate solutions provided in [18]. The methods outlined have been able to reproduce the results in [18] and moreover improve upon the numerical precision.

The second order corrections consist of a total of 60 Feynman diagrams that must be calculated as shown in Figure 3.7. Using `FIRE` (see previous section) these integrals can be re-written in terms of 32 master integrals. The values and diagrams for the master integrals have been presented in [32] and are included in Appendix A. In order to calculate the contributions from each diagram as accurately as possible, a combination of techniques that are described in Chapter 2 is used.

The results and calculation in [18] are done in the so-called Fried-Yennie gauge. This gauge sets the gauge parameter $\xi = \frac{2}{1-2\epsilon}$ and has the important property that, in this gauge, each Feynman diagram is infrared finite. This allows numerical calculations to be done without worrying about divergences. The calculation was carried out in a general gauge to make sure the gauge parameter disappeared in the sum of all diagrams. Specializing to the Fried-Yennie gauge allows a comparison of the results diagram by diagram with [18]. The results for the electron self-interaction and vertex correction diagrams are presented in Table 3.1.

It can be seen that most of the results presented here agree well with those of [18]. There are, however, a few diagrams that differ significantly: diagrams $o, s, k$ and $r$. As stated in [32] it is possible that these differences arise because of the different regularization schemes used. If the full result is considered instead, the change in

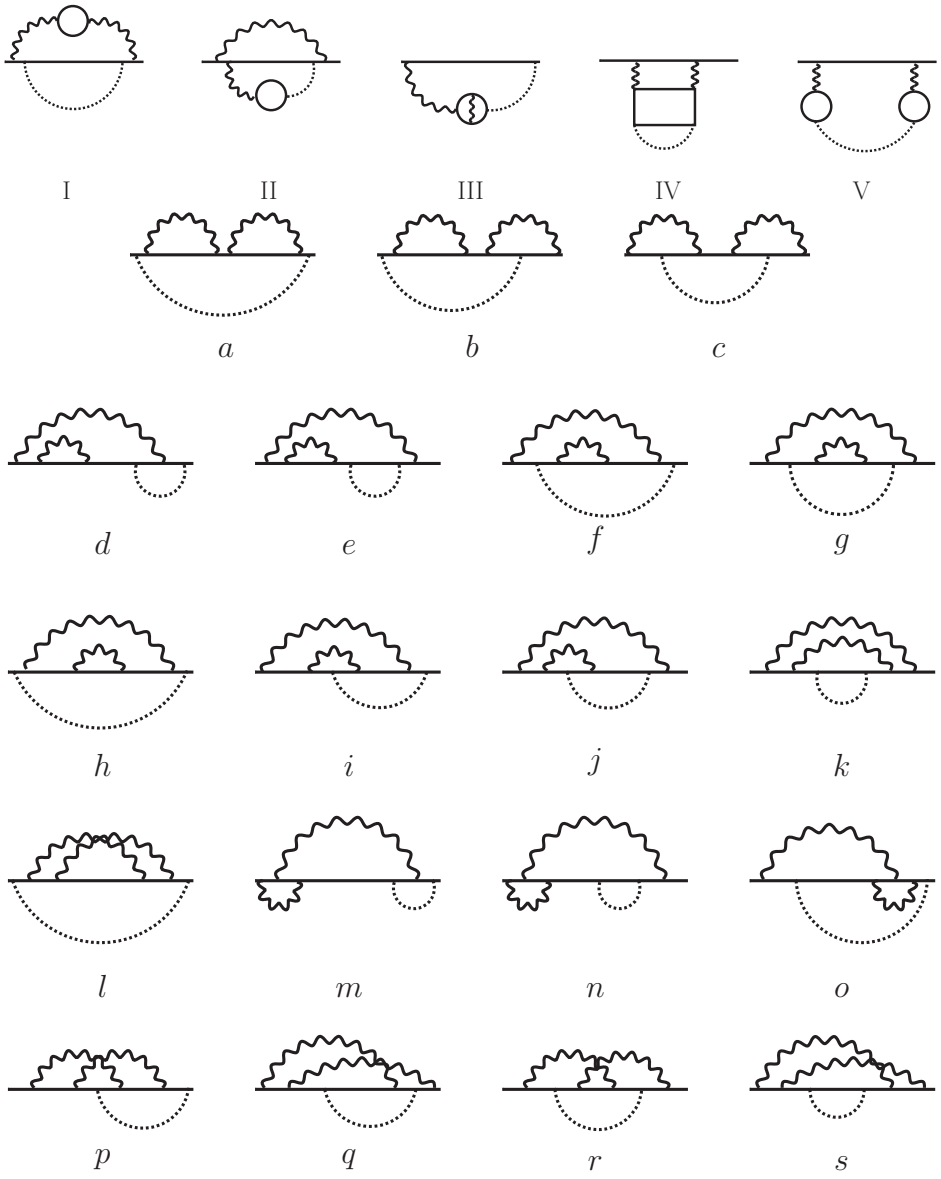


**Figure 3.7:** The second order Feynman diagrams needed for the $\mathcal{O}\left(\alpha^2(Z\alpha)^5\right)$ corrections to the Lamb shift. The diagrams I-V are vacuum polarization diagrams and each represents a collection of diagrams with every possible permutation of the propagators. The diagrams $a-s$ are the electron self-interaction and vertex corrections. The naming schemes used in [18, 19] have been used here as well.

energy is found to be

$$\delta E_{a-s} = \frac{\alpha^2(Z\alpha)^5}{\pi n^3}\left(\frac{\mu}{m}\right)^3 m[-7.72381(4)], \tag{3.20}$$

which is in perfect agreement with the result in [18],

$$\delta E_{a-s} = \frac{\alpha^2(Z\alpha)^5}{\pi n^3}\left(\frac{\mu}{m}\right)^3 m[-7.724(1)]. \tag{3.21}$$

| Diagram | This Calculation | Ref. [18] |
|---|---|---|
| $a$ | 0 | 0 |
| $b$ | 2.955090809... | 2.9551(1) |
| $c$ | $-2.22312657\ldots$ | $-2.2231(1)$ |
| $d$ | $-5.2381153272259(2)$ | $-5.238023(56)$ |
| $e$ | 5.0561650638185(4) | 5.056278(81) |
| $f$ | $6\ln(2) - 207/40$ | $-1.016145(21)$ |
| $g$ | $6\ln(2) - 147/80 - \pi^2/4$ | $-0.1460233(52)$ |
| $h$ | 153/80 | 153/80 |
| $i$ | $-5.51731(2)$ | $-5.51658(54)$ |
| $j$ | $-7.76838(1)$ | $-7.76813(18)$ |
| $k$ | 1.9597582447795(2) | 1.959589(33) |
| $l$ | 1.74834(4) | 1.74815(38) |
| $m$ | 1.87510512(6) | 1.87540(17) |
| $n$ | $-1.30570289(7)$ | $-1.30584(18)$ |
| $o$ | $-12.06904(9)$ | $-12.06751(47)$ |
| $p$ | 6.13815(1) | 6.13748(30) |
| $q$ | $-7.52425(2)$ | $-7.52525(74)$ |
| $r$ | 14.36962(7) | 14.36733(44) |
| $s$ | $-0.9304766935602(5)$ | $-0.930268(72)$ |

**Table 3.1:** Comparison between the results for diagrams $a$-$s$ (in the Fried-Yennie gauge) and those of [18]. Numbers ending in an ellipsis indicate an analytic result, which are given in Appendix 3.

Here, $\mu$ is the reduced mass of the system. The error in the result presented here comes from the master integrals. The diagrams denoted I-V were calculated in [19]. These diagrams have also been calculated using the method presented in this chapter and the sum of diagrams is improved by about two orders of magnitude. The results are shown in Table 3.2.

| Set | This paper | Refs. [19] |
|---|---|---|
| I | $-0.07290996446926(4)$ | $-0.0729098(3)$ |
| II | 0.61133839226... | $0.61133839226\ldots$ |
| III | 0.50814858506... | $0.50814858506\ldots$ |
| IV | $-0.12291623(3)$ | $-0.122915(3)$ |
| V | $-23/278$ | $-23/278$ |

**Table 3.2:** Comparison between the results calculated here for the different vacuum-polarization sets (in the Fried-Yennie gauge) and those of [19]. Numbers ending in an ellipsis indicate an analytic result, which are shown in Appendix 3.

The sum gives the energy corrections from vacuum polarization diagrams.

$$\delta E_{vp} = \frac{\alpha^2 (Z\alpha)^5}{\pi n^3} \left(\frac{\mu}{m}\right)^3 m \left[0.86281422(3)\right]. \tag{3.22}$$

The full energy correction is

$$\delta E = \frac{\alpha^2 (Z\alpha)^5}{\pi n^3} \left(\frac{\mu}{m}\right)^3 m[-6.86100(4)]. \tag{3.23}$$

As can be seen, the method used improves upon the previous results by a bit more than an order of magnitude. The error in this result comes from the numerical methods used in computing the master integrals. These methods are the limiting factor in the precision of our result. The achieved improvement shows the power of our method and provides an important check before applying it to the calculation of the bound $g$-factor of the electron in the next chapter.

# Chapter 4

# Bound Electron $g$-Factor

Along with the Lamb shift, the calculation of the $g$-factor of the electron was one of the first tests of QED, in particular perturbation theory. The success of the theoretical description of the $g$-factor continues today by providing the most precise determination of the fine structure constant, $\alpha$. This is the most precise measurement of any coupling constant and is a testament to how successful the SM is.

This chapter focuses on the $g$-factor of a bound electron. An electron in an atom has a $g$-factor that differs from the $g$-factor of a free electron because of interactions with the nucleus. With the use of Penning traps, the value of the bound electron $g$-factor can be measured accurately. The value is then used to determine the mass of the electron. This currently provides the most accurate value of the electron mass as shown in [16]. Two values are provided in that paper: one for a carbon atom and one for an oxygen atom (in atomic mass units):

$$m_e({}^{12}C^{5+}) = 0.000\,548\,579\,909\,32(29) \tag{4.1}$$
$$m_e({}^{16}O^{7+}) = 0.000\,548\,579\,909\,60(41). \tag{4.2}$$
$$\tag{4.3}$$

As can be seen, the two values agree well and provide the current CODATA recommended value [3]. It should be mentioned here that the measurements and calculations are done using so called hydrogen like atoms. This means that there is only one electron orbiting the nucleus. As well, recalling the expression used for determining the bound $g$-factor given in Equation 1.15,

$$g_b = 2\frac{\omega_L}{\omega_c}\frac{m_e}{m_{\text{ion}}}\frac{Q}{e}. \tag{4.4}$$

shows how the electron mass can be determined from the value of the bound $g$-factor. Importantly, the mass of the ion used needs to be known with great precision to obtain such a precise value of the electron mass.

In the following, the historical description of the free and bound $g$-factor will be discussed. With this perspective, a more modern method of calculating corrections will be introduced that follows the methods used in the Lamb shift calculation. This new approach will eventually allow a determination of the unknown $\alpha(Z\alpha)^5$ corrections as the calculation is ongoing.

## 4.1 The $g$-Factor

### 4.1.1 From the Dirac Equation

In naïv non-relativistic quantum mechanics with semiclassical reasoning, the interaction of the spin of an electron with an external magnetic field is given by

$$V = -\vec{\mu} \cdot \vec{\mathbf{B}} = \frac{e}{2m_e}\vec{\mathbf{S}} \cdot \vec{\mathbf{B}}. \tag{4.5}$$

Comparing this with experimental measurements shows that it is off by a factor of almost exactly two. To account for this extra factor, the interaction term is modified to include what is known as the $g$-factor.

$$V = -\vec{\mu} \cdot \vec{\mathbf{B}} = \frac{ge}{2m_e}\vec{\mathbf{S}} \cdot \vec{\mathbf{B}} \tag{4.6}$$

As it turns out, this factor can be explained by treating the electron relativistically using the Dirac equation. Indeed, the first major success of the Dirac equation, and one of the factors contributing to its acceptance, is the fact that the magnetic moment of the electron comes out with the proper factors of two. Today, this factor is known as the $g$-factor of the electron and is known to be slightly different from two. To start, let's see how this factor of two comes about. Consider the Dirac equation for an electron in the presence of an external field:

$$(i\gamma^\mu D_\mu - m_e)\psi = 0, \tag{4.7}$$

where $D_\mu = \partial_\mu - ieA_\mu$, $A_\mu$ is the electromagnetic vector field and $\psi$ is the electron spinor. Multiplying by $(i\gamma^\mu D_\mu + m_e)$ from the left, gives

$$-(\gamma^\mu\gamma^\nu D_\mu D_\nu + m_e^2)\psi = 0. \tag{4.8}$$

The factor of $\gamma^\mu\gamma^\nu$ can be written in terms of commutators and anti-commutators.

$$\gamma^\mu\gamma^\nu = \frac{1}{2}(\{\gamma^\mu, \gamma^\nu\} + [\gamma^\mu, \gamma^\nu]) = g^{\mu\nu} - i\sigma^{\mu\nu} \tag{4.9}$$

This identity gives

$$(D_\mu D^\mu - i\sigma^{\mu\nu} D_\mu D_\nu + m_e^2)\psi = 0. \tag{4.10}$$

Using the same trick from Equation 4.9 on the second term, the $D's$ can be rewritten. Notice that since $\sigma^{\mu\nu}$ is anti-symmetric and $\{D_\mu, D_\nu\}$ is symmetric, only the commutator contributes.

$$\begin{aligned} 0 &= (D_\mu D^\mu - i\frac{\sigma^{\mu\nu}}{2}[D_\mu, D_\nu] + m_e^2)\psi & (4.11)\\ &= (D_\mu D^\mu - \frac{e}{2}\sigma^{\mu\nu}F_{\mu\nu} + m_e^2)\psi & (4.12) \end{aligned}$$

Since the interaction between the spin of an electron and a magnetic field is what is required, the term proportional to $\sigma^{\mu\nu}F_{\mu\nu}$ is what is needed. By taking the non-relativistic limit of this term, it is possible to obtain the interaction term that appears in the Schrödinger equation with the correct factors of two:

$$\frac{e}{m_e}\vec{\mathbf{S}} \cdot \vec{\mathbf{B}}. \tag{4.13}$$

### 4.1.2 In Field Theory

The $g$-factor is now known to differ very slightly from two. This difference is known as the anomalous magnetic moment of the electron and is expressed by

$$a_e = \frac{1}{2}(g-2). \tag{4.14}$$

It arises from self-energy corrections to the electron-photon vertex. To see how this happens, consider the matrix element of the electromagnetic current

$$\langle p', s|J^\mu(q)|p, s\rangle. \tag{4.15}$$

Using Lorentz invariance and charge conservation, it is possible to write down a general form of the current:

$$\langle p', s|J^\mu(q)|p, s\rangle = \overline{u}(p', s')\left[\gamma^\mu F_1(q^2) + \frac{i\sigma^{\mu\nu}q_\nu}{2m_e}F_2(q^2)\right]u(p, s), \tag{4.16}$$

where $F_1(q^2)$ and $F_2(q^2)$ are known as form factors and $q = p' - p$ is the momentum transfer. The Gordon decomposition can be used to show that at leading order in momentum transfer, the matrix element becomes

$$\overline{u}(p', s')\left[\frac{(p'+p)^\mu}{2m_e}F_1(0) + \frac{i\sigma^{\mu\nu}q_\nu}{2m_e}(F_1(0) + F_2(0))\right]u(p, s). \tag{4.17}$$

The coefficient of the first term $F_1(0)$ is defined to be one as it corresponds to the electric charge seen in experiments. The second term gives the magnetic moment of the electron, which is shifted by an amount $F_2(0) = a_e$. It is this factor that will be calculated here.

Before this can be done though, the different contributions and factors need to be separated so that in the end only $F_2(0)$ remains. The authors of [33] show how this can be done in a simple but effective way. Their procedure is followed here. In order to get $F_2(0)$, $J_\mu(q)$ is expanded to first order in $q_\mu$:

$$\begin{aligned} J_\mu(q) &\approx J_\mu(0) + q_\nu \frac{\partial}{\partial q_\nu}J_\mu(q)\bigg|_{q=0} && (4.18)\\ &= V_\mu + q_\nu T^\nu_\mu. && (4.19)\end{aligned}$$

The result contains terms proportional to $q_\mu q_\nu$ and $q_\mu$. To deal with these, the average over spatial dimensions is computed. As dimensional regularization is used for the final calculation, the number of spatial dimensions is taken as $D-1$. This procedure gives

$$\begin{aligned} \langle q_\mu q_\nu\rangle &= \frac{q^2}{D-1}\left(g_{\mu\nu} - \frac{(p'+p)_\mu(p'+p)_\nu}{(p'+p)^2}\right), && (4.20)\\ \langle q_\mu\rangle &= 0. && (4.21)\end{aligned}$$

In order to extract $F_2(0)$ from the result, an operator known as a projector is used. Such a projector, say $P_\mu$, can be contracted by multiplying by the expansion of $J^\mu(0)$ and taking the trace. The most general form of $P_\mu$ is

$$P_\mu = (\not{p}' + m_e)\left[g_1\gamma_\mu - \frac{g_2}{m_e}(p'+p)_\mu - \frac{g_3}{m_e}(p'-p)_\mu\right](\not{p} + m_e). \tag{4.22}$$

Taking the trace leads to a system of equations showing that $g_3$ is zero and $F_2(0)$ is given by

$$\begin{aligned} F_2(0) &= \frac{1}{2(D-1)(D-2)m_e^2}\mathrm{Tr}\left[\frac{D-2}{2}\left(m_e^2\gamma_\mu - Dp_\mu \not{p} - (D-1)m_e p_\mu\right)V^\mu \right. \\ &+ \left. \frac{m_e}{4}(\not{p}+m_e)[\gamma_\nu,\gamma_\mu](\not{p}+m_e)T^{\mu\nu}\right]. \end{aligned} \tag{4.23}$$

Higher order corrections to the anomalous magnetic moment can be computed by expanding the diagram to first order in $q$ and replacing the $V^\mu$ and $T^{\mu\nu}$ terms in Equation 4.23 with the corresponding terms from the expansion, before traces are taken.

## 4.2 The Bound $g$-Factor

So far only the free electron $g$-factor has been considered. To treat the bound case, there are two options. The first is to use bound wave functions for the incoming and outgoing electrons. In the historical computation of the bound electron $g$-factor this is not how it was done. The use of bound wave functions will be explored more in Chapter 5.

The second option, which will be used here, is to treat the binding as a perturbation and build it up in a series similar to the $Z\alpha$ series from the Lamb shift. In this case, the leading order term is just the free electron $g$-factor; the first order involves the exchange of one photon with the nucleus and so on. The corrections to the form factor $F_2$ are built up in a double expansion. Self-energy corrections to the electron provide an expansion in $\alpha$ and interactions with the nucleus result in an expansion in $Z\alpha$. In this expansion, all leading order terms in the $\alpha$ expansion are known. They were calculated to all orders in $Z\alpha$ by Breit in [34]. Other than this correction, the $\alpha$ and $\alpha^2$ expansions are known up to $(Z\alpha)^4$. Similar to the Lamb shift, the wave function of the electron evaluated at the origin provides a factor of $(Z\alpha)^3$ to the $\alpha$ and $\alpha^2$ expansions. This means that the $(Z\alpha)^4$ contributions come from a single photon exchange with the nucleus and the $(Z\alpha)^5$ contributions have two photons exchanged.

In this chapter the method from Chapter 3 is applied to start the calculation of the $\alpha(Z\alpha)^5$ and the known contributions are reproduced. The evaluation of the other terms are ongoing.

### Breit Correction

Before computing the $\alpha(Z\alpha)^5$ corrections it will be informative to derive the leading order term in the Breit correction. The method is similar to the methods currently used in calculations of higher orders. As well, this exercise will help to highlight the difference between this approach and the method that will be introduced in the next section. For this correction, there are three diagrams that can contribute shown in Figure 4.1. The Dirac spinors are

$$u(\vec{p}) = \sqrt{\frac{2E_p}{E_p+m_e}}P_+(\vec{p})\omega, \tag{4.24}$$

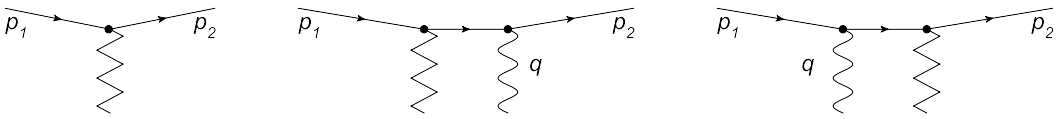


**Figure 4.1:** The tree-level contributions to the bound electron $g$-factor. The zig-zag line indicates the magnetic field interaction and the photon line shows an interaction with the Coulomb field.

where $\omega$ is the four-spinor of a particle at rest and $P_+$ is the projector on the positive electron energy states. The projectors on positive and negative energy states are

$$P_\pm(\vec{p}) = \frac{1}{2}\left(1 \pm \frac{\vec{\alpha}\cdot\vec{p} + \beta m_e}{E_p}\right). \tag{4.25}$$

Expanding the spinor $u(\vec{p})$ in terms of $\vec{p}$ gives the corrections to the $g$-factor.

The $g$-factor as determined by the diagrams in Figure 4.1 comes from the amplitude, which is equal to the negative of the potential. To start, consider the first diagram with no Coulomb interaction. The amplitude is

$$i\mathcal{M} = \overline{u}(\vec{p_2})\left(-ie\gamma_0\vec{\alpha}\cdot\vec{A}\right)u(\vec{p_1}). \tag{4.26}$$

Note that the definitions of $\vec{\alpha}$ and $\beta$ used are

$$\alpha = \begin{pmatrix} 0 & \vec{\sigma} \\ \vec{\sigma} & 0 \end{pmatrix}, \quad \beta = \begin{pmatrix} 1 & 0 \\ 0 & -1 \end{pmatrix}, \tag{4.27}$$

where $\vec{\sigma}$ are the Pauli matrices and 1 indicates the unit matrix. The corrections in this diagram come from expanding the spinor in $p_1$ and $p_2$.

$$u(p) = \frac{1}{\sqrt{2E_p(E_p+m_e)}}\begin{pmatrix} (E_p+m_e)\phi \\ \hat{p}\phi \end{pmatrix} \tag{4.28}$$

$$\approx \begin{pmatrix} \left(1-\frac{p^2}{8m_e^2}\right)\phi \\ \left(1-\frac{3p^2}{8m_e^2}\right)\frac{\hat{p}}{2m_e}\phi \end{pmatrix}, \tag{4.29}$$

where $\vec{\sigma}\cdot\vec{p}$ has been denoted as $\hat{p}$. This notation will be used frequently in this discussion. Using the expanded expression for the spinor, multiplying by $i$ to give the negative of the amplitude, and keeping only terms up to third order in the momenta gives

$$\begin{aligned} V_1 = \frac{e}{2m_e}\Big[&\left(\hat{A}\hat{p}_1 + \hat{p}_2\hat{A}\right) \\ &-\frac{1}{8m_e^2}\left(p_2^2\hat{A}\hat{p}_1 + 3\hat{A}\hat{p}_1p_1^2 + 3p_2^2\hat{p}_2\hat{A} + \hat{p}_2\hat{A}p_1^2\right)\Big]. \end{aligned} \tag{4.30}$$

Now, instead of using the eigenvalues $p_1$ and $p_2$ it will be more convenient to use the operator $P$. This also allows the relation $P = -i\vec{\nabla}$ to be used. Writing out the indices of the vectors explicitly and using the anti-commutator relation of the Pauli matrices gives

$$V_1 = \frac{e}{2m_e}\epsilon^{ijk}\sigma^k\left[[A^i, \nabla^j]\right.$$

$$+\frac{1}{8m_e^2}\left(\Delta A^i\nabla^j + 3A^i\nabla^j\Delta - 3\Delta\nabla^j A^i - \nabla^j A^i\Delta\right)\Big]. \tag{4.31}$$

Note that only the term with a spin interaction contributes to the $g$-factor. This allows the $\delta^{ij}$ term to be dropped from the anti-commutator of the Pauli matrices.

Next the magnetic field can be explicitly included with the relation $A^i = \frac{1}{2}\epsilon^{iln}B^l r^n$. Using the commutator of $P$ and $r$ also gives the relation $\Delta r^n = 2\nabla^n + r^n\Delta$. This can be used to commute the $r^n$s to the left. The resulting expression is

$$V_1 = \frac{e}{2m_e}\epsilon^{ijk}\sigma^k\left[\epsilon^{iln}B^l\left(\frac{\delta^{jn}}{2} - \frac{1}{4m_e^2}(\nabla^n\nabla^j + \delta^{jn}\Delta)\right)\right]. \tag{4.32}$$

The spatial average of $\nabla^n\nabla^j$ is taken and is equal to $\frac{1}{3}\delta^{nj}\Delta$ giving

$$\begin{aligned} V_1 &= \frac{e}{2m_e}\sigma^k B^k\left[1 + \frac{P^2}{3m_e^2}\right] && (4.33)\\ &= \frac{e}{2m_e}\left(1 - \frac{2}{3}(Z\alpha)^2\right)\vec{\sigma}\cdot\vec{\mathbf{B}} && (4.34)\\ &= \frac{e}{2m_e}\left(2 - \frac{4}{3}(Z\alpha)^2\right)\vec{\mathbf{S}}\cdot\vec{\mathbf{B}}, && (4.35) \end{aligned}$$

where $\vec{\mathbf{S}} = \frac{\vec{\sigma}}{2}$ has been used and $P^2$ is replaced by its expectation value. The $g$-factor is given by the bracketed term. It shows that this diagram correctly reproduces the leading order of 2 and the first correction is proportional to $(Z\alpha)^2$.

To obtain the rest of the $(Z\alpha)^2$ correction, the other two diagrams in Figure 4.1 must be computed. This time, the negative energy projectors will also be needed. These projectors come with an extra minus sign when used in the potential. The sum of the two diagrams is

$$V_2 = eP_+(p_2)\left[\frac{-P_-(p_2-q)}{-2m_e}\vec{\alpha}\cdot\vec{\mathbf{A}} + \vec{\alpha}\cdot\vec{\mathbf{A}}\frac{-P_-(p_1+q)}{-2m_e}\right]P_+(p_1)\frac{Z\alpha}{r}. \tag{4.36}$$

The two projectors can be combined with

$$\begin{aligned} P_+(p_2)P_-(p_2-q) &= \frac{1}{4}\left(1 + \frac{\vec{\alpha}\cdot\vec{p_2} + \beta m}{E_{p_2}}\right)\left(1 - \frac{\vec{\alpha}\cdot(\vec{p_2}-\vec{q}) + \beta m_e}{E_{p_2-q}}\right) && (4.37)\\ &\approx \frac{1}{4}\left(1 + \frac{\vec{\alpha}\cdot\vec{p_2} + \beta m_e}{m_e} - \frac{\vec{\alpha}\cdot\vec{p_2} - \vec{\alpha}\cdot\vec{q} + \beta m_e}{m_e}\right) && (4.38)\\ &\approx \frac{1}{4}\left(1 + \frac{\vec{\alpha}\cdot\vec{p_2} + \beta m_e}{m_e}\right)\frac{\vec{\alpha}\cdot\vec{q}}{m_e} && (4.39)\\ &= P_+(p_2)\left(\frac{\vec{\alpha}\cdot\vec{q}}{2m_e}\right). && (4.40) \end{aligned}$$

Similarly

$$P_-(p_1+q)P_+(p_1) \approx \left(-\frac{\vec{\alpha}\cdot\vec{q}}{2m_e}\right)P_+(p_1). \tag{4.41}$$

Using this in the expression for the potential gives

$$V_2 = \frac{e}{(2m_e)^2}\left(\hat{\mathbf{A}}\hat{\mathbf{q}} - \hat{\mathbf{q}}\hat{\mathbf{A}}\right)\frac{Z\alpha}{r}. \tag{4.42}$$

The rest of the analysis follows the same procedure carried out previously. The required identities are $\nabla^i \frac{1}{r} = -\frac{r^i}{r^3}$ and the average over the directions of $r$: $r^j r^n \to \frac{\delta^{jn}}{3} r^2$. Finally, the contribution to the potential from the two diagrams with a Coulomb contribution is

$$V_2 = \frac{e}{2m_e}\left(\frac{2}{3}(Z\alpha)^2\right)\vec{\mathbf{S}}\cdot\vec{\mathbf{B}} \tag{4.43}$$

Summing $V_1$ and $V_2$ then gives the full $(Z\alpha)^2$ corrections to the potential.

$$V_1 + V_2 = \frac{e}{2m_e}\left(2 - \frac{2}{3}(Z\alpha)^2\right)\vec{\mathbf{S}}\cdot\vec{\mathbf{B}}. \tag{4.44}$$

Comparing this expression with Equation 4.6 shows that the $(Z\alpha)^2$ correction to the bound electron $g$-factor is

$$\Delta g = -\frac{2}{3}(Z\alpha)^2. \tag{4.45}$$

A similar calculation can be carried out using the full bound electron wave functions in a hydrogen-like atom. This gives the full Breit correction valid at all orders in $Z\alpha$:

$$g = \frac{2}{3}\left(1 + 2\sqrt{1-(Z\alpha)^2}\right). \tag{4.46}$$

## 4.3 The $\alpha(Z\alpha)^5$ Correction

In this section, the same method used to calculate the $\mathcal{O}(\alpha(Z\alpha)^5)$ corrections to the Lamb shift are used to compute the similar order correction for the bound electron $g$-factor. With the required magnetic insertion, however, the number of diagrams at this order increases from four to nine. The diagrams only provide part of the

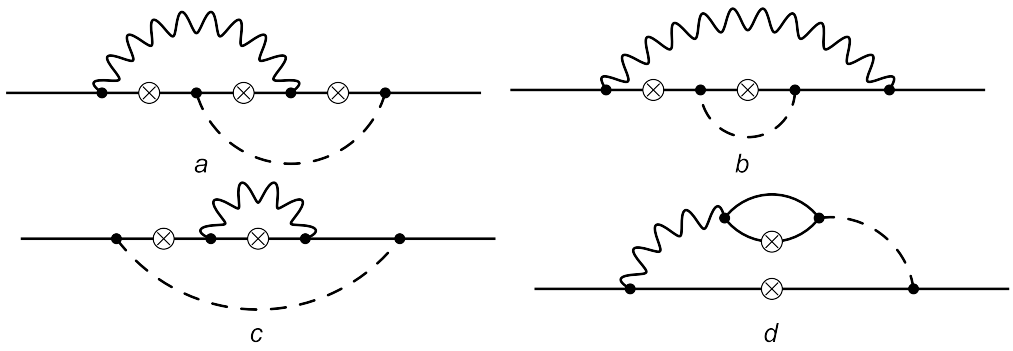


**Figure 4.2:** Contributions to the bound electron $g$-factor. The solid lines indicate the electron, while the wavy lines indicate photons and the dotted lines indicate the ph3D propagator used. The circled x's indicate unique places where the interaction with an external magnetic field is included.

contribution to the corrections to the $g$-factor as they correspond to the two diagrams with a Coulomb interaction in Figure 4.1. The analogue of the other diagram comes in the form of the Lamb shift. This contribution is made explicit in [35] where it is shown that the contribution to the $g$-factor is twice the Lamb shift contribution.

The calculation has been completed for diagram $d$ in Figure 4.2. In this calculation, the projector found in Equation 4.23 is used. The two diagrams are first computed such that a list of the integrals that will need to be computed is generated. This list is comprised of 93 unique integrals all belonging to the topology N53d from Figure 3.5, reproduced in Figure 4.3 for convenience. This list is then fed into the

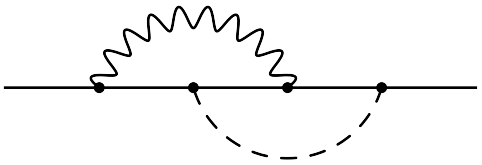

**Figure 4.3:** The single topology (N53d) required for the $\alpha(Z\alpha)^5$ contribution to the Lamb shift.

Laporta algorithm `FIRE` in order to reduce the list of integrals to a small set of master integrals. The reduction produces the same two master integrals that contribute to the Lamb shift and are shown in Figure 3.6. A more detailed description of the use of these programs is given in Appendix B.

From here, the values of the master integral can be plugged into the expression. The result of diagram $d$ is

$$d = \frac{5}{36}\alpha(Z\alpha)^5. \tag{4.47}$$

Adding the Lamb shift contribution from Equation 3.19 then gives the result

$$\delta g_{vp} = \frac{5}{9}\alpha(Z\alpha)^5, \tag{4.48}$$

where the $vp$ refers to the fact that these are the vacuum polarization corrections. This result is in agreement with the known result in [36]. The other diagrams are still being calculated and the full result will be published when available.

# Chapter 5

# Majoron

Neutrinos were first discovered in 1956 by Frederick Reines and collaborators, but to this day, relatively little is known about them. One of the major properties that has been established is that neutrinos can oscillate between the three different flavours: electron, muon and tau. The observed pattern of oscillations requires that at least two neutrino states be massive. What the masses of the neutrinos are, along with the origin of these masses, is still unknown. There are two possible types of fermion mass that can occur. All known elementary fermions, other than neutrinos, have what is called a Dirac mass. The other more intriguing type of mass is known as a Majorana mass, named after Ettore Majorana who first proposed this property. The major difference between Dirac and Majorana particles is that a Majorana particle is its own antiparticle. The possibility of neutrinos being Majorana particles is intriguing, because as will be seen, this may lead to beyond the standard model effects, including new particles and forces.

One of the processes looked at that would confirm the Majorana nature of neutrinos is neutrinoless double beta decay. In this process, a nucleus will decay twice through the conversion $n \to pe\overline{\nu}_e$. If neutrinos are Majorana, the two emitted electron neutrinos can annihilate with an end result of only two electrons being emitted. This would violate lepton number conservation.

In field theories, conservation rules like lepton number conservation are associated with a symmetry that exists in the theory. A violation of lepton number conservation would require a mechanism to be added to the theory describing how this happens. Three possibilities exist for how this symmetry breaking can occur. The first is that it is explicitly broken in the Lagrangian. The second is spontaneous local symmetry breaking, similar to the Higgs mechanism. Finally, the method of interest here, is spontaneous global symmetry breaking. At first glance, this seems to be an odd choice as Goldstone's theorem [37] says that a broken global symmetry necessarily involves the creation of a new massless Goldstone boson. Naïvely, one would expect a massless boson to be ruled out by the fact that it would give rise to a new long range force, which has never been seen. This can be reconciled by having the Goldstone boson coupling very weakly to matter so that its effects fit within experimental error. In Appendix D, a model is introduced that leads to a new massless Goldstone boson called the Majoron. Although the particular model has been ruled out by experiments, it is possible to create supersymmetric theories that lead to a Majoron with similar properties as the one introduced in the model: in particular the muon-

electron coupling is the same [38, 39]. Along with introducing a mechanism for lepton number violation, this model also includes lepton flavour violation. The fact that neutrinos oscillate means that lepton flavour is violated. The addition of the Majoron, enhances muon to electron conversions.

The aim of this chapter is to provide the theory that will underlie a new way to search for Majorons and is based on [40].

## 5.1 Limits on Majoron Emission

The standard method of placing limits on Majoron production comes from looking for free muon decays of the form $\mu \to eJ$, where the Majoron is denoted by $J$. By comparing the expected decay rate to the SM decay, it is possible to put a limit on the branching ratio of a muon decaying to an electron and Majoron. The current limit is [41]

$$B(\mu \to eJ) = \frac{\Gamma(\mu \to eJ)}{\Gamma(\mu \to e\nu_\mu \overline{\nu}_e)} < 8.4 \times 10^{-6}. \tag{5.1}$$

Using free muons presents some problems in searching for a new two body decay. The most important of these comes from comparing the SM electron energy spectrum to that of the Majoron decay. In a two body decay, the kinematics force the outgoing particles to have equal and opposite momentum and equal energies (in the rest frame of the parent). The outgoing electron in the decay $\mu \to eJ$ has an energy of $m_\mu/2$ in the center of momentum frame of the muon, where $m_\mu$ is the mass of the muon. The SM decay is a three body decay making the electron spectrum a bit more interesting, with the general shape known as a Michel spectrum. Figure 5.1 shows the electron spectrum for the SM decay at tree level where it is seen that the maximum energy of the electron is approximately $m_\mu/2$. This means that any signal from the Majoron

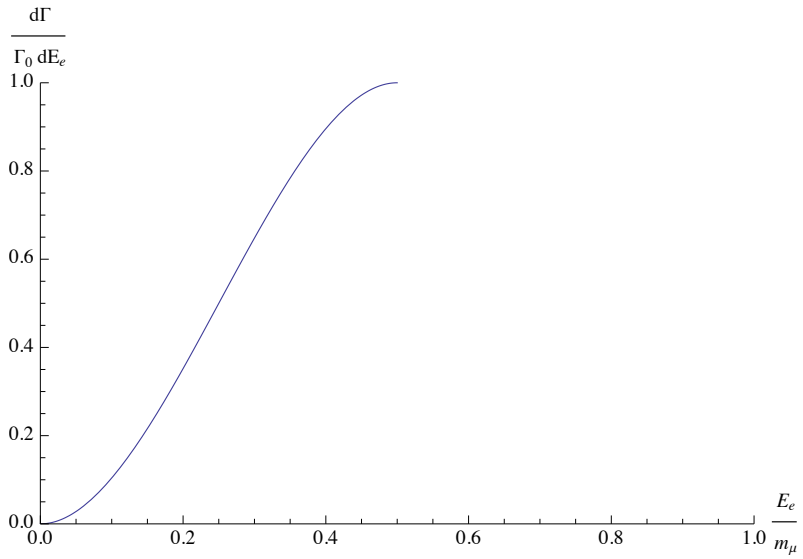


**Figure 5.1:** The Michel spectrum for a muon decaying to an electron and neutrinos. Only the tree level decay is plotted, as the known corrections do not change the properties significantly. $\Gamma_0$ is an overall factor of $\frac{G_F^2 m_\mu^5}{192\pi^3}$.

decay would appear as an excess of events at $E_e = m_\mu/2$. Experimentally, extracting a signal from this region is difficult. This begs the question, is there an easier place/way to search for a very weak signal?

The answer comes from considering not free but bound muon decays. When the muon is bound to a nucleus, the electron spectrum now extends all the way to the point where $E_e \approx m_\mu$. This occurs for both the SM decay and Majoron decay. As the energy of the electron approaches its maximum, the spectrum drops off very rapidly. A recent paper calculates the SM spectrum, paying close attention to the high energy region so that an accurate estimate of the SM background can be given in this region [42]. Using the results from that paper and assuming an experimental energy resolution of approximately 250 keV, the SM background is expected to be approximately 0.22 events at the high energy endpoint after a two year run. Furthermore, it is shown in [42] that the spectrum is suppressed as $(E_{\mu e} - E_e)^5$ near the endpoint. Here, $E_{\mu e}$ denotes the maximum energy of the electron and is given by

$$E_{\mu e} = E_\mu - E_e - E_{rec}, \tag{5.2}$$

where $E_{rec}$ is the recoil energy of the nucleus. This area provides a much cleaner place to search for new decays like Majoron decay.

Studies of the high-energy endpoint of the muon decay spectrum will be performed in the planned searches for muon-electron conversion [43, 44], $\mu(A,Z) \to e(A,Z)$, where $A$ and $Z$ characterize the nuclear properties of the target used. In the absence of a signal, those experiments are able to put limits on the branching ratio

$$B(\mu \to eJ) = \frac{\Gamma(\mu \to eJ)}{\Gamma(\mu \to e\nu_\mu \overline{\nu}_e)} \tag{5.3}$$

by first determining the ratio

$$\frac{\Gamma(\mu(A,Z) \to e(A,Z))}{\Gamma_{\text{capture}}} = R_{\mu e}. \tag{5.4}$$

Here, $\Gamma_{\text{capture}}$ is the rate of nuclear muon capture (i.e. instead of decaying, the muon is captured by the nucleus). If there is no signal, experiments are able to provide an upper bound for $R_{\mu e}$. This ratio can be related to Majoron emission in muon decay using the relation

$$N_R R_{\mu e} = \frac{\Gamma(\mu \to eJ) \times f_J}{\Gamma_{\text{capture}}}, \tag{5.5}$$

where $N_R$ is a factor used to correct for the phase space region used by the experiment and $f_J$ is the fraction of $\mu \to eJ$ events that occur in the region of interest. It is the factor $f_J$ that will be determined in this chapter. The limit on the branching ratio is given by bringing these relations together.

$$B(\mu \to eJ) = \frac{\Gamma(\mu \to eJ)}{\Gamma(\mu \to e\nu_\mu \overline{\nu}_e)} = \frac{N_R R_{\mu e}}{f_J} \frac{\Gamma_{\text{capture}}}{\Gamma(\mu \to e\nu_\mu \overline{\nu}_e)} \tag{5.6}$$

In order to compute the fraction of events $f_J$, an expression for the spectrum of the decay rate of the $\mu \to eJ$ process when the muon is bound to a nucleus is needed. The high energy limit requires treating both the muon and electron fully relativistically. To start, the muon and electron wave functions are needed as they exist in hydrogen-like ions.

## 5.2 Nuclear $\mu \to eJ$ Decay

### 5.2.1 Dirac Equation for Hydrogen

The decay spectrum of the electrons can only be properly computed by considering the solution of the hydrogen atom using the Dirac equation. This is because the the endpoint spectrum where the electron and muon are both relativistic particles will be considered. Thus, the Dirac equation needs to be solved for an electron in a central field.

The Dirac equation in terms of $\alpha_i$ and $\beta$ matrices instead of the usual $\gamma^\mu$ is

$$W\psi = (\vec{\alpha} \cdot \vec{\mathbf{p}} + \beta m + V(r))\psi \tag{5.7}$$

Here $V(r)$ is the potential and $W$ the energy of the state $\psi$. Now the fact that $\vec{\mathbf{p}} = -i\vec{\nabla}$ is used to rewrite this equation in polar form. Using the triple cross product identity provides

$$\hat{r} \times (\hat{r} \times \vec{\nabla}) = (\hat{r} \cdot \vec{\nabla})\hat{r} - (\hat{r} \cdot \hat{r})\vec{\nabla}. \tag{5.8}$$

Rearranging to solve for $\vec{\nabla}$ gives

$$\begin{aligned} \vec{\nabla} &= \hat{r}(\hat{r} \cdot \vec{\nabla}) - \hat{r} \times (\hat{r} \times \vec{\nabla}) & (5.9) \\ &= \hat{r}\partial_r - i\frac{\hat{r}}{r} \times \vec{l}, & (5.10) \end{aligned}$$

where $\vec{l} = -i\vec{r} \times \vec{\nabla}$ is the orbital angular momentum. Using this in the term $\vec{\alpha} \cdot \vec{\mathbf{p}}$ gives

$$\vec{\alpha} \cdot \vec{\mathbf{p}} = -i\alpha_r\partial_r - \frac{1}{r}\vec{\alpha} \cdot (\hat{r} \times \vec{l}). \tag{5.11}$$

Finally, the $r \times \vec{l}$ term can be re-written by using the identity

$$(\vec{\sigma} \cdot \hat{r})(\vec{\sigma} \cdot \vec{l}) = \hat{r} \cdot \vec{l} + i\vec{\sigma} \cdot (\hat{r} \times \vec{l}). \tag{5.12}$$

Using this allows the relation

$$\vec{\alpha} \cdot \vec{\mathbf{p}} = -i\alpha_r\partial_r + i\frac{\alpha_r}{r}\vec{\alpha} \cdot \vec{l}. \tag{5.13}$$

Plugging this into the Dirac equation gives

$$W\psi = \left[i\gamma_5\sigma_r\left(\partial_r + \frac{1}{r} - \frac{\beta}{r}K\right) + V(r) + \beta m\right]\psi, \tag{5.14}$$

where the operator $K = \beta(1 + \vec{\sigma} \cdot \vec{l})$ has been defined. The matrix $\sigma_r$ is given by

$$r\sigma_r = \begin{pmatrix} \vec{\sigma} \cdot \vec{r} & 0 \\ 0 & \vec{\sigma} \cdot \vec{r} \end{pmatrix}, \tag{5.15}$$

where $\vec{\sigma}$ are the usual Pauli matrices. This is the equation that must be solved for the electron and muon wave functions.

### 5.2.2 Electron Spectrum

#### Free Decay

The decay rate is normalized to its free decay, so the free decay of a muon into an electron and a Majoron is considered first. For simplicity, the left and right hand projectors are denoted $P_L = \frac{1}{2}(1-\gamma_5)$ and $P_R = \frac{1}{2}(1+\gamma_5)$.

$$\begin{aligned}
\mathcal{M} &= \overline{u}(e)\left(g_1 P_L + g_2 P_R\right) u(\mu) J && (5.16)\\
|\mathcal{M}|^2 &= \left[\overline{u}(e)\left(g_1 P_L + g_2 P_R\right) u(\mu)\right]\left[\overline{u}(\mu)\overline{\left(g_1 P_L + g_2 P_R\right)} u(e)\right] && (5.17)\\
&= \left[\overline{u}(e)\left(g_1 P_L + g_2 P_R\right) u(\mu)\right]\left[\overline{u}(\mu)\left(g_1 P_R + g_2 P_L\right) u(e)\right] && (5.18)\\
&= \frac{1}{8}\mathrm{Tr}\Big[\left(\not{p}_e + m_e\right)\left((g_1+g_2) - \gamma^5(g_1-g_2)\right)\left(\not{p}_\mu + m_\mu\right)\\
&\quad \left((g_1+g_2) + \gamma^5(g_1-g_2)\right)\Big] && (5.19)\\
&= 2m_e m_\mu g_1 g_2 + \frac{1}{2}(m_e^2 + m_\mu^2)(g_1^2 + g_2^2) && (5.20)\\
&\approx \frac{m_\mu^2}{2}(|g_1|^2 + |g_2|^2). && (5.21)
\end{aligned}$$

In the last line, the possibility of complex couplings has been included and $m_e$ is set to zero. The decay rate is

$$\Gamma_0 = \frac{|\mathcal{M}|^2}{8\pi}\frac{|p_e|}{m_\mu^2}. \quad (5.22)$$

With $|p_e| \approx m_\mu/2$ and $|\mathcal{M}|^2$ from Equation 5.21, the decay rate becomes

$$\Gamma_0 = \frac{m_\mu}{32\pi}\left(g_1^2 + g_2^2\right). \quad (5.23)$$

#### Bound Decay

For the bound decay there are a few extra criteria that need to be met. The muon needs to start in a bound state (1S for this calculation). As well, the electron has a significant interaction with the nucleus as it leaves which needs to be accounted for. The diagram representing this decay is shown in Figure 5.2

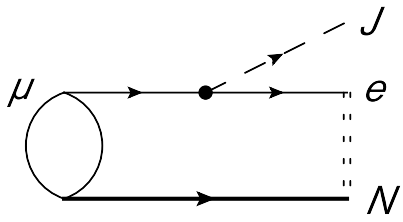


**Figure 5.2:** A diagram representing the bound decay of a muon. The circle attaching the muon line to the nucleus indicates that the muon is bound and the double line connecting the electron to the nucleus indicates that the electron wave function is solved in the presence of a Coulomb potential.

The matrix element for the free decay is as in Equation 5.16

$$\mathcal{M} = \overline{u}(p_e)\left(g_1 P_L + g_2 P_R\right) u(p_\mu) J. \tag{5.24}$$

To change from the free decay to the bound case, the wave functions of the muon and electron need to be replaced with their respective bound/interacting cases. This is done by replacing the previous expression with

$$\int d^3 r e^{-i\vec{p}_J\cdot\vec{r}}\overline{\phi}_e\left(g_1 P_L + g_2 P_R\right)\varphi_\mu. \tag{5.25}$$

The substitution can be made more intuitive with the relation

$$(2\pi)^3\delta^{(3)}(\vec{p}_\mu - \vec{p}_e - \vec{p}_J)\overline{u}(p_e)\Gamma u(p_\mu) = \int d^3 r e^{-i\vec{p}_J\cdot\vec{r}}\langle e|\overline{\psi}_e\Gamma\psi_\mu|\mu\rangle. \tag{5.26}$$

The matrix elements

$$\langle e|\overline{\psi}_e|0\rangle \text{ and } \langle 0|\psi_\mu|\mu\rangle \tag{5.27}$$

are then replaced with their interacting counterparts

$$\sqrt{2E_e}\overline{\phi}_e \text{ and } \sqrt{2E_\mu}\varphi_\mu. \tag{5.28}$$

The matrix element is now

$$\mathcal{M} = 2\sqrt{E_e E_\mu}\int d^3 r e^{-i\vec{p}_J\cdot\vec{r}}\overline{\phi}_e\left(g_1 P_L + g_2 P_R\right)\varphi_\mu J. \tag{5.29}$$

Squaring this and plugging it into the equation for the decay rate gives the starting point of the calculation.

$$\begin{aligned}\Gamma &= \int \frac{d^3 p_J}{(2\pi)^3 2E_J}\frac{d^3 p_e}{(2\pi)^3}(2\pi)\delta(E_\mu - E_e - E_J)\left[\int d^3 r e^{-i\vec{p}_J\cdot\vec{r}}\overline{\phi}_e(g_1 P_L + g_2 P_R)\varphi_\mu\right] \\ &\times \left[\int d^3 r' e^{-i\vec{p}_J\cdot\vec{r}'}\overline{\varphi}_\mu(g_1^* P_R + g_2^* P_L)\phi_e\right]\end{aligned} \tag{5.30}$$

From here, the best place to start is the $p_J$ integral to get rid of the delta function. Using

$$d^3\vec{p}_J = dE_J E_J|\vec{p}_J|d\Omega_J \tag{5.31}$$

gives

$$\begin{aligned}\Gamma &= \frac{1}{2(2\pi)^5}\int d\Omega_J\int d^3 p_e|\vec{p}_J|\left[\int d^3 r e^{-i\vec{p}_J\cdot\vec{r}}\overline{\phi}_e(g_1 P_L + g_2 P_R)\varphi_\mu\right] \\ &\times \left[\int d^3 r' e^{-i\vec{p}_J\cdot\vec{r}'}\overline{\varphi}_\mu(g_1 P_R + g_2 P_L)\phi_e\right].\end{aligned} \tag{5.32}$$

To simplify the expression, a single $r$ integral is considered. The best way to evaluate this is to write the wave functions in terms of the upper and lower components.

$$\varphi_\mu(\vec{r}) = \sum_s a_s\begin{pmatrix} G(r)\chi^s_{-1} \\ iF(r)\chi^s_1\end{pmatrix} \tag{5.33}$$

and

$$\phi_e(\vec{r}) = \sum_{t\kappa\mu} a_{\kappa\mu t} \begin{pmatrix} g_\kappa(r)\chi^\mu_\kappa \\ if_\kappa(r)\chi^\mu_{-\kappa} \end{pmatrix}, \tag{5.34}$$

where the definition

$$\chi^\mu_\kappa = \sum_m C(l\frac{1}{2}j;\mu - m m\mu) Y_l^{\mu-m}\chi^m, \tag{5.35}$$

has been used, and the electron wave function has been expanded in terms of partial waves. The Rayleigh expansion is also used for the exponential terms,

$$e^{i\vec{q}\cdot\vec{r}} = 4\pi \sum_{JM} i^J j_J(qr) Y_J^{M*}(\hat{q}) Y_J^M(\hat{r}), \tag{5.36}$$

where $j_J$ is a Bessel function. This gives

$$\begin{aligned} I_r &= 4\pi \int d^3r \sum_{JM} (-i)^J j_J(pr) Y_J^{M*}(\hat{p}) \sum_{s\kappa t\mu} a^*_{\kappa\mu t} a_s (g_\kappa \chi^{\mu\dagger}_\kappa \ - i f_\kappa \chi^{\mu\dagger}_{-\kappa}) \\ &\times \ \gamma_0 \left(g_1 P_L + g_2 P_R\right) \begin{pmatrix} G\chi^s_{-1} \\ iF\chi^s_1 \end{pmatrix} Y_J^M(\hat{r}). \end{aligned} \tag{5.37}$$

When the wave functions and gamma matrices are then multiplied out

$$\begin{aligned} &\frac{1}{2}\Big[(g_1+g_2)\left(g^*_\kappa \chi^{\mu\dagger}_\kappa G\chi^s_{-1} - f^*_\kappa \chi^{\mu\dagger}_{-\kappa} F\chi^s_1\right)\delta_{Jl_\kappa} \\ &-i(g_1-g_2)\left(g^*_\kappa \chi^{\mu\dagger}_\kappa F\chi^s_1 + f^*_\kappa \chi^{\mu\dagger}_{-\kappa} G\chi^s_{-1}\right)\delta_{Jl_{-\kappa}}\Big]. \end{aligned} \tag{5.38}$$

It is important to note that the other term is the hermitian conjugate, and as seen in the free decay, this switches the left and right projectors. For later use, the resulting term is

$$\begin{aligned} &\frac{1}{2}\Big[(g_1+g_2)\left(G^*\chi^{s\dagger}_{-1} g_\kappa \chi^\mu_\kappa - F^*\chi^{s\dagger}_1 f_\kappa \chi^\mu_{-\kappa}\right)\delta_{Jl_\kappa} \\ &+i(g_1-g_2)\left(G^*\chi^{s\dagger}_{-1} f_\kappa \chi^\mu_{-\kappa} + F^*\chi^{s\dagger}_1 g_\kappa \chi^\mu_\kappa\right)\delta_{Jl_{-\kappa}}\Big]. \end{aligned} \tag{5.39}$$

This has the right structure to produce the $g_1^2 + g_2^2$ term from the free decay.

The first integral that can be evaluated is the angular integral $d\Omega_r$. This is accomplished by using

$$\begin{aligned} \int d\Omega_r \chi^{\mu\dagger}_\kappa \chi^s_{-1} Y_J^M(\hat{r}) &= \int d\Omega_r \left(-\frac{1}{r}\vec{\sigma}\cdot\vec{r}\right)\chi^{\mu\dagger}_{-\kappa}\left(-\frac{1}{r}\vec{\sigma}\cdot\vec{r}\right)\chi^s_1 Y_J^M(\hat{r}) \\ &= \int d\Omega_r \chi^{\mu\dagger}_{-\kappa}\chi^s_1 Y_J^M(\hat{r}). \end{aligned} \tag{5.40}$$

Substituting in the expressions for $\chi$ gives

$$\begin{aligned} \int d\Omega_r \chi^{\mu\dagger}_\kappa \chi^s_{-1} Y_J^M(\hat{r}) &= \int \frac{d\Omega_r}{\sqrt{4\pi}} \sum_m C(\ell\frac{1}{2}j;\mu - m\ m\ \mu) Y_\ell^{\mu-m*}(\hat{r}) \chi^{m\dagger}\chi^s Y_J^M(\hat{r}) \\ &= \frac{1}{\sqrt{4\pi}} C(J\frac{1}{2}j;Ms\mu). \end{aligned} \tag{5.41}$$

Placing this into the expression in the $r$ integral produces

$$\begin{aligned} I_r &= \frac{4\pi}{2\sqrt{4\pi}} \int dr r^2 \sum_{JM} (-i)^J j_J(pr) C(J\frac{1}{2}j; Ms\mu) Y_J^{M*}(\hat{p}) \sum_{s\kappa t\mu} a^*_{\kappa t\mu} a_s \\ &\times \left[ (g_1+g_2)(g_\kappa G - f_\kappa F) - i(g_1-g_2)(g_\kappa F + f_\kappa G) \right]. \qquad (5.42) \\ &= \sqrt{4\pi} \sum_{s\kappa t\mu} a^*_{\kappa\mu t} a_s \sum_{Kr} (-1)^{j_\kappa + \frac{1}{2} + K} C(\frac{1}{2} K j_\kappa; sr\mu) \frac{1}{2} \\ &\quad \left[ (-1)(-i)^K Y_K^{r*}(\hat{p}) S_{K\kappa} \right], \qquad (5.43) \end{aligned}$$

where

$$\begin{aligned} S_{K\kappa} &= \int dr r^2 j_K(pr) \left\{ (g_1+g_2) \left( \frac{1+(-1)^{l_\kappa + K}}{2} \right) (g^*_\kappa G - f^*_\kappa F) \delta_{K l_\kappa} \right. \\ &- \left. i(g_1-g_2) \left( \frac{1+(-1)^{l_\kappa + K + 1}}{2} \right) (g^*_\kappa F + f^*_\kappa G) \delta_{K l_{-\kappa}} \right\}. \qquad (5.44) \end{aligned}$$

The decay rate is given by

$$\Gamma = \frac{1}{2(2\pi)^5} \int d\Omega_J \int d^3 p_e |\vec{p}_J| |I_r|^2. \qquad (5.45)$$

Looking at the spherical harmonics that appear the $\Omega_J$ integral can then be immediately calculated as

$$\int d\Omega_J Y_K^{r*}(\hat{p}) Y_{K'}^{r'}(\hat{p}) = \delta_{KK'} \delta_{rr'}. \qquad (5.46)$$

The partial wave coefficients for the electron are given by

$$a_{\kappa\mu t} = 4\pi i^{l_\kappa} C(l_\kappa \frac{1}{2} j_\kappa; \mu - t\ t\ \mu) Y_{l_\kappa}^{\mu - t*}(\hat{p}_e) e^{-i\delta_\kappa}, \qquad (5.47)$$

where the extra exponential term arises as a result of the phase shift from the interaction with the Coulomb potential. The other coefficient $a_s$ can be written in the unpolarized case as

$$a_s a^*_{s'} = \frac{1}{2} \delta_{ss'}. \qquad (5.48)$$

The angular part of the $p_e$ integral can be carried out using these terms and gives

$$\int d\Omega_{p_e} Y_{l_\kappa}^{\mu - t*} Y_{l_{\kappa'}}^{\mu' - t'} = \delta_{l_\kappa l_{\kappa'}} \delta_{\mu - t, \mu' - t'}. \qquad (5.49)$$

The four remaining Clebsch-Gordon coefficients can now be simplified with

$$\sum_{rs} C(\frac{1}{2} K j_\kappa; sr\mu) C(\frac{1}{2} K j_{\kappa'}; sr\mu') = \delta_{j_\kappa j_{\kappa'}} \delta_{\mu\mu'} \delta(K - \frac{1}{2} - j_\kappa), \qquad (5.50)$$

and

$$\sum_{tt'\mu n} C(l_\kappa \frac{1}{2} j_\kappa; nt\mu) C(l_\kappa \frac{1}{2} j_\kappa; nt'\mu) = 2j_\kappa + 1, \qquad (5.51)$$

where the delta functions have been used as needed. Finally, this just leaves the sums over $K$ and $\kappa$ and an integral over $|p_e| = E_e$ to give the electron spectrum,

$$\frac{d\Gamma}{dE_e} = \frac{4}{\pi m_\mu} \left( \frac{m_\mu}{32\pi} \right) (E_\mu - E_e) E_e^2 \sum_{K\kappa} (2j_\kappa + 1) |S_{K\kappa}|^2. \qquad (5.52)$$

The final requirement is $|S_{K\kappa}|^2$. In each term of this sum, there are factors of

$$\left(\frac{1+(-1)^{l_\kappa+K}}{2}\right)\delta_{Kl_\kappa} \quad \text{and} \quad \left(\frac{1+(-1)^{l_\kappa+K+1}}{2}\right)\delta_{Kl_{-\kappa}}. \tag{5.53}$$

With the Kroneker delta, the factor on the left is simply one. The other factor is not as clear. Making the substitution $\kappa \to -\kappa'$ and using the relation between $l_\kappa$ and $j$ gives

$$\begin{aligned} l_\kappa &= j + \frac{1}{2}\frac{\kappa}{|\kappa|} && (5.54)\\ l_\kappa + l_{-\kappa} &= 2j && (5.55)\\ &= 2|\kappa| - 1. && (5.56) \end{aligned}$$

In the Equation 5.56, $j = |\kappa| - 1/2$ has been used. The second term then becomes

$$\left(\frac{1+(-1)^{2|\kappa|-1+1}}{2}\right) = 1. \tag{5.57}$$

This greatly simplifies our expression for $|S_{K\kappa}|^2$;

$$\begin{aligned} |S_{K\kappa}|^2 &= \int dr dr' j_K(pr) j_K(pr') && (5.58)\\ &\times \left[(g_1+g_2)(g^*_\kappa G - f^*_\kappa F)\delta_{Kl_\kappa} - i(g_1-g_2)(g^*_\kappa F + f^*_\kappa G)\delta_{Kl_{-\kappa}}\right]\\ &\times \left[(g_1+g_2)(g_\kappa G - f_\kappa F)\delta_{Kl_\kappa} + i(g_1-g_2)(g_{-\kappa} F + f_{-\kappa} G)\delta_{Kl_{-\kappa}}\right]. \end{aligned}$$

It is preferable to write everything in terms of $-\kappa$ instead of $\pm\kappa$. To do this, the relations $g_{-\kappa} = if_\kappa$ and $f_{-\kappa} = -ig_\kappa$ can be used. These can be worked out from the massless Dirac equation for the electron (note that the relations no longer hold if we consider a massive electron).

Before starting, there are a few relations between $\kappa$ and $K$ that are worth reviewing. The first of these is $\kappa = \pm K, \pm(K+1)$. As well, $\kappa \neq 0$ and from the relations in Equations 5.54-5.56 $l_\kappa = j + \frac{1}{2}\frac{\kappa}{|\kappa|} = |\kappa| + \frac{1}{2}(\frac{\kappa}{|\kappa|} - 1)$. Combining these relations with the delta functions from Equation 5.58 gives

$$\delta_{Kl_\kappa} \to \kappa = K, -(K+1), \tag{5.59}$$

and

$$\delta_{Kl_{-\kappa}} \to \kappa = -K, (K+1). \tag{5.60}$$

One can now look at a single $K$ term in the sum where $\kappa$ can take on four values. Summing these gives

$$\begin{aligned} |S_{K\kappa}|^2 &= \int dr dr' j_K(pr) j_K(pr')\\ &\times \Big\{ g_p^2 (g^*_{-(K+1)} G - f^*_{-(K+1)} F)(g_{-(K+1)} G^* - f_{-(K+1)} F^*)\\ &+ g_m^2 (g^*_{-K} F + f^*_{-K} G)(g_{-K} F^* + f_{-K} G^*)\\ &+ g_p^2 (g^*_K G - f^*_K F)(g_K G^* - f_K F^*)\\ &+ g_m^2 (g^*_{(K+1)} F + f^*_{(K+1)} G)(g_{(K+1)} F^* + f_{(K+1)} G^*) \Big\}. \end{aligned} \tag{5.61}$$

Here, $g_p = (g_1 + g_2)$ and $g_m = (g_1 - g_2)$ have been used for simplicity. The positive $\kappa$ terms can be re-written as negative terms via the above relations.

$$\begin{aligned}
\sum_{\kappa} |S_{K\kappa}|^2 &= \int dr dr' j_K(pr) j_K(pr') \\
&\times \Big[ g_p^2 (g^*_{-(K+1)} G - f^*_{-(K+1)} F)^2 + g_m^2 (g^*_{-(K+1)} G - f^*_{-(K+1)} F)^2 \\
&+ g_p^2 (f^*_{-K} G + g^*_{-K} F)^2 + g_m^2 (f^*_{-K} G + g^*_{-K} F)^2 \Big] \qquad (5.62) \\
&= 2(g_1^2 + g_2^2) \int dr dr' j(pr) j_K(pr') \\
&\times \Big[ (g^*_{-(K+1)} G - f^*_{-(K+1)} F)^2 + (1 - \delta_{K0}) (g^*_{-K} F + f^*_{-K} G)^2 \Big] \qquad (5.63)
\end{aligned}$$

The full spectrum of the electron is finally given by

$$\begin{aligned}
N(E_e) &= \frac{1}{\Gamma_0} \frac{d\Gamma}{dE_e} = \frac{8}{\pi m_\mu} E_e^2 (E_\mu - E_e) \sum_K \int dr dr' r^2 r'^2 j_K(pr) j_K(pr') \qquad (5.64) \\
&\times \Big[ (2K+2) (g^*_{-(K+1)} G - f^*_{-(K+1)} F)^2 + 2K (1 - \delta_{K0}) (g^*_{-K} F + f^*_{-K} G)^2 \Big],
\end{aligned}$$

where the sum over $K$ goes from 0 to $\infty$. From here, functions for $f, g, F$ and $G$ are introduced. If the finite size of the nucleus is ignored, these functions can be worked out analytically [45]. For the results to be experimentally viable though, larger nuclei will need to be considered where the size of the nucleus cannot be ignored. To include these effects, the wave functions must be solved for numerically, meaning that from this point onwards the spectrum needs to computed numerically. Before the results of this calculation are presented, the expansion of the spectrum in terms of energy and $\alpha$ will be explored.

## 5.3 Energy Expansion

Ultimately the high energy region of the electron spectrum will be of interest and the results will be completely numerical. The required information will be extracted from this, but it would also be nice to be able to pick out some properties of the high energy endpoint of the spectrum analytically. One way of doing this is to carry out an expansion near the endpoint.

In the previous section, the spectrum of the electron in terms of the muon and electron wave functions is solved for. If the nucleus is assumed to be infinitely heavy and small, the wave functions, $g, f, G$ and $F$ can be solved for analytically. Using the bound state solutions for the muon and the continuum state solutions for the electron, it is possible to Taylor expand the spectrum near the maximum energy point.

The muon wave functions in the 1S state are given by

$$\begin{aligned}
G &= \frac{(2\zeta m_\mu)^{\gamma+1/2}}{[2m_\mu \Gamma(2\gamma+1)]^{1/2}} (m_\mu + \gamma)^{1/2} r^{\gamma - 1/2} e^{-\zeta m_\mu r}, \qquad (5.65) \\
F &= -\frac{(2\zeta m_\mu)^{\gamma+1/2}}{[2m_\mu \Gamma(2\gamma+1)]^{1/2}} (m_\mu - \gamma)^{1/2} r^{\gamma - 1/2} e^{-\zeta m_\mu r}, \qquad (5.66)
\end{aligned}$$

where $\zeta = Z\alpha$, and $\gamma = \sqrt{1-\zeta^2}$. The electron wave functions are given by

$$\begin{aligned} g_\kappa &= \frac{(2E_e r)^{\gamma_\kappa} e^{\frac{\pi\zeta}{2}} |\Gamma(\gamma_\kappa + i\zeta)|}{2\pi^{1/2}\Gamma(2\gamma_\kappa+1)} \left[ e^{-iE_e r} \sqrt{-\frac{\kappa}{\gamma_\kappa + i\zeta}} (\gamma_\kappa + i\zeta) \right. \\ &\times \left. {}_1F_1(\gamma_\kappa + 1 + i\zeta, 2\gamma_\kappa + 1, 2iE_e r) + c.c. \right], \qquad (5.67) \\ f_\kappa &= \frac{i(2E_e r)^{\gamma_\kappa} e^{\frac{\pi\zeta}{2}} |\Gamma(\gamma_\kappa + i\zeta)|}{2\pi^{1/2}\Gamma(2\gamma_\kappa+1)} \left[ e^{-iE_e r} \sqrt{-\frac{\kappa}{\gamma_\kappa + i\zeta}} (\gamma_\kappa + i\zeta) \right. \\ &\times \left. {}_1F_1(\gamma + 1 + i\zeta, 2\gamma_\kappa + 1, 2iE_e r) - c.c. \right], \qquad (5.68) \end{aligned}$$

where, $\gamma_\kappa = \sqrt{\kappa^2 - \zeta^2}$, and $E_e$ is the electron energy. The muon wave functions are normalized such that $\int (G^2 + F^2) r^2 dr = 1$ while the electron wave functions introduce a factor of $\frac{1}{4E_e^2}$ to the coefficient of our spectrum.

For now, only the leading order of the expansion is required. If the expansion in terms of $E_e$ about the point $E_\mu$, the maximum energy, is considered the electron wave functions have a leading order of $\delta = \frac{(E_\mu - E_e)}{E_\mu}$ and the muon wave functions are simply constants.

Next, consider the Bessel functions that appear. The series form for these can be used to find

$$j_K(m_\mu \delta r) = 2^K (E_\mu \delta r)^K \sum_{n=0}^{\infty} \frac{(-1)^n (n+K)!}{n!(2n+2K+1)!} (E_\mu \delta r)^{2n}. \qquad (5.69)$$

The only term contributing to the leading order is the $K = 0, i = 0$ term for which $j_0(E_\mu \delta r) = 1$. Putting this all into the expression for the decay spectrum gives

$$\frac{1}{\Gamma_0}\frac{d\Gamma}{dE_e} = \frac{2}{\pi m_\mu} E_\mu \delta \left( \int dr (g_{-1}^* G - f_{-1}^* F) r^2 \right)^2, \qquad (5.70)$$

where the factor of $\frac{1}{4E_e^2}$ from the electron wave function has been taken into account. This integral can be evaluated analytically and gives zero.

Thus, to obtain the leading order for the spectrum, the second order terms in all of the above expressions are required. Expanding the electron wave functions in $\delta$ increases both by one order. As well, if the next term in $j_0(m_\mu \delta r)$ is included, it is seen that it goes like $\delta^2$. The next important term in the leading order is when $K = 1$. In this case, the spherical Bessel function gives

$$j_1(E_\mu \delta r) \approx \frac{E_\mu \delta r}{3}. \qquad (5.71)$$

Writing just the terms that involve $\delta$ gives

$$\begin{aligned} \frac{d\Gamma}{dE_e} &\propto \delta \left\{ \left[ (g_{-1}^{(0)} + g_{-1}^{(1)}\delta) G - (f_{-1}^{(0)} + f_{-1}^{(1)}\delta) F \right]^2 \right. \\ &+ \left. \delta^2 \left[ (g_{-2}^{(0)} G - f_{-2}^{(0)} F)^2 + (g_{-1}^{(0)} F + f_{-1}^{(0)} G)^2 \right] \right\} \qquad (5.72) \\ &= \delta \left\{ \delta^2 \left[ g_{-1}^{(1)} G - f_{-1}^{(1)} F \right]^2 \right. \\ &+ \left. \delta^2 \left[ (g_{-2}^{(0)} G - f_{-2}^{(0)} F)^2 + (g_{-1}^{(0)} F + f_{-1}^{(0)} G)^2 \right] \right\}, \qquad (5.73) \end{aligned}$$

where the $n$th coefficients of the $\delta$ series in the wave functions are denoted by $g_\kappa^{(n)}, f_\kappa^{(n)}$. The leading order in the expansion is not linear or even quadratic; it goes like $\delta^3$. Fortunately these integrals can also be calculated analytically. The result is long and complicated (to the point that Mathematica would not recognize the first term calculated as zero analytically), so the calculation is done analytically and then numbers are introduced into the result to obtain the expansion. Expanding to $\mathcal{O}(\delta^6)$ gives

$$\frac{1}{\Gamma_0}\frac{d\Gamma}{dE_e} \approx \frac{(Z\alpha)^5}{m_\mu}\delta^3\left(41.892 + 374.536\delta + 2180.640\delta^2 + 10198.429\delta^3 + \mathcal{O}(\delta^4)\right). \tag{5.74}$$

The full expression for the leading term is

$$\begin{aligned}\frac{1}{\Gamma_0}\frac{d\Gamma}{dE_e} &\approx \frac{2}{\pi m_\mu}\delta^3\left\{2\left[g_{-1}^{(1)}G - f_{-1}^{(1)}F\right]^2\right. \\ &+ \left. 2\left[g_{-1}^{(0)}F + f_{-1}^{(0)}G\right]^2 + 4\left[g_{-2}^{(0)}G - f_{-2}^{(0)}F\right]^2\right\}. \end{aligned}\tag{5.75}$$

Here, $\delta$ goes from zero to one. Figure 5.3 shows that the expansion is converging on the proper values.

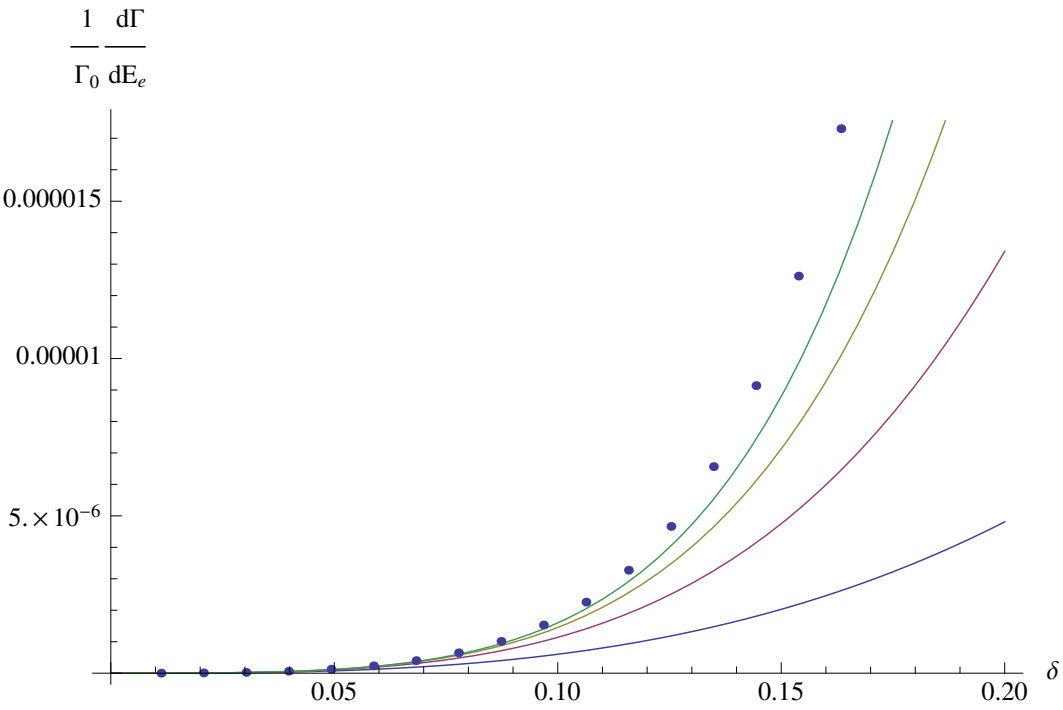


**Figure 5.3:** The Taylor expansion of the electron spectrum. The contributions from $\mathcal{O}(\delta^3)$ to $\mathcal{O}(\delta^6)$ are shown in order to illustrate how the series is converging on the full result (dots). Looking at the right side of the curves, the bottom one is $\mathcal{O}(\delta^3)$. Moving up, the curves go in order up to the top one which is $\mathcal{O}(\delta^6)$. The units of the spectrum are in fm.

### 5.3.1 Expansion in $Z\alpha$

As the expressions for the Taylor expansion are so complicated that numbers must be input, it may be beneficial to expand the expression in Equation 5.75 in terms of $Z\alpha$. A full expansion in $Z\alpha$ would include an infinite sum because $K$ is unbounded, so only the leading term in the energy expansion is considered. This should, at the very least, simplify things so that the expression can be written down analytically. As well, this can be compared with the leading order result obtained from perturbation theory and provide a check of the full results.

Again, the wave functions from [45] are used. To carry out the expansion in Mathematica, each term in Equation 5.75 must be considered separately (i.e. $g_{-1}^{(1)}G$, $f_{-1}^{(1)}F$, etc.). The results can then be used in Equation 5.75 to obtain the expansion in $Z\alpha$. Everything can be expanded and a very simple expression for the leading order term is obtained.

$$\frac{1}{\Gamma_0}\frac{d\Gamma}{dE_e} = \frac{(Z\alpha)^5}{m_\mu \pi}\frac{512}{3}\delta^3 \approx 54.3\frac{(Z\alpha)^5}{m_\mu}\delta^3 \tag{5.76}$$

This agrees with the perturbative version of this calculation. Comparing this result with the full result in Equation 5.74, shows that the coefficient is accurate to only about 25%. This justifies a full relativistic treatment as opposed to carrying out a perturbative calculation.

## 5.4 Results

For the full electron spectrum, the electron and muon wave functions must be solved numerically, taking into account the finite size and mass of the nucleus. A Fermi distribution $\rho(r)$ is used as a model for the nucleus and characterized by two parameters, $a$ and $r_0$.

$$\rho(r) = \frac{\rho_0}{1 + e^{\frac{r-r_0}{a}}}, \tag{5.77}$$

where $\rho_0$ is a normalization constant chosen such that the integral over all space of $r^2\rho(r)$ is $-Z\alpha$. In order to account for the finite mass of the nucleus,the nuclear-recoil energy is approximated with [46],

$$E_{\text{rec}} \approx \frac{E_e^2}{2m_N}, \tag{5.78}$$

where $m_N$ is the mass of the nucleus. For this calculation to be useful to experiments, the spectrum for various nuclei is needed. The results for gold (used by SINDRUM II [47]), aluminum, and titanium (considered for use by both Mu2e [43] and COMET [44]) are included. Table 5.1 shows the parameters used for each of the nuclei considered as found in [48].

The numerical values for the full range of energies for the electron spectrum have been calculated. Figure 5.4 shows the results for Al, Ti, and Au. In addition to these, the analysis has been refined at the endpoints for Al, Au and Ti so accurate results for the corresponding fractions $f_J$ can be obtained. The endpoints of Al and Au are plotted in Figure 5.5 against the standard muon decay in orbit results to highlight the difference in the shape. Note that the Majoron emission plots have been scaled to facilitate the shape comparison.

| Nucleus | $r_0$ (fm) | $a$ (fm) | $m_N$ (MeV) | $E_\mu$ (MeV) | $E_{\mu e}$ (MeV) |
|---|---|---|---|---|---|
| Al($Z = 13$) | 2.84 | 0.569 | 25133 | 105.194 | 104.973 |
| Ti($Z = 22$) | 3.84 | 0.588 | 44588 | 104.394 | 104.272 |
| Au($Z = 79$) | 6.38 | 0.535 | 183473 | 95.533 | 95.508 |

**Table 5.1:** Values for the parameters in the Fermi distribution in Equation 5.77, nuclear masses, muon energy $E_\mu$, and endpoint energy $E_{\mu e}$ for the elements used.

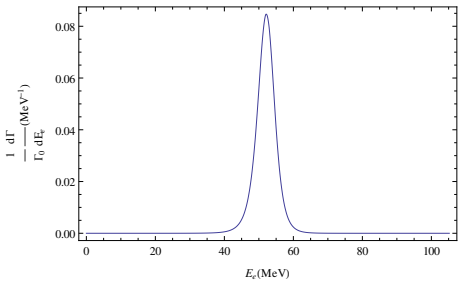


(a) Aluminum

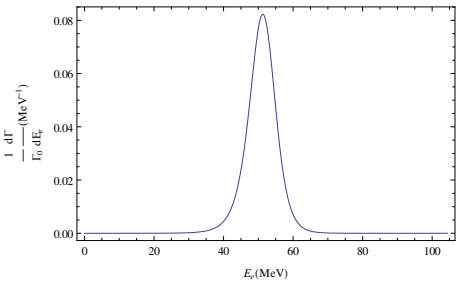


(b) Titanium

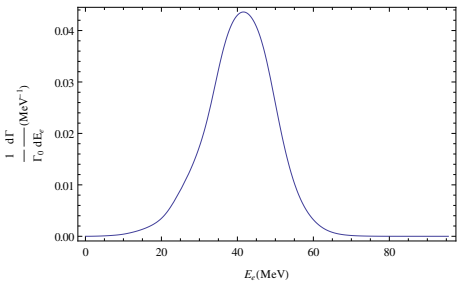


(c) Gold

**Figure 5.4:** The full electron spectrum for aluminum, titanium, and gold.

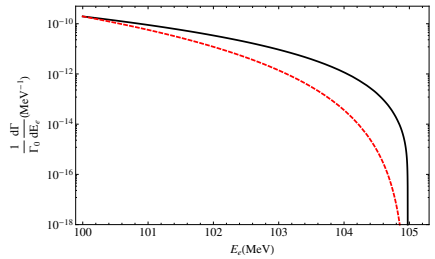


(a) Aluminum

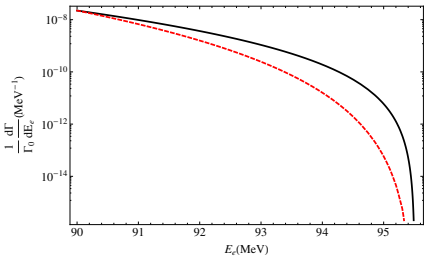


(b) Gold

**Figure 5.5:** A comparison of the endpoints for aluminum and gold (solid lines) with the SM spectrum (dashed lines). The Majoron spectra have been scaled to match the SM spectra at 100 MeV (Al) and 90 MeV (Au).

## SINDRUM II

The SINDRUM II Collaboration used gold nuclei to measure the electron spectrum of muon decay in orbit processes in the region from 90MeV to $E_{\mu e}$. They were able to put a limit on $R_{\mu e}$ of

$$R_{\mu e}^{\text{SINDRUM II}} < 7 \times 10^{-13} (90\% \text{ C.L.}). \tag{5.79}$$

The electron spectrum when a Majoron is produced has been calculated as well and it is found that the numerical results near the endpoint are fit very accurately with the function

$$\left.\frac{1}{\Gamma_0}\frac{d\Gamma}{dE_e}\right|_{Au, E_e > 90\text{MeV}} = \frac{1}{m_\mu}(5.292 \times 10^{-3}\delta^3 + 9.629 \times 10^{-2}\delta^4 + 1.125\delta^5 + 22.94\delta^6), \tag{5.80}$$

where

$$\delta = \frac{E_\mu - E_e - \frac{E_e^2}{2m_N}}{m_\mu}. \tag{5.81}$$

Using Equation 5.80 the fraction, $f_J$, of Majoron events in the region of interest is

$$f_{J,Au} = \int_{90\text{MeV}}^{E_{\mu e}} \frac{1}{\Gamma_0}\frac{d\Gamma}{dE_e} dE_e = 2.4 \times 10^{-8}. \tag{5.82}$$

As a result, only $N_R$ is required in order to place a limit on the branching ratio $B(\mu \to eJ)$.

$N_R$ corresponds to the number of $\mu \to e$ events seen in the detection region. In the SINDRUM II experiment, six events were seen. This matches the SM decay in orbit predictions so it is likely that none of these events correspond to a signal. Typically, one would then perform a subtraction of the background in order to extract any signal. In this case there are so few events that background subtraction is not a desirable method. Instead, to put an upper limit on the Majoron emission branching ratio, it is assumed that the number of Majoron events is no larger than the total number of events seen. This is only a single result, and it is not likely that another run of the experiment would provide exactly six signal events again. To account for this, the number of events is assumed to follow a Gaussian distribution with a mean and variance of six. Projecting up to the 90% C.L. means that 90% of the time, nine events or less are seen. Since there is actually no signal, a Poisson distribution can be used to find the mean upper limit of events that could possibly be seen by running the experiment multiple times. In this case, at 90% C.L. the mean upper limit is found to be $a = 2.3$. Now $a$ is the number of sample events multiplied by the probability of an event being a signal, $1/N_R$

$$a = \frac{9}{N_R}. \tag{5.83}$$

Solving for $N_R$, gives $N_R = \frac{9}{2.3}$.

Finally, with the capture rate $\Gamma_{\text{capture}} = \frac{1}{88\text{ns}}$ and the SM decay rate $\Gamma(\mu \to e\nu_\mu\overline{\nu}_e) = \frac{1}{2.197\mu\text{s}}$ an upper limit on the branching ratio for Majoron emission can be obtained. From Equation 5.6

$$B(\mu \to eJ) < \frac{\frac{9}{2.3}7 \times 10^{-13}}{2.4 \times 10^{-8}} \frac{2.197\mu\text{s}}{88\text{ns}} \approx 3 \times 10^{-3} \text{ @ } 90\% \text{ C.L.} \tag{5.84}$$

Unfortunately this is much larger than the current limit, so the results are not able to improve upon the limits using current data. A more robust limit can be obtained with the use of Bayesian limit calculations (see for example [49]) but is not expected to improve the limit by the two orders of magnitude required to match the current limits.

### Mu2e and COMET

Although current data does not provide a more stringent upper limit on the branching ratio $B(\mu \to eJ)$, future $\mu \to e$ experiments may be able to do so using the results from our calculation. The experiments Mu2e at Fermilab [43] and COMET at J-PARC [44] aim to improve sensitivity to the $10^{-16}$ level. They also intend on using an aluminum target.

The aluminum target both helps and hinders the evaluation of the branching ratio. On one side, the ratio between the muon capture width and free muon width in Al is about 1.5, as compared to 25 for Au. The fraction of events $f_J$, however, is much smaller due to a much lower value of $Z$. For Al, it is found that the endpoint of the spectrum (above 100 MeV) is closely approximated by

$$\begin{aligned}\left.\frac{1}{\Gamma_0}\frac{d\Gamma}{dE_e}\right|_{Al,E_e>100\,\mathrm{MeV}} &= \frac{1}{m_\mu}(3.289\times10^{-10}\delta + 3.137\times10^{-7}\delta^2 \\ &\quad +1.027\times10^{-4}\delta^3 + 1.438\times10^{-3}\delta^4 + 2.418\times10^{-3}\delta^5 \\ &\quad +1.215\times10^{-1}\delta^6). \end{aligned} \tag{5.85}$$

In the region $E_e > 100\,\mathrm{MeV}$, $f_J = 2.2\times10^{-10}$. Using $N_R = 27$, this time based on background subtraction of the decay in orbit background, gives an upper limit

$$B(\mu \to eJ) < 1.9\times10^{-5}. \tag{5.86}$$

This is comparable to the current limit. Note that it is possible to obtain a more accurate estimate of the bounds these experiments will be able produce by including the effects of the energy resolution in the experiment [40]. The limit does not change significantly so the effect is not considered here.

Both experiments also consider Ti as a possible target. For completeness, the calculation has been carried out for this nucleus as well. The endpoint of the spectrum is approximated by

$$\begin{aligned}\left.\frac{1}{\Gamma_0}\frac{d\Gamma}{dE_e}\right|_{Ti,E_e>99\,\mathrm{MeV}} &= \frac{1}{m_\mu}(5.404\times10^{-10}\delta + 9.301\times10^{-7}\delta^2 \\ &\quad +5.552\times10^{-4}\delta^3 + 8.113\times10^{-3}\delta^4 + 5.470\times10^{-2}\delta^5 \\ &\quad +4.244\times10^{-1}\delta^6), \end{aligned} \tag{5.87}$$

with the bounds on $B(\mu \to eJ)$ being similar to that of Al.

With this analysis, Mu2e and COMET may produce more stringent bounds on the branching ratio $B(\mu \to eJ)$. This is even more likely if suggestions to push the sensitivity to the $10^{-18}$ level are undertaken. Also, if the experiment is able to improve the energy resolution used, a better bound can be placed on the branching ratio. The results given here require no modification or extra analysis of the conversion experiment – the bound comes as a free byproduct. In addition to providing a

method of finding limits of the branching ratio, it is shown that the endpoint of the spectrum is an ideal place to search for new types of muon decays. This is because the SM muon decay has stronger suppression, $(E_{\mu e} - E_e)^5$ at the endpoint than the Majoron emission, which goes as $(E_{\mu e} - E_e)^3$.

# Chapter 6

# Semileptonic $b$-quark Decay

## 6.1 Introduction

### The CKM Matrix

In QCD the particles that interact via the strong force are known as quarks, while the force carrying particles are the gluons. The quarks are arranged into three doublets,

$$\begin{pmatrix} u \\ d \end{pmatrix}, \begin{pmatrix} c \\ s \end{pmatrix} \text{ and } \begin{pmatrix} t \\ b \end{pmatrix}.$$

They are the only particles in the SM that interact via all three forces: electromagnetic, weak and strong. $d$-type quarks have an electric charge of $-\frac{1}{3}e$, while $u$-type quarks have an electric charge of $\frac{2}{3}e$. One of the peculiarities of quarks is that they never have (and in theory never will) been seen in a state that is not bound to another quark or antiquark. The qualitative argument for the cause of this is that the strong force becomes stronger as the distance between quarks increases. When the quarks are far enough apart, the potential energy between them becomes large enough to cause the production of a new quark anti-quark pair, leading to two bound states instead of one. The inability of quarks to be free is called confinement.

With the property of confinement, calculating the decays of quarks becomes a more difficult task than for leptons. The fact that the quark of interest is not a free quark, but is bound, must be taken into account. In order to compute a true decay rate, the non-perturbative effects of the strong force potential need to be included. Fortunately, methods have been developed to separate the non-perturbative effects of this binding interaction with other perturbative effects. This chapter focuses on the perturbative aspects of quark decays.

Through the weak interaction, quarks are able to change their flavour from an up-type ($u$) to a down-type ($d$) quark. This allows the process $b \to c\ell\overline{\nu}$ to occur. The strength of this mixing is described by the Cabibbo-Kobayashi-Maskawa (CKM) matrix,

$$\begin{pmatrix} V_{ud} & V_{us} & V_{ub} \\ V_{cd} & V_{cs} & V_{cb} \\ V_{td} & V_{ts} & V_{tb} \end{pmatrix}.$$

Typically, one would invoke unitarity requirements to rewrite this matrix in terms of three unknown parameters and a complex phase. Nevertheless it is important

to measure the values of each of these matrix terms. Doing so allows the unitarity requirements to be overconstrained and tested for new physics. If this unitarity was found to be broken, this would be an indication of new physics, such as a fourth generation of quarks.

### The Parameter $V_{cb}$

The parameter of interest in this chapter is $|V_{cb}|$. Experimentally, two approaches are used to extract a value of $|V_{cb}|$ from data. The first is by looking at the exclusive decays $B \to D\ell\nu_\ell$ and $B \to D^*\ell\nu_\ell$ that give values [50]

$$|V_{cb}| = (39.6 \pm 0.6_{\text{exp}} \pm 0.8_{\text{theo}}) \times 10^{-3} \quad (\overline{B} \to D^*\ell\overline{\nu}_\ell),$$
$$|V_{cb}| = (39.4 \pm 1.4_{\text{exp}} \pm 1.3_{\text{theo}}) \times 10^{-3} \quad (\overline{B} \to D\ell\overline{\nu}_\ell).$$

Both of these values involve lattice QCD calculations and are used to give the average exclusive value of $V_{cb}$

$$|V_{cb}| = (39.6 \pm 0.9) \times 10^{-3} \quad \text{(exclusive)}.$$

The other approach involves extracting $V_{cb}$ from the inclusive decay of the $B$ meson. This method uses all decay products that have leptons and a meson with a $c$-quark in the final state ($X_c$): $\overline{B} \to X_c\ell\overline{\nu}_\ell$. Currently, this approach gives the most precise determination of $|V_{cb}|$ with a value [50]

$$|V_{cb}| = (41.96 \pm 0.45 \pm 0.07) \times 10^{-3} \quad \text{(inclusive 1S)}.$$

Here, 1S refers to the renormalization scheme used in the mass definition of the $b$-quark. As can be seen, there is some tension between the exclusive and inclusive measurements. This motivates more precise measurements and a deeper investigation of the theory.

In order to extract $|V_{cb}|$ from the decay rate, a sufficiently accurate theoretical expression is required. The expression for the total decay rate $\Gamma(\overline{B} \to X_c\ell\overline{\nu}_\ell)$ is given by [51]

$$\begin{aligned}\Gamma \;=\; & \frac{G_F^2 m_b^5(\mu)}{192\pi^3}|V_{cb}|^2(1+A_{ew})A^{\text{pert}}(r,\mu) \times \\ & \left[ z_0(r)\left(1 - \frac{\mu_\pi^2(\mu) - \mu_G^2(\mu) + \frac{\rho_D^3(\mu)+\rho_{LS}^3(\mu)}{m_b(\mu)}}{2m_b^2(\mu)}\right)\right. \\ & \left. -2(1-r)^4\frac{\mu_G^2(\mu) - \frac{\rho_D^3(\mu)+\rho_{LS}^3(\mu)}{m_b(\mu)}}{2m_b^2(\mu)}m_b^2(\mu) + d(r)\frac{\rho_D^3(\mu)}{m_b^3(\mu)} + \ldots\right]. \qquad (6.1)\end{aligned}$$

Here $A_{ew}$ are electroweak corrections, and $A^{\text{pert}}$ are perturbative corrections, $z_0(r)$ is the tree-level phase space, $r$ is the mass ratio $m_c^2(\mu)/m_b^2(\mu)$ and $\mu$ is the renormalization scale. The $\mu_i$ and $\rho_i$ are expectation values of non-perturbative operators. This result is obtained using the method of Operator Product Expansion, which is able to separate the perturbative and non-perturbative parts. A review of semileptonic $b$-decay, including a discussion of all these terms, can be found in [51]. The perturbative part, $A^{\text{pert}}$, is calculated by applying perturbation theory to the partonic decay $b \to c\ell\overline{\nu}_\ell$. These are the corrections that will be focused on here.

## Perturbative Corrections

This chapter is based on [52], which calculates the second order (also called next to next to leading order or NNLO) corrections to the decay $b \to c\ell\overline{\nu}$ by expanding around the limit that the daughter quark is as heavy as the parent. The NNLO corrections to this decay have been studied using various expansions in an attempt to provide an accurate determination of the decay rate. The first methods used an approximation scheme where the leptons were replaced by a virtual boson ($W^*$) with a mass that allowed the calculation to be carried out in a specific kinematic region. This replacement can be done rigorously by looking at the decay rate of $b \to X\ell\overline{\nu}_\ell$.

$$d\Gamma(b \to X\ell\overline{\nu}_\ell) = \frac{(2\pi)^4}{2m_b}|\mathcal{M}|^2 d\Phi(b \to X\ell\overline{\nu}_\ell), \tag{6.2}$$

$$i\mathcal{M}(b \to X\ell\overline{\nu}_\ell) = Q_\mu \frac{-i}{q^2 - m_W^2}\left(g^{\mu\nu} - \frac{q^\mu q^\nu}{m_W^2}\right)\overline{u}\frac{ig_w}{2\sqrt{2}}\gamma^\nu(1+\gamma^5)v, \tag{6.3}$$

where $d\Phi$ is an element of the phase space for the decay, $Q_\mu$ is the quark current and $q$ is the momentum of the $W$. The phase space integral can be separated with the identity,

$$d\Phi(b; X\ell\nu_\ell) = d\Phi(b; XW^*)d\Phi(W^*; \ell\nu_\ell)(2\pi)^3 dq^2. \tag{6.4}$$

The differential decay rate is then,

$$\begin{aligned} d\Gamma(b \to X\ell\nu_\ell) &= \frac{(2\pi)^4}{2m_b}\frac{g_w^2}{8}\frac{Q_\mu Q_\nu^*}{\left(q^2 - m_W^2\right)^2}\left(g^{\mu\alpha} - \frac{q^\mu q^\alpha}{m_W^2}\right)\left(g^{\nu\beta} - \frac{q^\nu q^\beta}{m_W^2}\right) \\ &\quad \times d\Phi(b; XW^*)dq^2 \\ &\quad \times \frac{1}{2}\mathrm{Tr}\left[\not{p}_\ell\gamma_\alpha(1+\gamma^5)\not{p}_\nu\gamma_\beta(1+\gamma^5)\right](2\pi)^3 d\Phi(W^*; \ell\nu_\ell) \qquad (6.5) \\ &= \frac{(2\pi)^4}{2m_b}\frac{g_w^2}{8}\frac{Q_\mu Q_\nu^*}{\left(q^2 - m_W^2\right)^2}\left(g^{\mu\alpha} - \frac{q^\mu q^\alpha}{m_W^2}\right)\left(g^{\nu\beta} - \frac{q^\nu q^\beta}{m_W^2}\right) \\ &\quad \times d\Phi(b; XW^*)dq^2 \\ &\quad \times \delta^4(q - p_\ell - p\nu)\frac{d^3\mathbf{p}_\ell}{(2\pi)^3 2E_\ell}\frac{d^3\mathbf{p}_\nu}{(2\pi)^3 2E_\nu} \\ &\quad \times 4(2\pi)^3\left(p_{\ell\alpha}p_{\nu\beta} + p_{\nu\alpha}p_{\ell\beta} - g_{\alpha\beta}p_\ell \cdot p_\nu - \epsilon_{\alpha\beta\sigma\rho}p_\ell^\sigma p_\nu^\rho\right). \qquad (6.6) \end{aligned}$$

Notice that it is now possible to carry out the phase-space integral for the leptons. The method of computing these types of tensor integrals is commonly used as follows below.

### Phase Space Integral

Consider the tensor integral

$$\mathcal{I}^{\alpha\beta} = \int \frac{d^3\mathbf{p}_\ell}{(2\pi)^3 E_\ell}\frac{d^3\mathbf{p}_\nu}{(2\pi)^3 E_\nu}(2\pi)^3 p_\ell^\alpha p_\nu^\beta \delta^4(q - p_\ell - p_\nu) \tag{6.7}$$

The only tensors that can appear in the final result are $g^{\alpha\beta}$ and $q^\alpha q^\beta$, so the result must be of the general form

$$\mathcal{I}^{\alpha\beta} = Ag^{\alpha\beta} + B\frac{q^\alpha q^\beta}{q^2}. \tag{6.8}$$

The two unknowns $A$ and $B$ can be solved for by multiplying both equations by $g^{\alpha\beta}$ or $q^\alpha q^\beta$. It is then possible to carry out the integrals to create a system of two equations that can be used to solve for $A$ and $B$. Multiplying by $g^{\alpha\beta}$ gives

$$4A + B = \int \frac{d^3\mathbf{p}_\ell d^3\mathbf{p}_\nu}{(2\pi)^3 E_\ell E_\nu} p_\ell \cdot p_\nu \delta(E_q - E_\ell - E_\nu)\delta^3(\mathbf{p}_\ell + \mathbf{p}_\nu). \tag{6.9}$$

For simplicity, the rest frame of the $W^*$ is considered. In addition, since the mass of the leptons is so small compared to the other scales in this problem, they are considered to be massless.

$$\begin{aligned} 4A + B &= \int \frac{d^3\mathbf{p}_\ell}{(2\pi)^3} \frac{(E_\ell^2 + \mathbf{p}_\ell^2)}{E_\ell^2} \delta(E_q - 2E_\ell), && (6.10)\\ &= \int \frac{dE_\ell}{2\pi^2} E_\ell^2 \delta\left(\frac{E_q}{2} - E_\ell\right), && (6.11)\\ &= \frac{q^2}{8\pi^2}. && (6.12) \end{aligned}$$

Here, the fact that $q^2 = E_q^2$ has been used to write the final result in a Lorentz invariant form. Carrying out the same procedure after multiplying by $q^\alpha q^\beta$ gives the condition

$$A + B = \frac{q^2}{16\pi^2}. \tag{6.13}$$

Finally, solving for $A$ and $B$ gives

$$A = \frac{q^2}{48\pi^2}, \qquad B = \frac{q^2}{24\pi^2}, \tag{6.14}$$

which produces the result of the integral.

$$\mathcal{I}^{\alpha\beta} = \frac{q^2}{48\pi^2}\left(g^{\alpha\beta} + 2\frac{q^\alpha q^\beta}{q^2}\right) \tag{6.15}$$

Using the result for $\mathcal{I}^{\alpha\beta}$, the decay rate is

$$\begin{aligned} d\Gamma(b \to X\ell\nu_\ell) &= \frac{(2\pi)^4}{2m_b}\frac{g_w^2}{8}\frac{Q_\mu Q_\nu^*}{\left(q^2 - m_W^2\right)^2} d\Phi(b; XW^*) dq^2 \\ &\quad \times \frac{q^2}{48\pi^2}\left(g^{\mu\alpha} - \frac{q^\mu q^\alpha}{m_W^2}\right)\left(g^{\nu\beta} - \frac{q^\nu q^\beta}{m_W^2}\right) \\ &\quad \times \left[4\left(-g_{\alpha\beta} + \frac{q_\alpha q_\beta}{q^2}\right) + \epsilon_{\alpha\beta\sigma\rho}\left(g_{\alpha\beta} + 2\frac{q_\alpha q_\beta}{q^2}\right)\right] && (6.16)\\ &= \frac{(2\pi)^4 g_w^2}{2m_b(96\pi^2)}\frac{Q_\mu Q_\nu^*}{m_W^4} d\Phi(b; XW^*) q^2 dq^2 \left(g^{\mu\nu} - \frac{q^\mu q^\nu}{q^2}\right) && (6.17) \end{aligned}$$

where the limiting case $q^2 \ll m_W^2$ has been taken, which is valid for this decay.

Now, consider the decay rate of the process $b \to XW^*$ where the $W^*$ has a mass $m_W = \sqrt{q^2}$.

$$d\Gamma(b \to XW^*) = \frac{(2\pi)^4}{2m_b} Q_\mu Q_\nu^* \left(g^{\mu\nu} - \frac{q^\mu q^\nu}{q^2}\right) d\Phi(b; XW^*) \tag{6.18}$$

Comparing the two expressions, it is now possible to relate the full semi-leptonic decay rate to the virtual boson decay rate

$$d\Gamma(b \to X\ell\overline{\nu}_\ell) = \frac{g_w^2}{96\pi^2 m_{W^*}^4} \int dq^2 q^2 d\Gamma(b \to XW^*)|_{m_{W^*}=\sqrt{q^2}}. \tag{6.19}$$

This equation allows the decay rate for $b \to XW^*$ to be computed and related to a specific point in the mass spectrum of the decay $b \to X_c\ell\overline{\nu}_\ell$. With enough points in the mass spectrum, it is possible to provide a good estimate of the full $b$ decay rate.

## Kinematics

With the leptons replaced by a virtual boson, one can map the kinematically available phase space onto a triangle as shown in Figure 6.1.

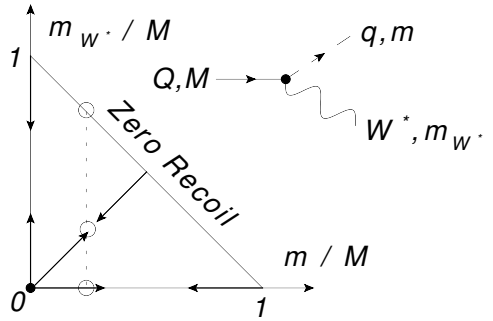


**Figure 6.1:** The kinematic region allowed for the decay $Q \to qW^*$. The known expansions are seen to cover the borders of the region plus the bisecting expansions, where the mass configuration $m_{W^*} = m$ was considered. The dashed line and circles show the points used to obtain an approximate result for the full decay with leptons.

The vertical axis corresponds to the mass ratio of the virtual boson ($W^*$) to the heavy quark ($Q$). The horizontal axis corresponds to the mass ratio of the light quark ($q$) to the heavy quark. When the sum of the masses of the boson and light quark equals the mass of the heavy quark, the light quark is produced at rest and the leptons have momenta in opposite directions. This situation provides the hypotenuse of the triangle, also known as the zero recoil line. Using various limits of the two mass ratios, the decay rate $\Gamma(Q \to W^*q)$ can be calculated as an expansion around the chosen limit. For this decay, calculations have been carried out for the configurations,

$$\frac{m}{M} = 0 \quad \tfrac{m_{W^*}}{M} \sim 0 \quad [53] \tag{6.20}$$

$$\frac{m}{M} = 0 \quad \tfrac{m_{W^*}}{M} \sim 1 \quad [54] \tag{6.21}$$

$$\frac{m}{M} \sim 0 \quad \tfrac{m_{W^*}}{M} = 0 \quad [55] \tag{6.22}$$

$$\frac{m}{M} \sim 1 \quad \tfrac{m_{W^*}}{M} = 0 \quad [56] \tag{6.23}$$

$$\frac{m}{M} \sim 0 \quad \tfrac{m_{W^*}}{M} = \tfrac{m}{M} \quad [57] \tag{6.24}$$

$$\frac{m + m_{W^*}}{M} \sim 1 \quad \frac{m_{W^*}}{M} = \frac{m}{M} \quad [58]. \tag{6.25}$$

Full analytic solutions are also known along the zero recoil line [59]. Using points in three of the expansions (denoted as circles in Figure 6.1) allowed an approximation of the full decay [58, 60].

The full calculation, including leptons, was first done both numerically and analytically in [61, 62] respectively. Both results are valid in the physical region of the quark mass ratio $\rho = m_c/m_b \approx 0.25 - 0.3$. In [62] the corrections were obtained as an expansion in the ratio of quark masses $\rho$. The calculation described here provides an additional check of the analytic result by expanding in the opposite limit, $\delta = 1 - \rho$. In addition, this calculation requires the application of the method of asymptotic expansion to a new kinematic configuration. The results agree well with the expansion in [62] and has interesting implications for calculating higher order corrections.

## 6.2 Calculation Method

The full NNLO corrections to this decay involve diagrams that have as many as five daughter particles: two leptons, a quark and up to two gluons. A convenient way to obtain the amplitudes needed for this calculation is through the use of the optical theorem. The decay can then be written in terms of four-loop $b$-quark self-energy diagrams, and the powerful loop integral techniques developed over the past few decades can be taken advantage of. These self-energy diagrams have two mass scales that need to be dealt with: $m_c$ and $m_b$. The mass scale $M_W$ is removed by using a four-fermion effective interaction with coupling $G_F$ that avoids the creation of a $W$ propagator. The occurrence of the two scales makes these integrals much more difficult than they would be if they had a single scale. Fortunately, asymptotic expansion can be used to separate the two scales in the problem.

Asymptotic expansion is a method of separating integrals into 'regions' such that the resulting regions have integrals with only one scale. The result is an expansion in the ratio of small scale to large scale. In the case of this calculation, this ratio is denoted $\delta = 1 - m_c/m_b$. The loop momenta in the diagrams can then have one of two characteristic scales, hard $m_b$ or soft $\delta m_b$. When all loop momenta have been separated into hard or soft regions, the result is a product of single scale loop integrals that can be calculated with the many tools and methods available.

As an example, consider the leading order contribution to this decay as shown in Figure 6.2. This diagram is a topology diagram like the one discussed in Chapter

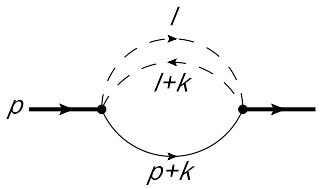


**Figure 6.2:** The leading order contribution to $b \to c$ decay. The dashed lines indicate massless leptons, the heavy lines denote $b$-quarks, and the light lines denote $c$-quarks.

1. It is possible to simplify any Feynman diagram to an expression that depends only on different powers of the propagators and possibly scalar products of momenta in the numerator. Thus, the vertices and external lines indicate only the flow of four-momenta. The diagram in Figure 6.2 represents the integral

$$I(\lambda_1) = \int \frac{d^D l}{(2\pi)^D} \frac{d^D k}{(2\pi)^D} \frac{1}{l^2} \frac{1}{(l+k)^2} \frac{1}{[(p+k)^2 + m_c^2]^{\lambda_1}} \tag{6.26}$$

Note that in this calculation the leptons are considered to be massless. First, it will be important to remember a few properties of this integral. In order to regularize infrared and ultraviolet divergences, the integrations are done in $D = 4 - 2\epsilon$ dimensions. This allows an expansion in $\epsilon$ after the integrals have been computed to make the divergences explicit. When all diagrams are summed, including any renormalization terms, the pole terms in $\epsilon$ should cancel to give a finite result in the limit $\epsilon \to 0$. This is known as dimensional regularization. The second thing that is noticed is that the massive propagator has been given a power $\lambda_1$. When considering the topology of a diagram, it is often convenient to use general powers of the propagator as it is likely that more than one configuration of powers will appear. If a result can be derived for general powers, then values can be plugged into the general result.

The integral over the lepton loop momentum is not very difficult. Fortunately, this is the form of the lepton loop that will appear in all diagrams at all orders as the leptons do not interact in this decay. As a result, it can be done once and result can be used in future calculations. Also, this is a sub-topology that appears often in this calculation, so the evaluation is done using general powers of the propagators here. Using Feynman parameters to combine the propagators gives

$$\begin{aligned} \mathrm{One}(a,b) &= \int \frac{d^D l}{(2\pi)^D} \frac{1}{(l^2)^a} \frac{1}{[(l+k)^2]^b} & (6.27) \\ &= \int \frac{d^D l}{(2\pi)^D} \int_0^1 dx \frac{\Gamma(a+b)}{\Gamma(a)\Gamma(b)} \frac{x^{b-1}(1-x)^{a-1}}{[l^2 + 2l\cdot kx + k^2 x]^{a+b}}. & (6.28) \end{aligned}$$

The square is completed for $l$ and a change variables $l \to l' - kx$ is made. This puts the denominator in a form that allows the $l$ integral to be carried out. The result is an integral over the Feynman parameter that gives a beta function,

$$\begin{aligned} \mathrm{One}(a,b) &= \int_0^1 dx \frac{\Gamma(a+b)}{\Gamma(a)\Gamma(b)} \int \frac{d^D l'}{(2\pi)^D} \frac{x^{b-1}(1-x)^{a-1}}{[l'^2 + k^2 x(1-x)]^{a+b}} & (6.29) \\ &= \int_0^1 dx \frac{\Gamma\left(a+b-\frac{D}{2}\right)}{(4\pi)^{D/2}\Gamma(a)\Gamma(b)} \frac{x^{b-1}(1-x)^{a-1}}{[k^2 x(1-x)]^{a+b-D/2}} & (6.30) \\ &= \frac{\Gamma\left(a+b-\frac{D}{2}\right)}{(4\pi)^{D/2}\Gamma(a)\Gamma(b)} \frac{1}{k^{2(a+b-D/2)}} & (6.31) \\ &\times \int_0^1 dx (1-x)^{\frac{D}{2}-b-1} x^{\frac{D}{2}-a-1} \\ &= \frac{\Gamma\left(a+b-\frac{D}{2}\right)\Gamma\left(\frac{D}{2}-b\right)\Gamma\left(\frac{D}{2}-a\right)}{(4\pi)^{D/2}\Gamma(D-a-b)\Gamma(a)\Gamma(b)} \frac{1}{k^{2(a+b-2+\epsilon)}}. & (6.32) \end{aligned}$$

$a = 1$ and $b = 1$ can now be plugged in as in the lepton loop from Equation 6.26. At this point, the $k$ integral is all that remains to be completed.

This second loop integral in Equation 6.26 is more complicated as the mass in the propagator is $m_c$, while the momentum depends on the external momentum which is proportional to $m_b$. Asymptotic expansion is used to deal with this complication. As mentioned earlier, the hard region is when the loop momentum is of order $m_b$ and the soft region is when the loop momentum is of order $\delta m_b$. To separate the integral into these two regions, the small scales are Taylor expanded out of the propagators, as shown in Figure 6.3. By including higher orders in this expansion, a series is built up in powers of $\delta$.

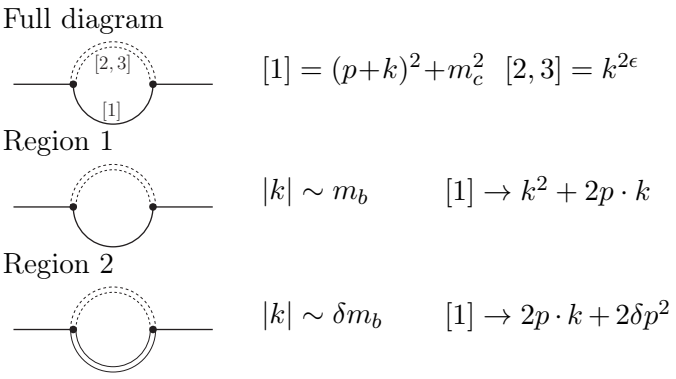


**Figure 6.3:** The asymptotic expansion of the diagram in Figure 6.2. The double dotted line represents the integrated lepton loop. The double solid line denotes the eikonal propagator $2p \cdot k + 2\delta p^2$.

There are two integrals that need to be calculated. On closer inspection, it is noted that the integral from Region 1 will not contribute to the final result as it is purely real while the decay rate is given by the imaginary part. In general this is true for the so-called 'hard' region when all loop momenta are of order $m_b$. Normally, the hard region is one of the more difficult regions to calculate meaning this kinematic configuration (the $\delta \to 0$ limit) leads to some strong simplifications. The other region gives

$$\text{eOne}(\lambda_1, \lambda_2) \quad = \quad \int \frac{d^D k}{(2\pi)^D} \frac{1}{(k^2)^{\lambda_1} \left[2p \cdot k + 2\delta p^2\right]^{\lambda_2}}. \tag{6.33}$$

To carry out this integral, a similar method of combining the denominators as Feynman parameters is used. The parameterization used here however, is slightly different.

$$\frac{1}{A^a B^b} = \frac{\Gamma(a+b)}{\Gamma(a)\Gamma(b)} \int_0^\infty d\lambda \frac{\lambda^{b-1}}{[A + B\lambda]^{a+b}} \tag{6.34}$$

The integral over $k$ is carried out in the same way as the integral over $l$ previously. This leaves an integral that can be rewritten to give a beta function. The final result is

$$\begin{aligned} \text{eOne}(\lambda_1, \lambda_2) \quad = \quad & \int \frac{d^D k}{(2\pi)^D} \frac{\Gamma(\lambda_1 + \lambda_2)}{\Gamma(\lambda_1)\Gamma(\lambda_2)} \\ & \int_0^\infty dx \frac{x^{\lambda_2 - 1}}{\left[k^2 + x(2p \cdot k + 2p^2\delta)\right]^{\lambda_1 + \lambda_2}} \end{aligned} \tag{6.35}$$

$$= \frac{\Gamma(\lambda_1+\lambda_2)}{\Gamma(\lambda_1)\Gamma(\lambda_2)}\int_0^\infty dx \int \frac{d^Dk}{(2\pi)^D}\frac{x^{\lambda_2-1}}{[k^2+p^2x(2\delta-x)]^{\lambda_1+\lambda_2}} \quad (6.36)$$

$$= \frac{\Gamma(\lambda_1+\lambda_2-\frac{D}{2})}{\Gamma(\lambda_1)\Gamma(\lambda_2)}\frac{(p^2)^{D/2-\lambda_1-\lambda_2}}{(4\pi)^{D/2}} \quad (6.37)$$

$$\times \int_0^\infty dx x^{D/2-\lambda_1-1}(2\delta-x)^{D/2-\lambda_1-\lambda_2}$$

$$= \frac{(p^2)^{D/2-\lambda_1-\lambda_2}}{(4\pi)^{D/2}}(-1)^{\lambda_1-D/2}(2\delta)^{D-2\lambda_1-\lambda_2} \quad (6.38)$$

$$\times \frac{\Gamma\left(\frac{D}{2}-\lambda_1\right)\Gamma\left(2\lambda_1+\lambda_2-D\right)}{\Gamma\left(\lambda_1\right)\Gamma\left(\lambda_2\right)}.$$

These two integrals, One and eOne, appear frequently in this calculation. With these general forms, calculation of diagrams only requires plugging in values for $a, b, \lambda_1$ and $\lambda_2$. Another simplifying feature of the integral in Figure 6.2 is the fact that this two loop integral can be done by carrying out two nested one loop integrals. This is not always possible in general, but occurs quite frequently in this calculation. In fact, this nesting of integrals appears in almost all regions for the four loop calculation. With this technique, only five unique topologies are required to carry out the full calculation. In addition, the topologies that appear have at most two loops, and the calculation of these is well known (see for example [28]).

The only regions where nesting does not work are those with a three-gluon vertex. An extra step is required for these diagrams. It turns out that it is possible to get rid of the dependence on one of the gluon propagators through recurrence relation techniques, such as IBP. The Laporta algorithm implemented in `FIRE` and `rows` [63] is used to do this reduction. The resulting integrals can then be calculated using the nesting technique described above. With these simplifications, this four loop problem is reduced to the calculation of five one or two loop integrals.

## 6.3 Second Order Corrections

The second order corrections to the decay rate involves the calculation of the 39 four loop diagrams shown in Figure C.1. These diagrams all fit into one of ten topologies that can be reduced to a total of five master integrals shown in Figure 6.4. The names in these diagrams come from [28] where they are evaluated, with the exception of eY2, which is related to the integral $I'$ in [64]. Note that eY2 is also a generalization of the eOne integral in Equation 6.33.

The total decay rate can be written as a series in terms of $\frac{\alpha_s}{\pi}$. The results presented here are given such that $\alpha_s$ is evaluated at the scale $m_b$ unless otherwise specified.

$$\Gamma = \frac{G_F^2|V_{cb}|^2 m_b^5}{192\pi^3}\left[X_0 + \frac{\alpha_s}{\pi}C_F X_1 + \left(\frac{\alpha_s}{\pi}\right)^2 X_2 + \ldots\right], \quad (6.39)$$

where

$$X_2 = C_F X_F + C_A X_A + T_F(n_l X_l + X_c + X_b). \quad (6.40)$$

Here, $X_F$ and $X_A$ are the abelian and non-abelian terms respectively, while $X_l, X_c$ and $X_b$ denote the contributions from diagrams with light, $c$- or $b$- quark loops

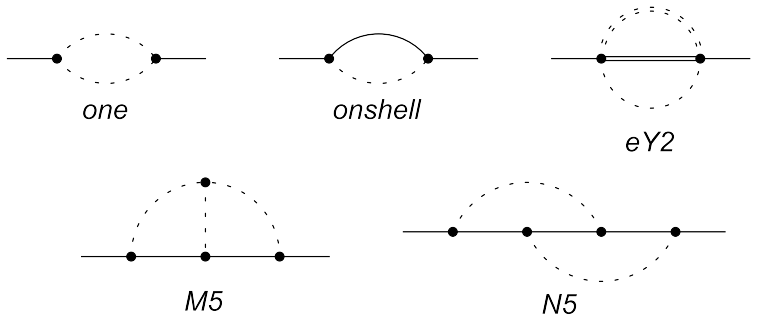


**Figure 6.4:** The five master integrals used to calculate every diagram for the NNLO corrections to the decay. The solid and dashed lines indicate massive and massless propagators respectively, while the double dashed and solid lines indicate propagators of the type $2p\cdot k$ or $2p\cdot k+\delta p^2$ respectively.

respectively. In QCD $C_F = 4/3, C_A = 3, T_F = 1/2$ and $n_l = 3$. The tree level and first order corrections have been reproduced as well,

$$X_0 = \frac{64}{5}\delta^5 - \frac{96}{5}\delta^6 + \frac{288}{35}\delta^7 + \ldots, \tag{6.41}$$

$$X_1 = -\frac{48}{5}\delta^5 + \frac{72}{5}\delta^6 + \left(\frac{512}{105}\ln(2\delta) - \frac{158152}{11025}\right)\delta^7 + \ldots. \tag{6.42}$$

The ellipses indicate higher order terms in $\delta$ that are not shown here. These results agree with the expansion of the full results found in [65]. Note that the expansions start at the order $\delta^5$. This means that the series is strongly suppressed in the region where $\delta \sim 0$ and leads to a highly convergent series. As will be seen, this has the important consequence that the expansion is valid over the whole range of $\delta$ and approximates the full result, even at $\delta = 1$, with fairly good accuracy.

The second order terms have been calculated up to $\mathcal{O}(\delta^{15})$ for the quark loop contributions. For the abelian and non-abelian terms the contributions are known up to $\delta^{12}$ and $\delta^{11}$ respectively. For simplicity, the results up to $\mathcal{O}(\delta^7)$ are presented here with the full results given in Appendix C.

$$\begin{aligned} X_F = {} & \left[\frac{35}{5}\pi^2(1-\ln(2)) - \frac{46}{5} + \frac{48}{5}\zeta_3\right]\delta^5 \\ & + \left[\frac{69}{5} - \frac{48}{5}\pi^2(1-\ln(2)) - \frac{72}{5}\zeta_3\right]\delta^6 \\ & + \left[\frac{39329}{3675} + \frac{3044}{945}\pi^2 - \frac{496}{105}\pi^2\ln(2) + \frac{248}{35}\zeta_3 - \frac{352}{105}\ln(2\delta)\right]\delta^7 + \ldots, \end{aligned} \tag{6.43}$$

$$\begin{aligned} X_A = {} & \left[-\frac{286}{15} - \frac{8}{5}\pi^2(1-2\ln(2)) - \frac{24}{5}\zeta_3\right]\delta^5 \\ & + \left[\frac{99}{5} + \frac{12}{5}\pi^2(1-2\ln(2)) + \frac{36}{5}\zeta_3\right]\delta^6 + \left[\frac{62206}{33075}\pi^2 + \frac{248}{105}\pi^2\ln(2)\right. \\ & \left. - \frac{99547376}{33075}\ln(2\delta) - \frac{256}{315}\pi^2\ln(2\delta) - \frac{1408}{315}\ln^2(2\delta)\right]\delta^7 + \ldots, \end{aligned} \tag{6.44}$$

$$
\begin{aligned}
X_l &= \frac{56}{15}\delta^5 - \frac{12}{5}\delta^6 + \left[\frac{25577548}{1157625} - \frac{417664}{33075}\ln(2\delta)\right. \\
&\quad \left. + \frac{512}{315}\left(\ln^2(2\delta) - \frac{\pi^2}{3}\right)\right]\delta^7 + \dots , \qquad (6.45) \\
X_c &= \left[\frac{184}{3} - \frac{32}{5}\pi^2\right]\delta^5 + \left[-\frac{828}{5} + \frac{88}{5}\pi^2\right]\delta^6 \\
&\quad + \left[\frac{108580}{567} - \frac{18968}{945}\pi^2\right]\delta^7 + \dots , \qquad (6.46) \\
X_b &= \left[\frac{184}{3} - \frac{32}{5}\pi^2\right]\delta^5 + \left[-12 + \frac{8}{5}\pi^2\right]\delta^6 \\
&\quad + \left[\frac{107444}{2835} - \frac{3848}{945}\pi^2\right]\delta^7 + \dots . \qquad (6.47)
\end{aligned}
$$

These results can be checked in a few ways. The first method is to look at the limiting case $\delta \to 0$. In this case, the results can be compared with the zero-recoil form factors calculated in [66, 59]. Specifically, both the $\delta^5$ and $\delta^6$ terms in the expansion here can be matched with the axial form factor $\eta_A$. When doing this comparison it is important to take into account the different scales used for $\alpha_s$. Here, $\alpha_s(m_b)$ is used while [66] uses $\alpha_s(\sqrt{m_c m_b})$. In order to compare the two results properly $\alpha_s$ must be run from $m_b$ to $\sqrt{m_c m_b}$ with four active flavours. This changes the full result by

$$
\delta X_2 = \frac{48}{5}\left(\frac{11}{12}C_A - \frac{1}{3}T_F(n_l + 1)\right)\delta^6 + \mathcal{O}(\delta^7). \qquad (6.48)
$$

Completing this change reproduces the first two terms of the expansion in [66] for the full result as well as the individual terms in Equation 6.40.

The second check is to compare the results here with the expansion from the opposite limit. Figure 6.5 shows the plots for the results presented here along with the expansions from [62]. As can be seen, the special kinematic configuration of the expansion done here has led to some very nice properties of the result when compared to the expansion in [62]. In particular, the expansion given here is converging quickly to the full result even at the point $\delta = 1$ where the expansion is not expected to converge. Also note that the $X_b$ expansion was able to reproduce the extremum at $\frac{m_c}{m_b} \approx 0.2$ that was found in [62].

The full result is shown in Figure 6.6, compared with the expansion from the opposite end. Here, terms up to $\mathcal{O}(\delta^{11})$ are plotted as that is the highest order in which all corrections are accounted for. The plot in Figure 6.6 clearly shows how well the expansion behaves all the way to $\delta = 1$. Combining this with the major simplifications that were found during the calculation implies that the third order corrections would not be much more difficult to calculate. Although this is not currently required in the quark sector, it could be applied to similar processes, such as muon decays.

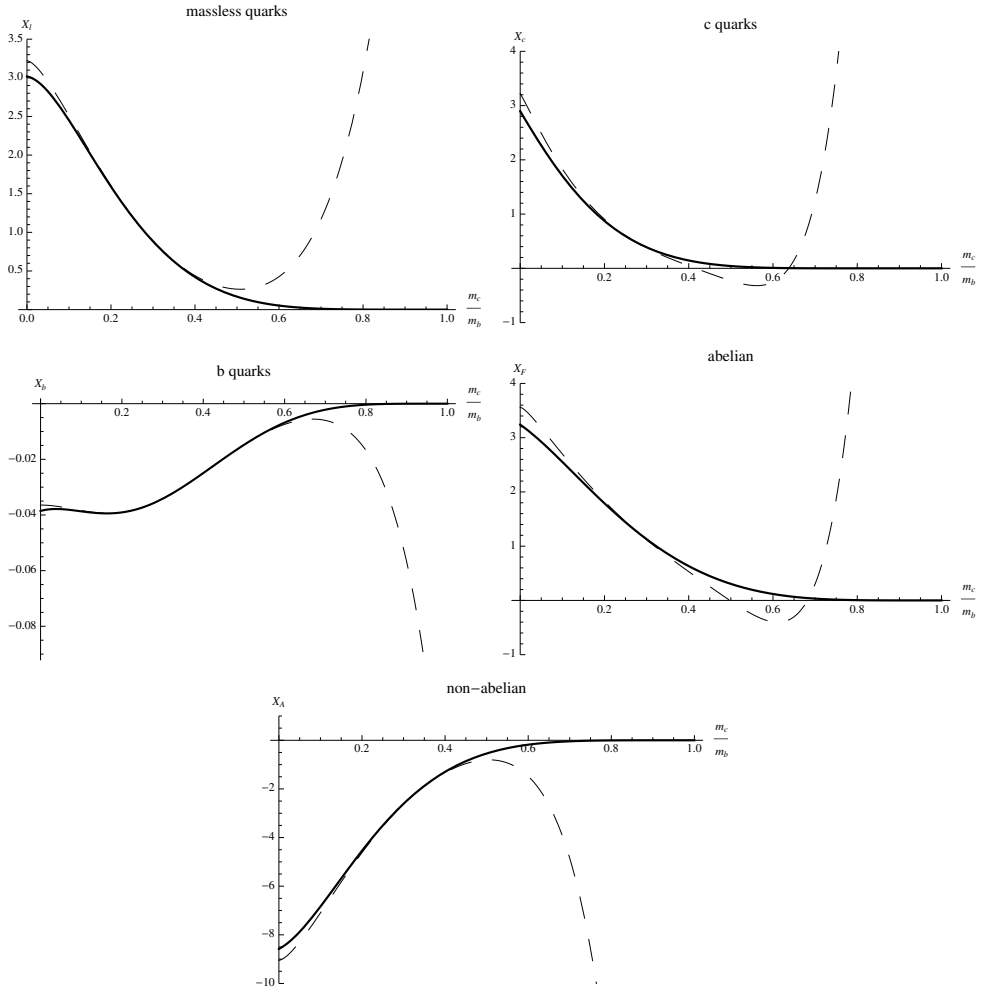


**Figure 6.5:** Plots of the different contributions to the $\mathcal{O}(\alpha_s^2)$ corrections to $b \to c\ell\overline{\nu}$ decay. Dashed lines indicate the expansion from $\frac{m_c}{m_b} = 0$ calculated in [62], while the solid line shows the expansion presented here and published in [52].

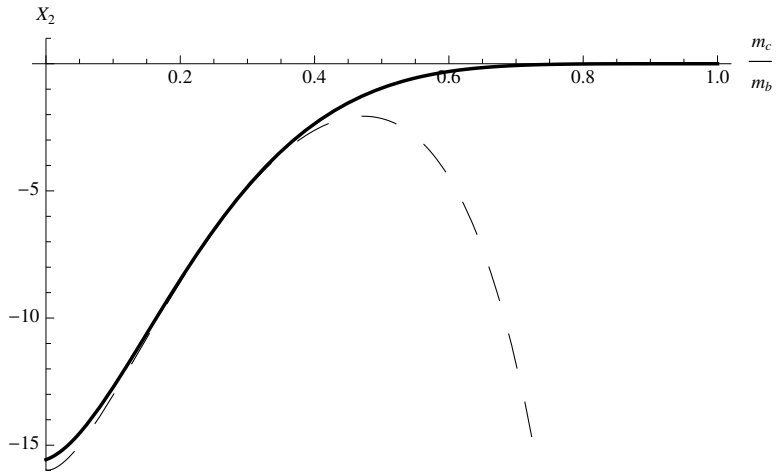


**Figure 6.6:** The full NNLO corrections, $X_2$, to semileptonic $b$ decay. The solid line shows the result presented here and the dashed line shows the expansion from [62].

# Chapter 7

# Muon Decay

In 1936 Carl D. Anderson and Seth Neddermeyer were studying cosmic radiation when they discovered particle tracks different from both electrons and protons [67]. The particle seemed to have the same charge as an electron but a mass in-between the electron and proton. Thus, they proposed this new particle be called the mesotron. Very quickly, this new particle went from being a discovery to being used as an experimental tool. In 1941 Bruno Rossi and David Hall performed an experiment [68] measuring the decay rate of muons with different momenta. They found that their results agreed with predictions only when time dilation effects were taken into account. This marks one of the first experimental confirmations of time dilation as predicted by special relativity.

It was eventually realized that the mesotron was a lepton just like the electron and was re-named the muon. In the SM, the muon is now used as a tool to carry out precision measurements. The fact that it has a large mass compared to the electron makes it ideal for testing the limits of the SM and searching for effects from possible new physics. For example, the Lamb shift of muonic hydrogen (a hydrogen atom with a muon instead of electron) has recently been used to make the most precise measurement of the proton charge radius [4]. This measurement disagrees with previous measurements by $7\sigma$. As another example, the experimental measurements and theoretical determinations of the anomalous magnetic moment of the muon currently have a $3.4\sigma$ discrepancy [69, 70].

In the SM, the muon can only decay in a few ways. Almost 100% of the time, the decay is of the form $\mu \to e^- \nu_\mu \overline{\nu}_e$ [50]. The other two decay modes quoted in [50] include the decay with an extra photon or electron positron pair. This property makes the SM decay of the muon a very clean process that is now used to extract a value for the SM constant $G_F$ [17]. In order to measure this fundamental constant as precisely as possible, it is necessary to compute the decay rate to high order. A review of the determination of $G_F$ from the muon lifetime cites three main sources of error limiting the measurements [71]: the electron mass in the $\mathcal{O}(\alpha^2)$ corrections, hadronic effects (which are small), and higher loops. The latest corrections to be computed were the $\mathcal{O}(\alpha^2)$ corrections [72], where it was found that an unexpected linear term in $m_e/m_\mu$ shifts the value of the decay rate by about 0.5ppm.

This small correction raises an important question: how accurate is the current theory regarding muon decay rates? Are higher loops a significant source of error? Looking at the order of magnitude of the most recent correction, it is found that the

change between the massless case and the linear mass corrections is of order

$$\mathcal{O}\left(\frac{m_e}{m_\mu}\right)\alpha^2 \sim \frac{m_e}{m_\mu}\alpha^2 \approx 0.005\alpha^2. \tag{7.1}$$

In terms of the expansion in $\alpha$, the order of the next correction can be estimated to be,

$$\alpha^3 \approx 0.007\alpha^2. \tag{7.2}$$

If the $\mathcal{O}(\alpha^3)$ contribution to the muon decay rate has a somewhat large coefficient, this correction could be important in a proper determination of the muon lifetime and in particular $G_F$.

This chapter focuses on a first effort to compute the third order corrections to the decay rate of the muon. To start, the relation between this decay and the QCD corrections of the semileptonic $b$-quark decay described in Chapter 6 is considered. The simplifications in that calculation also occur here and make this order of calculation possible. Next, some further simplifications are described that were skipped over in Chapter 6 but prove to help significantly here. After this, the calculation method used is expanded on as some extra techniques are needed. Finally, the results that are currently available are presented and some of the computing resources required to obtain them are discussed.

## 7.1 $b$-quark Decay Relation to Muon Decay

The semileptonic decay of quarks is very similar to the SM decay of muons. Taking a look at the tree level diagrams in Figure 7.1 it is seen that after the limit of large $W$ mass is taken, the decays can be related with the replacements,

$$b \to \mu, \quad c \to e, \quad l \to \nu_e, \quad \text{and} \quad \nu_l \to \nu_\mu. \tag{7.3}$$

This is achieved mathematically with a Fierz transformation. The equivalence of

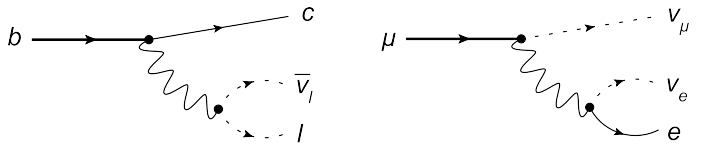


**Figure 7.1:** Tree level decay diagrams for semileptonic $b \to c$ and muon decays.

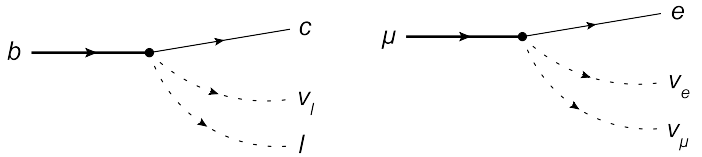


**Figure 7.2:** Tree level decay diagrams for semileptonic $b \to c$ and muon decays after the limit $M_W \to \infty$ is taken.

these two diagrams means that corrections to the semileptonic decay of $b$-quarks also give corrections to the SM muon decay. In fact, the first calculation of second order corrections to muon decay (including mass effects) were calculated in [72] as

part of the corrections to the $b$-decay. At higher orders, there is a difference between these two calculations. This difference comes from the fact that QCD corrections involve colour factors and interactions between three and four gluons. These kinds of interactions are not present in QED so the muon decay rate must be extracted from the semileptonic $b$-quark decay rate. Fortunately, the explicit separation of the different colour factor contributions as presented in Chapter 6 gives a very simple method of extracting the muon result. Specifically in QED

$$C_A = 0, \quad C_F = 1, \quad T_F = 1, \quad n_l = 0. \tag{7.4}$$

### Convergence

As seen in Chapter 6, the kinematic limit taken provided some significant advantages when carrying out the calculation. Remember, the expansion is being done in the limit where the electron is just as massive as the muon and regions where the loop momenta can be either large (hard) or small (soft) compared to the mass of the muon $M$ are considered. One of the advantages was the fact that the series in $\delta = (1 - \frac{m}{M})$ converges very rapidly and gives accurate results even at the point $\delta = 1$. For the muon decay, this convergence may change because, as mentioned before, the calculation involves only a subset of the diagrams that appear in the $b$-quark decay calculation. To make sure that the expansion still converges nicely, consider the $\mathcal{O}(\alpha^2)$ results. At tree level and first order in $\alpha$ the $b$-quark and muon decays are identical so there is no use in considering them here. Figure 7.3 shows the second order corrections for various orders in the expansion of $\delta$ between $\delta^7$ and $\delta^{10}$. The convergence is not quite as good as in the case of the $b$-decay. At order

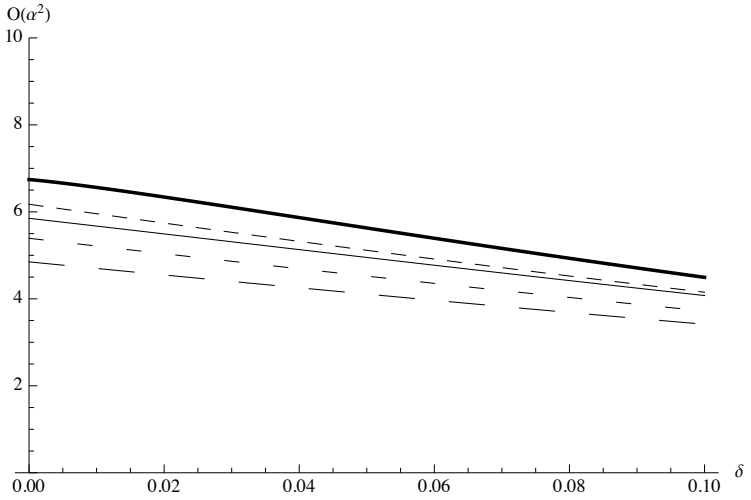


**Figure 7.3:** This plot shows the convergence of the second order corrections to muon decay. Starting at the bottom, the lines correspond to expansions up to order $\delta^7$, $\delta^8$, $\delta^{10}$, $\delta^9$ and the known expansion from $\delta = 1$ respectively.

$\delta^{10}$ using $\frac{m}{M} \approx \frac{1}{205}$ there is about a 13% difference between the full result and the expansion.

When the third order corrections are considered though, an accuracy of 10% - 20% would actually lead to a useful estimate of the full result. This is mainly due

to the fact that the size of the correction to the muon decay rate will likely be on the same order as the current experimental error. If it turns out to be the case that the corrections are actually larger than expected, this estimate would highlight the need for a more accurate calculation of this correction.

## 7.2 Features of the Expansion

At third order, $\mathcal{O}(\alpha^3)$, there are 249 five-loop Feynman diagrams that need to be computed. On top of this, each diagram is expanded asymptotically in the limit $\delta = 1 - \frac{m}{M} \approx 0$. In Chapter 6 a few of the features of this calculation were mentioned that result in making it much easier than if the diagrams had been expanded in the limit $\frac{m}{M} \approx 0$. One of these simplifying features was the fact that the purely hard region does not contribute because this region is real. In general, there are $2^{\#\text{ of loops -1}}$ regions that need to be considered. Remember, the neutrino loop is computed exactly so the asymptotic expansion is carried out on one fewer loops. At third order, getting rid of the purely hard region means that there are 15 regions to consider. Having to compute 249 diagrams 15 times over presents a challenge so let's look for a way to simplify the calculation further.

Before finding further simplifications, one important point must be made. The external momentum can be routed through the loops in a diagram in various ways. In this kinematic region, however, a very specific routing is convenient to use otherwise some regions can be missed. The condition that needs to be met is to have the external momentum pass through all massive lines. To see why this is helpful, consider the expansion of an electron propagator when the loop momentum, $k$, is soft. Without the external momentum, $p$, flowing though this propagator

$$[k^2 + m^2] = [k^2 + M^2(1-\delta)^2] \to [M^2]. \tag{7.5}$$

This makes the integral over $k$ scaleless and thus does not contribute. However, if the external momentum flows through the propagator, the expansion gives

$$[k^2 + 2p\cdot k + p^2 + m^2] = [k^2 + 2p\cdot k - M^2 + M^2(1-\delta)^2] \to [2p\cdot k - 2M^2\delta]. \tag{7.6}$$

As seen in Chapter 6, a propagator like this is not scaleless.

Note that the requirement for the external momentum to flow through all massive propagators includes any fermion loops that appear in the diagram. Normally, this is an unnecessary step that complicates the evaluation of the integral. In this case, however, it provides a check to make sure all of the regions have been accounted for. With these points taken into consideration the following simplifications become apparent.

To start, consider the diagrams with fermion loops. These diagrams can be further simplified by taking a closer look at the propagator structure and what happens after expanding. For a concrete example, consider the propagator structure that comes from the diagram in Figure 7.4. If the electron loop in the diagram is considered, it is seen that only those two propagators involve the loop momenta $k_3$. The $k_3$ integral would look like,

$$\int \frac{d^D k_3}{(2\pi)^D} \frac{1}{[(k_3+p)^2+m^2][(k_2+k_3+p)^2+m^2]}. \tag{7.7}$$

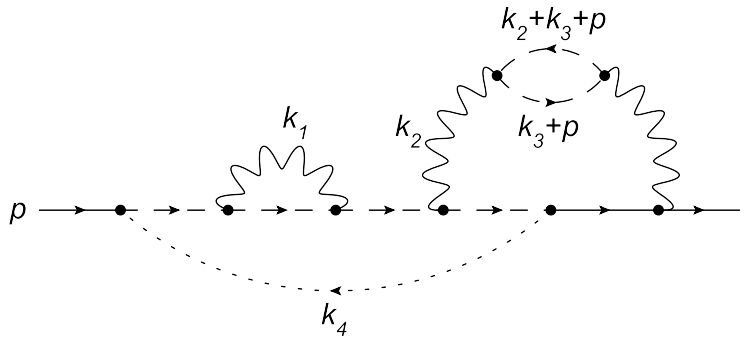


**Figure 7.4:** A third order diagram contributing to muon decay. The solid and dashed lines indicate muons and electrons respectively while the wavy lines indicate photons and the dotted line corresponds to the neutrino loop. The relevant momenta are labeled.

Carrying out the asymptotic expansion such that $k_3$ is soft and, for simplicity, $k_2$ is hard, gives

$$\int \frac{d^D k_3}{(2\pi)^D} \frac{1}{[2k_3 \cdot p - M^2\delta]}. \tag{7.8}$$

Equation 6.38 shows that this integral is zero because there is no massless propagator $k_3^2$. Note that the absence of the massless propagator is what makes this integral scaleless so considering the case where $k_2$ is hard would not change anything. In general, this will be true for any case as long as the momentum flowing through the fermion loop is soft (in this case $k_3$). Thus, regions where the fermion loop momentum is soft do not need to be considered. For diagrams with two fermion loops, only two regions need to be considered and for diagrams with a single fermion loop there are four regions to consider. With about one third of the diagrams having at least one fermion loop, this simplifies the calculation a considerable amount.

Next, a closer look is taken at the loop involving the neutrino line. It is possible to show that if the momentum flowing through this loop is hard, the resulting soft integral will be scaleless. To see this, lets look at the possible types of massive propagators that will appear.

$$\text{electron soft } k \quad : \quad [k^2 + 2p \cdot k + p^2 + m^2] \to [2p \cdot k - 2M^2\delta] \tag{7.9}$$

$$\text{muon soft } k \quad : \quad [k^2 + 2p \cdot k] \to [2p \cdot k] \tag{7.10}$$

$$\text{electron hard } k \quad : \quad [k^2 + 2p \cdot k + p^2 + m^2] \to [k^2 + 2p \cdot k] \tag{7.11}$$

$$\text{muon hard } k \quad : \quad [k^2 + 2p \cdot k], \tag{7.12}$$

where $p^2 = -M^2$. Now, the loop that includes the massless neutrino line only has electron propagators (other than the neutrino propagator). If the neutrino loop momentum is hard, the only types of propagators contributing to the soft region then are muon and photon propagators. Any electron propagator contributing to the soft region would be part of a fermion loop, which as just seen leads to a scaleless integral anyway. This means that when the neutrino momentum is hard, the only types of propagators that can appear in the soft region are,

$$k^2 \quad \text{and} \quad [2p \cdot k], \tag{7.13}$$

leading to a scaleless integral. This argument also works when there are more loop momenta to consider. Applying this condition gets rid of half of the original set of regions leaving at most eight that must be considered.

## 7.3 Calculation Methods

One of the requirements of carrying out a large calculation such as this is to automate the procedure as much as possible. For this problem, a private set of libraries written by M. Czakon is used to generate the diagrams and required information for the asymptotic expansion. These libraries generate `FORM` code that define the diagrams in such a way that the Feynman rules can be applied and asymptotic expansions carried out. The routing of the momenta in each diagram is also automatically determined using conservation of momentum at each vertex. In order to avoid any human error, custom routines have also been written in `FORM` for the neutrino integral, soft integrals and asymptotic expansions. All of these routines can be generally applied to any diagram of any order in $\alpha$ for the muon decay rate. The one exception to this is four-loop soft integrals which, as shall be seen soon, do not follow the same behaviour as soft integrals with three-loops or less. In this case, Czakon's libraries can be used to apply integration by parts (IBP) relations and simplify these four-loop soft integrals. These routines have been tested by re-computing all previous results from tree-level to $\mathcal{O}(\alpha^2)$.

Other than the four-loop soft integrals, the other step that is not completely automated is the hard integrals. Fortunately, routines have been implemented in `FORM` to carry out up to three-loop on-shell integrals. A package called `SHELL3` is used which has been used in various three-loop problems [73, 74, 75] All that needs to be done to use this package is to map the momenta from the diagram definitions from our code to the definitions required by `SHELL3`.

### Iterative integrals and IBP

In the process of carrying out this calculation, a situation came up that does not occur in the calculation of the $\mathcal{O}(\alpha^2)$ corrections. At the NNLO order, all soft integrals could be completed using an iterative integration procedure. For example, consider the following two-loop integral,

$$I = \int \frac{d^D k_1 d^D k_2}{(k_1)^2 (k_2)^2 [2p \cdot k_1 + 2\delta p^2][2p \cdot k_2 + 2\delta p^2][2p \cdot (k_1 + k_2) + 2\delta p^2]}. \tag{7.14}$$

This represents a worst case scenario for the second order calculation as it requires the most complex treatment of any integral. The integral is symmetric with respect to $k_1$ and $k_2$ so without loss of generality, lets take a look at the $k_1$ integral first. Finding a way to write this in the form of Equation 6.33 so that the result of that integral can be used would be best. The first problem encountered is that there are three propagators involving $k_1$ instead of two.

$$I = \int \frac{d^D k_1}{(k_1)^2 [2p \cdot k_1 + 2\delta p^2][2p \cdot (k_1 + k_2) + 2\delta p^2]}. \tag{7.15}$$

This problem can be easily circumvented by using partial fractions on the two massive-type propagators.

$$\frac{1}{[2p\cdot k_1+2\delta p^2][2p\cdot(k_1+k_2)+2\delta p^2]} = \frac{1}{[2p\cdot k_2]}\left(\frac{1}{[2p\cdot k_1+2\delta p^2]} - \frac{1}{[2p\cdot(k_1+k_2)+2\delta p^2]}\right) \quad (7.16)$$

This splits the integral into two terms, each of which only have two propagators involving $k_1$. Note that if the propagators appeared with larger powers, this relation could be introduced multiple times until the integral becomes a sum where each term only involves one of the two propagators.

The two $k_1$ integrals needed are

$$I_1 = \int \frac{d^D k_1}{(k_1)^2[2p\cdot k_1+2\delta p^2]}, \quad (7.17)$$

$$I_2 = \int \frac{d^D k_1}{(k_1)^2[2p\cdot k_1+2p\cdot k_2+2\delta p^2]}. \quad (7.18)$$

The first of these matches exactly the form of Equation 6.33, while the second integral is only slightly more complicated. In the case of $I_2$ the terms that don't depend on $k_1$ in the second propagator are grouped into a single term $\Delta = 2p\cdot k_2 + 2\delta p^2$. This makes the relation between Equation 6.33 and $I_2$ a bit more clear. The result of the integral ends up being proportional to $[2p\cdot k_2 + 2\delta p^2]$ instead of just $(2\delta p^2)$. Notice that the term in the result that depends on $k_2$ is exactly the same as the massive-type propagator from the original integral. This means that the $k_2$ integral becomes

$$I \propto \int \frac{d^D k_2}{(k_2)^2[2p\cdot k_2][2p\cdot k_2+2\delta p^2]^{a_1}}. \quad (7.19)$$

Here the factor of $[2p\cdot k_2]$ from the partial fractions has been included.

Typically, there would be an option of carrying out the integral as is or using partial fractions to simplify the integral. In this case however, partial fractions cannot be used because $a_1$ can depend on $\epsilon$, thus $a_1$ will never be zero. This means that the integral must be evaluated as is. Fortunately, the integral can be solved for general powers in much the same way as the eOne integral in Equation 6.33.

The above example shows the most difficult case encountered in the NNLO calculation. At third order, however these techniques do not work all of the time. It is possible for the propagators that appear to be of a form where partial fractioning will lead to no simplification. In particular, it will not produce integrals where the iterative integration technique that is outlined above can be applied. The integrals always end up in a form similar to

$$I = \int \frac{d^D k}{(2\pi)^D} \frac{1}{(k^2)^{n_1}[2p\cdot k+\Delta_1]^{n_2}[2p\cdot k+\Delta_2]^{n_3}} \quad (7.20)$$

As is, this integral can be solved for general powers of the propagators. The result is a hypergeometric function that depends on $\Delta_1$ and $\Delta_2$. This presents a problem when $\Delta_1$ and $\Delta_2$ depend on other loop momenta.

One way to further simplify the initial integral is to use integration by parts identities. Using this technique it may be possible to reduce the power of one or

more propagators to zero. This gives a better chance of being able to rewrite the initial integral in terms of integrals that can be solved using the iterative procedure. In the worst case scenario, this reduction leads to a small set of master integrals with terms similar to Equation 7.20 but with definite powers in the propagators. Techniques such as Mellin-Barnes or sector decomposition can then be used to compute the master integrals. This integration by parts procedure is, as will be seen, unfortunately the bottleneck in the calculation.

## 7.4 Results

Here, the currently available results for the $\mathcal{O}(\alpha^3)$ corrections to the muon decay rate are presented. The computational resources and time required for this calculation are not insignificant and are ultimately what will limit the accuracy of the final result. These time requirements mean that the computation is ongoing and only a subset of the final results are known. Note, however, that the only obstacle in the full calculation is the computing time required. All of the integrals and procedures needed have been implemented and successfully tested. In order to demonstrate the difficulty present in this calculation, some of the computing resources needed are looked at.

### Computing Resources

The first step in the calculation is to take traces and integrate the neutrino loop. Since this step is the same for each region that needs to be considered, it can be done separately. The results are stored in files that take up a total of 5GB for all 249 diagrams.

From here, each region needs to computed individually. To carry out the expansions as quickly as possible, a threaded version of `FORM` appropriately called `TFORM` is used. Using 12 cores, the expansion of all diagrams in all regions to the first two orders takes approximately two weeks. In all cases except for the purely soft region, the soft integrals are carried out in this step. It is possible for single regions to use 100GB of RAM when only the first two orders of the expansion are included. This does not really limit how high the expansion can be carried out as `FORM` will automatically use hard disk space when there is not enough RAM present. One important check that is carried out is to make sure that the sum of diagrams is gauge independent. Including the gauge dependence increases the size of the calculation dramatically. At a maximum, one region of a single diagram wrote over 994GB of data to temporary files while carrying out the soft integrals. This calculation was done with only the first order in the expansion included! The calculation would likely run out of disk space if it needed to be run to higher order.

The limiting step in this calculation is generating the integration by parts identities that are needed for the reduction of the four-loop soft integrals. For this step, there are 742 'prototype' integrals that identities need to be generated for. Fortunately, the identities for each of these prototypes can be generated separately enabling the use of large clusters to complete this step. Even with this massive parallelization, the longest running instance took 22 days to complete. In total, 3.12 years of computer time have been used with 3 897 849 400 identities generated. The bugaboo cluster on WestGrid was used which has nodes with either four or six core

processors running at 2.66GHz. As well, individual generation routines used over 20GB of RAM when running. This came close to using up all of the 24GB available per node. Finally, the identities are written to database files which total in size at 254GB. All of the above numbers are used to compute only the first two orders in the mass expansion. Clearly, in order to expand to higher orders, more time and RAM is required. Note that the $b$-decay calculation was ultimately limited by hard drive space which at the time was around 500GB.

Fortunately there is a way to further parallelize this by separating it into two steps. The first step generates the identities and writes them to files. This step can be run on more than one processor and uses very little RAM so that it is possible to take full advantage of the WestGrid resources. The second step reads the identity files and carries out any simplifications the can be done. This step can only use a single processor for each prototype and uses much more RAM. In order to deal with this, the second step can be run on local machines which have approximately 1-200GB of RAM. This has been set up and is currently running to obtain higher orders in the mass expansion.

### Master Integrals

In this calculation, there are two types of integrals. The first are the soft integrals with massless and eikonal propagators, and the second are the hard on-shell integrals. In the hard case, up to three-loop integrals appear and there end up being just six master integrals needed as shown in Figure 7.5. In the soft case, there is the master

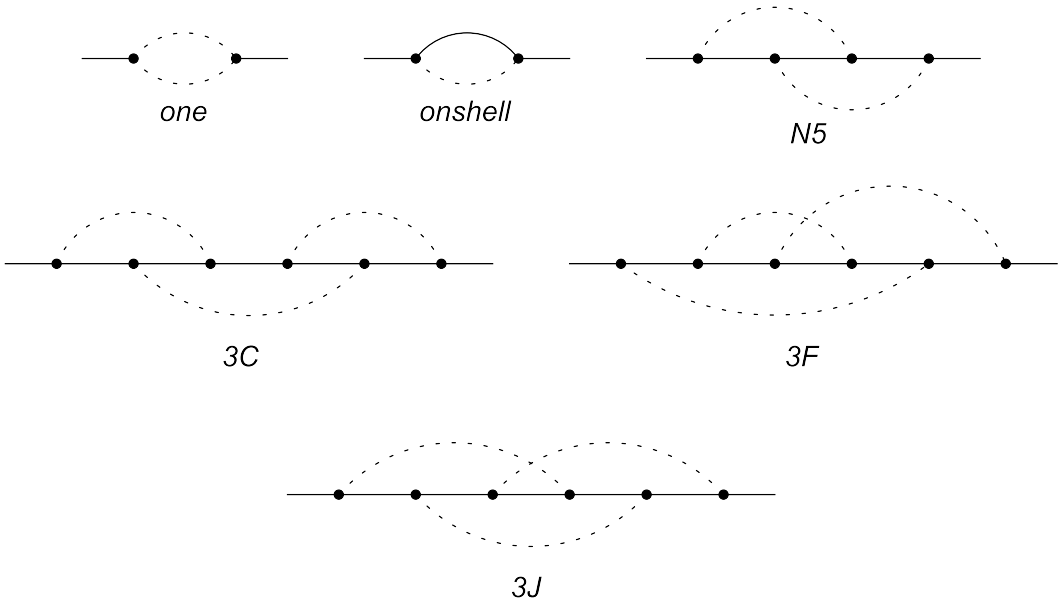


**Figure 7.5:** Master integrals for the hard loops. The solid lines are massive and the dotted lines are massless. The names are given according to the integration routines used.

integral eOne that is solved for general powers in addition to thousands of four-loop master integrals with fixed powers.

## Current Results

In Chapter 6 the results were presented in terms of the colour factors $C_A, C_F, T_F$ and $n_l$. In QED, these colour factors have values of $C_F = T_F = 1$ and $C_A = n_l = 0$ so it would not make much sense to present the results here in a similar fashion. If, however, the fact that the result here is a subset of the $(\mathrm{N})^3\mathrm{LO}$ semileptonic $b$-quark decay corrections is taken into account, it makes sense to keep these factors so that future calculations can make use of this result. For completeness, the muon decay rate is given by,

$$\Gamma(\mu \to e\overline{\nu}_e\nu_\mu) = \Gamma_0 \left[ X_0 + \frac{\alpha}{\pi} C_F X_1 + \left(\frac{\alpha}{\pi}\right)^2 C_F X_2 + \left(\frac{\alpha}{\pi}\right)^3 C_F X_3 + \ldots \right], \quad (7.21)$$

where

$$\Gamma_0 = \frac{G_F^2 m_\mu^5}{192\pi^3}, \quad (7.22)$$

$X_0$, $X_1$ are given in Chapter 6 and $X_2$ can be obtained from the results in Chapter 6 by setting $C_A$ and $n_l$ to zero. The factor $X_3$ is further parametrized by

$$X_3 = C_F^2 X_F + C_F T_F (X_\mu + X_e) + T_F^2 (X_{\mu\mu} + X_{\mu e} + X_{ee}), \quad (7.23)$$

where $X_F$ refers to contributions from diagrams with no muon or electron loops, and the other $X_i$'s refer to contributions from diagrams with one or two muon and electron loops.

All known results are presented here except for the case of diagrams with two fermion loops. For simplicity, only the first two orders of those results are presented here with the full results included in Appendix F.

$$X_{\mu\mu} = \delta^5 \left( -\frac{1688}{27} + \frac{256}{5}\zeta_3 \right) + \delta^6 \left( -\frac{4}{9} - \frac{128}{45}\pi^2 + \frac{128}{5}\zeta_3 \right) \quad (7.24)$$

$$X_{\mu e} = \delta^5 \left( -\frac{3376}{27} + \frac{512}{5}\zeta_3 \right) + \delta^6 \left( \frac{952}{9} + \frac{128}{15}\pi^2 - \frac{768}{5}\zeta_3 \right) \quad (7.25)$$

$$X_{ee} = \delta^5 \left( -\frac{1688}{27} + \frac{256}{5}\zeta_3 \right) + \delta^6 \left( \frac{956}{9} + \frac{512}{45}\pi^2 - \frac{896}{5}\zeta_3 \right) \quad (7.26)$$

$$X_e = \delta^5 \left( \frac{3539}{135} - \frac{5632}{405}\pi^2 + \frac{16}{25}\pi^4 + \frac{512}{45}\pi^2 \ln(2) - \frac{128}{15}\pi^2 \ln^2(2) \right.$$
$$\left. \frac{128}{15}\ln^4(2) + \frac{1024}{5}a_4 - \frac{568}{9}\zeta_3 \right) \quad (7.27)$$

$$X_\mu = \delta^5 \left( \frac{3539}{135} - \frac{5632}{405}\pi^2 + \frac{16}{25}\pi^4 + \frac{512}{45}\pi^2 \ln(2) - \frac{128}{15}\pi^2 \ln^2(2) \right.$$
$$\left. \frac{128}{15}\ln^4(2) + \frac{1024}{5}a_4 - \frac{568}{9}\zeta_3 \right) \quad (7.28)$$

$$(7.29)$$

Here, the symbol $a_4$ refers to the multiple polylogarithm $\mathrm{Li}(4, \frac{1}{2})$. The calculation to higher orders is under way and will be published when available.

It is important to be sure these results are accurate if they are to be used to estimate the size of the corrections to the physical decay rate. As discussed in

Chapter 6 if the form factor $\eta_A$ is known in the limit of equal $b$-quark(muon) and $c$-quark(electron) masses, it is possible to extract the first two orders of the corrections to the decay rate. The contribution to $\eta_A$ at $\mathcal{O}(\alpha_s^3)$ is actually known [73] so it should be possible to match the results presented above to these corrections providing a valuable check of their accuracy. Again, the authors of [73] used $\alpha_s(\sqrt{m_c m_b})$ which translates to $\alpha(\sqrt{m_e m_\mu})$ for muon decay. Running the coupling constant to $\alpha(m_\mu)$ allows a proper comparison of both results. This procedure has been carried out and it is found that the results here do indeed match the terms found from [73].

As another check, the leading orders of the known results were computed using a general gauge. The disappearance of this gauge parameter provides another check of the results. Note that only the leading orders were checked as including higher order terms would lead to expressions so large that the available disc space is exhausted.

## 7.5 Estimate Of The Decay Rate

Although the calculation is not yet complete, it is possible to use the known results to provide an estimate of the size of the physical corrections to the decay rate. In particular, it will be useful to estimate a lower bound for the absolute value of the correction. This lower bound would then give the smallest expected correction to the decay rate, and ultimately $G_F$.

To do this, at least the first order of $X_F$ will be needed. Fortunately, the form factor calculated in [73] can provide this. In fact, it is possible to obtain the first two orders of all terms using this method. For completeness, both orders will be provided in Appendix F with the leading order of the $X_F$ term given here:

$$\begin{aligned} X_F &= \delta^5 \left( -\frac{967}{30} - \frac{256}{3} a_4 + \frac{476}{45}\pi^2 - \frac{28}{45}\pi^4 - \frac{96}{5}\pi^2 \ln(2) + \frac{32}{9}\pi^2 \ln^2(2) \right. \\ &\quad \left. -\frac{32}{9}\ln^4(2) + \frac{1208}{5}\zeta_3 + \frac{56}{5}\pi^2\zeta_3 - 128\zeta_5 \right). \end{aligned} \tag{7.30}$$

Two methods will be used to estimate the physical decay rate. For the first method, consider the ratio between the full correction at the value $\delta = \frac{m_e}{m_\mu}$ and the value of the leading order of the expansion around $\delta = 1 - \frac{m_e}{m_\mu}$ at some small value of $\delta$ say, $\delta = 0.01$ for the tree level, and $\mathcal{O}(\alpha, \alpha^2)$ corrections. At a value of $\delta = 0.01$ the leading order of the expansion is accurate to 1% for all three contributions. The

| | Tree Level | NLO | NNLO |
|---|---|---|---|
| Full Correction | 1.000 | $-1.808$ | 6.664 |
| Leading Order | $1.28 \times 10^{-9}$ | $-9.6 \times 10^{-10}$ | $1.806 \times 10^{-9}$ |
| Ratio | $1.28 \times 10^{9}$ | $1.88 \times 10^{9}$ | $3.69 \times 10^{9}$ |

**Table 7.1:** A comparison between the full corrections to the muon decay and the leading order contribution from an expansion around $\delta = 0$ at tree level, first order and second order in $\alpha$.

values are shown in Table 7.1. As is, the numbers don't seem to mean anything. A closer look at the ratios, however, seems to indicate that the value of the ratio increases by approximately a factor of two every time the order of $\alpha$ is increased.

Another important property to notice is that the full correction and leading order always have the same sign. Assuming these trends hold, a lower bound on the $\alpha^3$ corrections would be obtained by multiplying the leading order correction, evaluated at $\delta = 0.01$ by $3.69 \times 10^9$. The factor of two is left out so as to provide a reasonable bound of

$$X_3 \approx -5. \tag{7.31}$$

This is a sizeable result and warrants a check with a different method.

The second method that will be used relies on the first two orders of the mass expansion. Figure 7.6 shows the $\mathcal{O}(\delta^5)$, $\mathcal{O}(\delta^6)$, and full corrections to the muon decay rate at all known orders. To be clear, the $\mathcal{O}(\delta^5)$ correction includes just the $\delta^5$ term and the $\mathcal{O}(\delta^6)$ correction includes both the $\delta^5$ and $\delta^6$ terms. A few general properties are apparent from these plots. First, the corrections up to $\mathcal{O}(\delta^5)$ have the same sign as the full result. This was seen in the previous estimate as well. Second and more importantly, the full result always lies between these two corrections and even seems to be located close to the mid-point. In fact, the thin solid line in the plots in Figure 7.6 shows the plot of the mid-point. As can be seen, this line follows the full result very closely. In the NLO and NNLO plots, this estimate is within 35% of the full result at the worst. Applying this to the $(\mathrm{N})^3\mathrm{LO}$ terms gives the plot in Figure 7.7. The estimate using this method is

$$X_3 \approx -6. \tag{7.32}$$

Both approximation methods discussed here give similar estimates. This shows that the correction $X_3$ is very likely close to $-6$. Based on the analysis presented in the second method, a conservative error is 50% giving a final estimate of

$$X_3 \approx -6 \pm 3. \tag{7.33}$$

Including this correction in the determination of $G_F$, it is found to shift the central value between $-0.02$ and $-0.07$ppm. This is an order of magnitude smaller than the current error in [17]. For the contribution to be large enough to get to the 0.1ppm level, $|X_3|$ would need to be larger than 13 which is roughly double the estimate given here.

In this chapter a method of calculating the $\mathcal{O}(\alpha^3)$ corrections has been presented. Results were given for some of the contributions, particularly those that come from diagrams with fermion loops, with the rest of the contributions still being calculated. Using the relation between the form factor $\eta_A$ and the muon decay rate, it was possible to obtain the first two orders in the mass expansion of all terms contributing to $X_3$. This allowed two estimates of the physical value of the decay rate, with both giving similar values. Although it is found that the change in $G_F$ due to this correction is small, any future measurements that improve on the lifetime of the muon given in [17] will need to take these $\mathcal{O}(\alpha^3)$ corrections into account.

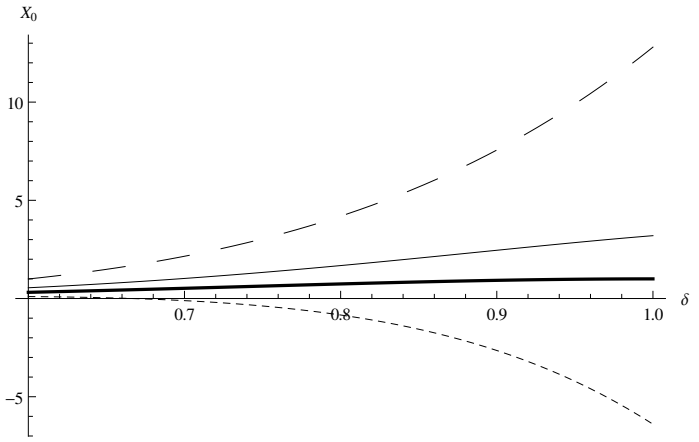


(a) Tree Level

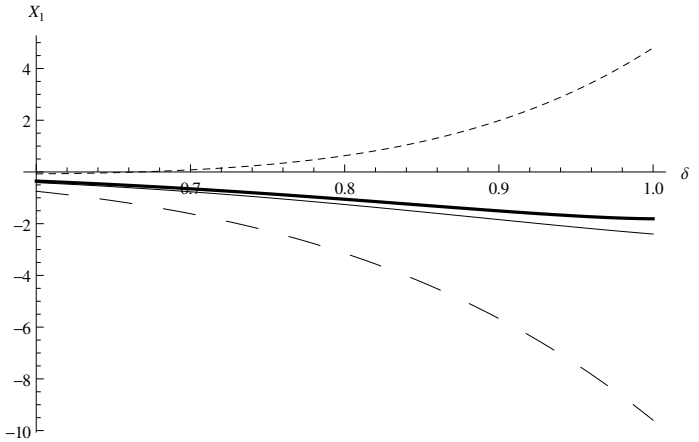


(b) NLO

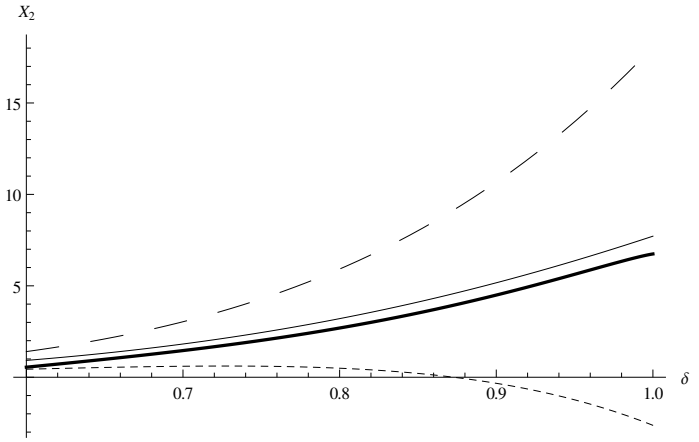


(c) NNLO

**Figure 7.6:** Plots of different order contributions to the muon decay rate at tree level, $\mathcal{O}(\alpha)$ and $\mathcal{O}(\alpha^2)$. The dashed and dotted lines indicate the corrections up to $\mathcal{O}(\delta^5)$ and $\mathcal{O}(\delta^6)$ respectively. The thick solid line shows the full known results while the thin solid lines show the mid-point between the two expansions.

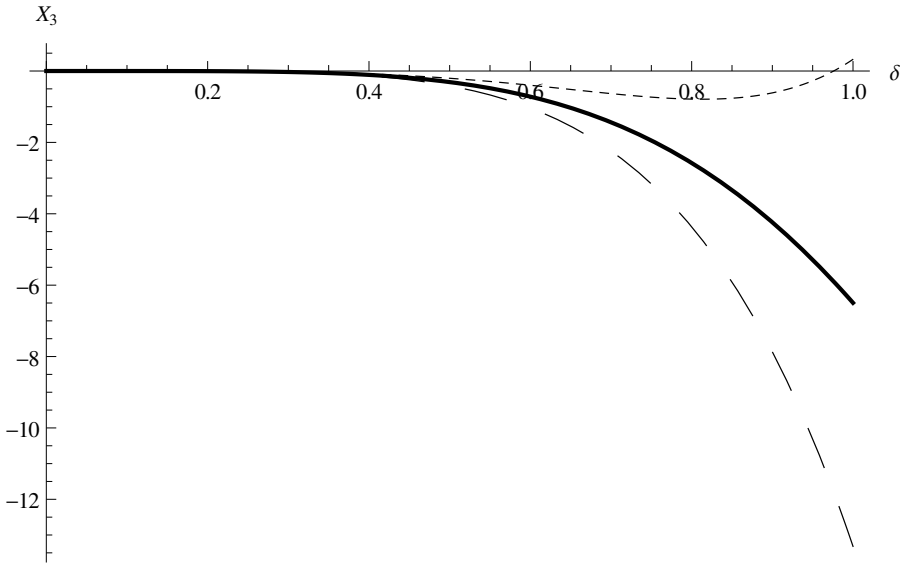


**Figure 7.7:** This plot shows the expansion of $X_3$ to first order and second order in $\delta$. The dashed line corresponds to the $\mathcal{O}(\delta^5)$ expansion and the dotted line corresponds to the $\mathcal{O}(\delta^6)$ expansion. The solid line shows the midpoint between these two expansions and approximates the full $\mathcal{O}(\alpha^3)$ corrections to the decay rate of a muon.

# Chapter 8

# Conclusion

One of the main focuses in particle physics today is the search for new physics. In addition to the more direct methods employed at colliders like the LHC and Tevatron, it is possible to search for new physics by looking for its effects in precision measurements. These high precision measurements require very precise predictions from theory. Most importantly, the fundamental constants that the measurements and theory depend on must be known as precisely as possible. In an effort to aid in this endeavour high order corrections to the standard processes used to extract the most precise values of various fundamental constants have been considered.

Another main goal of this thesis was to show how well developed techniques in field theory could be used to produce results that have previously been difficult to obtain. In Chapters 3 and 4 loop integral techniques were applied to problems where historically only atomic physics methods had been used. This approach led to an improvement of the precision of the $\mathcal{O}(\alpha^2(Z\alpha)^5)$ contributions to the Lamb shift by an order of magnitude. In Chapter 5 a new kind of muon decay was considered that required the use of full solutions to the electromagnetic Dirac equation as opposed to a perturbative approach. The results provide the theoretical foundation for a different method of searching for a new massless boson called a Majoron. Finally, in Chapters 6 and 7 corrections to the decay rates of two related processes in a new kinematic configuration are considered. Although the kinematic limit considered seems to be an inappropriate choice at first glance, a number of significant simplifications are found. These features allowed an accurate description of the second order corrections to semileptonic $b$-decay as well as access the $(\mathrm{N})^3\mathrm{LO}$ corrections to muon decay.

The calculation of Lamb shift corrections was looked at in Chapter 3 using modern techniques developed in particle physics instead of the atomic theory procedures that had been used previously. Compared to previous calculations of the $\mathcal{O}\left(\alpha^2(Z\alpha)^5\right)$ corrections, this approach provided a few advantages. One advantage was the ability to use dimensional regularization allowing explicit calculation of the $\epsilon$ poles. In [18, 19] the calculations were done in the Fried-Yenni gauge to avoid the $\epsilon$ poles. This gauge has the property that individual Feynman diagrams are infrared finite and thus the poles do not appear. Using this property, it is possible to carry out the calculations numerically for each diagram. With dimensional regularization and the techniques outlined in Chapter 2 the calculation could be carried out in a general gauge.

The calculation was reduced to the evaluation of 32 master integrals. It was possible to obtain almost half of these master integrals analytically, improving the previous result by close to two orders of magnitude. In addition, four new analytic results for individual diagrams were found. These improvements give a full correction to the energy of

$$\delta E = \frac{\alpha^2 (Z\alpha)^5}{\pi n^3} \left(\frac{\mu}{m}\right) m[-6.86100(4)], \tag{8.1}$$

as compared to

$$\delta E = \frac{\alpha^2 (Z\alpha)^5}{\pi n^3} \left(\frac{\mu}{m}\right) m[-6.861(1)], \tag{8.2}$$

from [18, 19].

Finally, the set of master integrals providing this result appears in the calculation of the same order correction to the bound electron $g$-factor. Re-calculating the corrections to the Lamb shift provides an important check of the methods used as well as values of the master integrals.

In Chapter 4 the leading order contribution at all orders in $Z\alpha$, known as the Breit correction, was reproduced as a starting point. A procedure for computing the $\mathcal{O}\left(\alpha(Z\alpha)^5\right)$ corrections was then described following the same methodology used in the Lamb shift. Work is continuing on evaluating the contributions at $\mathcal{O}\left(\alpha(Z\alpha)^5\right)$.

The goal of Chapter 5 was to provide the theoretical background needed by experiments to search for a new particle called the Majoron. The introduction of the Majoron comes from considering the possibility of neutrinos having a Majorana mass. Building this into the SM theory by assuming a global symmetry breaking causes the Majoron to emerge.

With the Majoron interacting very weakly with SM particles, it is argued that the best method of searching for them is in the high energy region of the electron energy spectrum in bound muon decays. In this region the SM decay of the muon has a suppression proportional to $(E_{\mu e} - E_e)^5$. It is shown that the Majoron decay does not follow this same suppression and is instead proportional to $(E_{\mu e} - E_e)^3$. As well, by expanding to leading order in $\alpha$ it was argued that a perturbative calculation would not provide an accurate estimate of the electron spectrum. For this reason, the calculation of the the spectrum had to include effects such as the finite size of the nucleus, full relativistic wave functions and the recoil of the nucleus.

Using data from the SINDRUM II collaboration, an upper limit of the branching ration of the decay $\mu \to eJ$ was found to be

$$B(\mu \to eJ) < 3 \times 10^{-3}\,(90\% C.L.). \tag{8.3}$$

This is approximately three orders of magnitude larger than the current limit

$$B(\mu \to eJ) < 8.4 \times 10^{-6}. \tag{8.4}$$

As the SINDRUM II data is unable to produce a more stringent limit, future experiments Mu2e and COMET were considered to estimate the limits they may be able to provide for the Majoron branching ratio. It was found that, with current design parameters, it may be possible to match the current limit and an upper limit of

$$B(\mu \to eJ) < 1.9 \times 10^{-5} \tag{8.5}$$

was estimated for both experiments. An increase in sensitivity with proposed upgrades would likely enable the experiments to place a more stringent limit on the branching ratio than is currently available. In order to allow these upper limits to be extracted from the data in the future, fits to the endpoint spectra for the three nuclei considered: aluminum, titanium and gold were provided.

In Chapters 6 and 7 the related decays of a $b$-quark to a $c$-quark and leptons and a muon to electron and neutrinos were considered. The $\mathcal{O}(\alpha_s^2)$ corrections to the $b$-quark semileptonic decay rate were presented. These corrections were previously computed numerically and analytically in [61] and [72] respectively. The approach used was to compute the corrections in the opposite limit to that of [72], namely around $\delta = (1 - \frac{m_e}{m_\mu}) \approx 0$.

This new kinematic configuration provided some surprising simplifications to the calculation as compared to that of [72]. One of the first simplifications was the fact that the purely hard region (the region where all loop momenta are large) does not contribute. This has the consequence of removing three-loop on-shell integrals from the calculation. In fact, the full calculation was reduced to five different integrals with at most two loops.

Another advantage of carrying out the calculation in this limit is that the expansion in $\delta$ converges well to the full result. Combined with the fact that the leading order in the expansion is proportional to $\delta^5$, this allowed a confirmation of the expansion in [72] with very good accuracy. The results were even able to reproduce an unusual local maximum in the mass spectrum of the contribution from diagrams with a $b$-quark loop that appears around $\delta = 0.8$. In the end the result was within 2.5% of the full result at a value of $\delta = 1$ demonstrating the fast convergence of this expansion.

Perhaps the most important consequence of this calculation is that the simplifications and convergence provide a method of computing the next order in the decay rate. Indeed, this calculation led directly to the muon decay rate calculation in Chapter 7 as all of the simplifying properties are general and hold at all orders.

In Chapter 7 it was argued that the $\mathcal{O}(\alpha^3)$ corrections to the muon decay rate could very well be of the same size as the linear mass correction at order $\alpha^2$ found in [72]. Consequently, the $(\text{N})^3\text{LO}$ correction will be important in a proper determination of the SM parameter $G_F$. During this calculation it was found that the purely soft integrals (when all loop momenta are small) do not fully benefit from the nesting procedure that was implemented in the $b$-decay calculation. This makes the calculation more difficult because, even with IBPs, a large number of master integrals must be calculated. As well, the expansion of these five-loop diagrams produces a large number of terms causing the limits provided by the computing hardware used to be a limiting factor. Nevertheless, results for diagrams with one and two fermion loops have been provided. Combining these with results extracted from the $\mathcal{O}(\alpha_s^3)$ corrections to the form factor $\eta_A$ made it possible to provide an estimate for the full corrections at the physical value of $\frac{m_e}{m_\mu}$ of

$$X_3 \approx -6 \pm 3. \tag{8.6}$$

This was seen to change the value of $G_F$ by between -0.02 and -0.07ppm. Although this is an order of magnitude smaller than the current error, this result will be important in any future measurements that improve on the precision of the lifetime of the muon.

With these results, the effectiveness of the methods used has been shown. The methods used are not specific to the problems considered so it will be possible in the future to compute other required high order corrections with them. For example, the method of computing the bound electron $g$-factor and Lamb shift can be used to compute higher order corrections of both effects. It should be possible to use the master integrals from the $\mathcal{O}(\alpha^2(Z\alpha)^5)$ contribution to the Lamb shift to compute the similar order correction of the bound electron $g$-factor. In addition, the methods used in the Lamb shift calculation can be used at order $\mathcal{O}(\alpha^3(Z\alpha)^5)$. One of the main difficulties in that calculation would be the evaluation of the four loop master integrals once the reduction is complete.

A major portion of the contributions to the $\mathcal{O}(\alpha_s^3)$ corrections to semileptonic $b$-quark decay will be complete when the muon calculation is finished. It should also be possible to compute the non-abelian and massless loop parts. The three and four gluon vertices provide a complication making these diagrams the most difficult part of the $\mathcal{O}(\alpha_s^3)$ corrections.

This thesis has concentrated on high order corrections to a few of the fundamental constants in the SM. It has been shown how the application of methods based on loop calculations can be successfully applied to problems in atomic physics. As well, the calculation of heavy to light decays similar to the decay of a muon has been made possible by considering a new kinematic configuration. The methods developed in this thesis will help searches for new physics by allowing a comparison of ever more precise theoretical predictions and experimental results.

The endeavour to probe the standard model at high precision is one that gets more and more difficult with every step forward. It is exciting to be able to provide methods that allow the state of the art measurements of fundamental constants to be pushed beyond their current limits. I hope the methods presented here will continue to be useful in providing a means to make these steps forward however small or large they may be.

# Bibliography


[1] G. Aad *et al.*, (2012), hep-ex/1207.7214.

[2] S. Chatrchyan *et al.*, (2012), hep-ex/1207.7235.

[3] P. J. Mohr, B. N. Taylor, and D. B. Newell, (2012), atom-ph/1203.5425.

[4] R. Pohl *et al.*, Nature **466**, 213 (2010).

[5] R. J. Hill and G. Paz, Phys. Rev. **D82**, 113005 (2010), hep-ph/1008.4619.

[6] R. J. Hill and G. Paz, Phys.Rev.Lett. **107**, 160402 (2011), hep-ph/1103.4617.

[7] R. Feynman, Phys. Rev. **76**, 769 (1949).

[8] J. S. Schwinger, Phys. Rev. **74**, 1439 (1948).

[9] J. S. Schwinger, Phys. Rev. **75**, 651 (1948).

[10] F. Dyson, Phys. Rev. **75**, 486 (1949).

[11] T. Aoyama, M. Hayakawa, T. Kinoshita, and M. Nio, (2012), hep-ph/1205.5368.

[12] D. Hanneke, S. F. Hoogerheide, and G. Gabrielse, (2010), atom-ph/1009.4831.

[13] S. Lundeen and F. Pipkin, Phys. Rev. Lett. **46**, 232 (1981).

[14] E. Hagley and F. Pipkin, Phys. Rev. Lett. **72**, 1172 (1994).

[15] N. Ramsey, *Molecular Beams* (Clarendon Press, 1956).

[16] K. Pachucki, A. Czarnecki, U. D. Jentschura, and V. A. Yerokhin, Phys. Rev. **A72**, 022108 (2005), physics/0506227.

[17] D. Webber *et al.*, Phys. Rev. Lett. **106**, 041803 (2011), hep-ex/1010.0991.

[18] M. I. Eides and V. A. Shelyuto, Phys. Rev. **A52**, 954 (1995), hep-ph/9501303.

[19] K. Pachucki, Phys. Rev. **A48**, 2609 (1993).

[20] S. Laporta, Int. J. Mod. Phys. **A15**, 5087 (2000), hep-ph/0102033.

[21] T. Gehrmann and E. Remiddi, Nucl. Phys. **B601**, 248 (2001), hep-ph/0008287.

[22] T. Binoth and G. Heinrich, Nucl. Phys. **B585**, 741 (2000), hep-ph/0004013.

[23] G. Heinrich, Int. J. Mod. Phys. **A23**, 1457 (2008), hep-ph/0803.4177.

[24] A. Smirnov and M. Tentyukov, Comput. Phys. Commun. **180**, 735 (2009), hep-ph/0807.4129.

[25] W. E. Lamb and R. C. Retherford, Phys. Rev. **72**, 241 (1947).

[26] H. A. Bethe, Phys. Rev. **72**, 339 (1947).

[27] M. I. Eides, H. Grotch, and V. A. Shelyuto, *Theory of Light Hydrogenic Bound States* (Springer, 2007).

[28] I. R. Blokland, *Multiloop calculations in perturbative quantum field theory*, PhD thesis, University of Alberta, 2004.

[29] A. Smirnov, JHEP **0810**, 107 (2008), hep-ph/0807.3243.

[30] M. Baranger, H. A. Bethe, and R. P. Feynman, Phys. Rev. **92**, 482 (1953).

[31] R. Karplus, A. Klein, and J. Schwinger, Phys. Rev. **86**, 288 (1952).

[32] M. Dowling, J. Mondejar, J. H. Piclum, and A. Czarnecki, Phys. Rev. **A81**, 022509 (2010), hep-ph/0911.4078.

[33] A. Czarnecki and B. Krause, Nucl. Phys. Proc. Suppl. **51C**, 148 (1996), hep-ph/9606393.

[34] G. Breit, Nature **122**, 1 (1928).

[35] S. G. Karshenboim, Phys. Lett. **A266**, 380 (2000).

[36] U. D. Jentschura, (2009), hep-ph/0904.0835.

[37] J. Goldstone, A. Salam, and S. Weinberg, Phys. Rev. **127**, 965 (1962).

[38] M. Hirsch, A. Vicente, J. Meyer, and W. Porod, Phys. Rev. **D79**, 055023 (2009), hep-ph/0902.0525.

[39] A. Masiero and J. Valle, Phys. Lett. **B251**, 273 (1990).

[40] X. Garcia i Tormo, D. Bryman, A. Czarnecki, and M. Dowling, Phys. Rev. **D84**, 113010 (2011), hep-ph/1110.2874.

[41] R. D. Bayes, *Measurement of the decay parameter rho and a search for non-Standard Model decays in the muon decay spectrum*, PhD thesis, University of Victoria, 2010.

[42] A. Czarnecki, X. Garcia i Tormo, and W. J. Marciano, Phys. Rev. **D84**, 013006 (2011), hep-ph/1106.4756.

[43] R. Carey *et al.*, Proposal to search for $\mu N \to eN$ with a single event sensitivity below $10^{-16}$, 2008.

[44] Y. Cui *et al.*, Conceptual design report for experimental search for lepton flavor violating mu- - e- conversion at sensitivity of $10^{-16}$ with a slow-extracted bunched proton beam (COMET), 2009.

[45] M. Rose, *Relativistic Electron Theory* (Wiley, 1961).

[46] O. U. Shanker, Phys. Rev. **D25**, 1847 (1982).

[47] W. H. Bertl *et al.*, Eur. Phys. J. **C47**, 337 (2006).

[48] H. De Vries, C. De Jager, and C. De Vries, Atom. Data Nucl. Data Tabl. **36**, 495 (1987).

[49] http://www-d0.fnal.gov/Run2Physics/limit_calc/limit_calc.html .

[50] Particle Data Group, J. Beringer *et al.*, Phys. Rev. **D86**, 010001 (2012).

[51] D. Benson, I. Bigi, T. Mannel, and N. Uraltsev, Nucl. Phys. **B665**, 367 (2003).

[52] M. Dowling, J. H. Piclum, and A. Czarnecki, Phys. Rev. **D78**, 074024 (2008), hep-ph/0810.0543.

[53] I. R. Blokland, A. Czarnecki, M. Slusarczyk, and F. Tkachov, Phys. Rev. **D71**, 054004 (2005), hep-ph/0503039.

[54] A. Czarnecki and K. Melnikov, Phys. Rev. Lett. **88**, 131801 (2002), hep-ph/0112264.

[55] A. Pak, I. R. Blokland, and A. Czarnecki, Phys. Rev. **D73**, 114009 (2006), hep-ph/0604233.

[56] A. Czarnecki and K. Melnikov, Phys. Rev. Lett. **78**, 3630 (1997), hep-ph/9703291.

[57] M. Dowling, A. Pak, and A. Czarnecki, Phys. Rev. **D78**, 074029 (2008), hep-ph/0809.0491.

[58] A. Czarnecki and K. Melnikov, Phys. Rev. **D59**, 014036 (1999), hep-ph/9804215.

[59] A. Czarnecki and K. Melnikov, Nucl. Phys. **B505**, 65 (1997), hep-ph/9703277.

[60] M. E. Dowling, *Second order corrections to semileptonic b-quark decay*, Master's thesis, University of Alberta, 2008.

[61] K. Melnikov, Phys. Lett. **B666**, 336 (2008), hep-ph/0803.0951.

[62] A. Pak and A. Czarnecki, Phys. Rev. **D78**, 114015 (2008), hep-ph/0808.3509.

[63] A. Pak, unpublished.

[64] E. Bagan, P. Ball, and P. Gosdzinsky, Phys. Lett. **B301**, 249 (1993), hep-ph/9209277.

[65] Y. Nir, Phys. Lett. **B221**, 184 (1989).

[66] A. Czarnecki, Phys. Rev. Lett. **76**, 4124 (1996), hep-ph/9603261.

[67] S. Neddermeyer and C. Anderson, Phys. Rev. **51**, 884 (1937).

[68] B. Rossi and D. B. Hall, Phys. Rev. **59**, 223 (1941).

[69] U. Jentschura, Annals Phys. **326**, 500 (2011), hep-ph/1011.5275.

[70] U. Jentschura, Annals Phys. **326**, 516 (2011), hep-ph/1011.5453.

[71] T. van Ritbergen and R. G. Stuart, Nucl. Phys. **B564**, 343 (2000), hep-ph/9904240.

[72] A. Pak and A. Czarnecki, Phys. Rev. Lett. **100**, 241807 (2008), hep-ph/0803.0960.

[73] J. P. Archambault and A. Czarnecki, Phys. Rev. **D70**, 074016 (2004), hep-ph/0408021.

[74] K. Melnikov and T. van Ritbergen, Phys. Lett. **B482**, 99 (2000), hep-ph/9912391.

[75] K. Melnikov and T. van Ritbergen, Phys. Rev. Lett. **84**, 1673 (2000), hep-ph/9911277.

[76] P. Nogueira, J. Comput. Phys. **105**, 279 (1993).

[77] R. Harlander, T. Seidensticker, and M. Steinhauser, Phys. Lett. **B426**, 125 (1998), hep-ph/9712228.

[78] T. Seidensticker, (1999), hep-ph/9905298.

[79] J. A. M. Vermaseren, (2000), math-ph/0010025.

[80] Y. Chikashige, R. N. Mohapatra, and R. Peccei, Phys. Lett. **B98**, 265 (1981).

[81] Y. Chikashige, G. Gelmini, R. Peccei, and M. Roncadelli, Phys. Lett. **B94**, 499 (1980).

[82] S. Bekavac, A. Grozin, D. Seidel, and M. Steinhauser, JHEP **0710**, 006 (2007), hep-ph/0708.1729.

[83] K. Melnikov and T. van Ritbergen, Nucl. Phys. **B591**, 515 (2000), hep-ph/0005131.

[84] P. Marquard, L. Mihaila, J. Piclum, and M. Steinhauser, Nucl. Phys. **B773**, 1 (2007), hep-ph/0702185.

# Appendix A

# Lamb Shift

## A.1 Master Integrals

The Lamb shift calculation can be reduced to the evaluation of 32 master integrals. The topologies are shown here along with the results for each master integral.

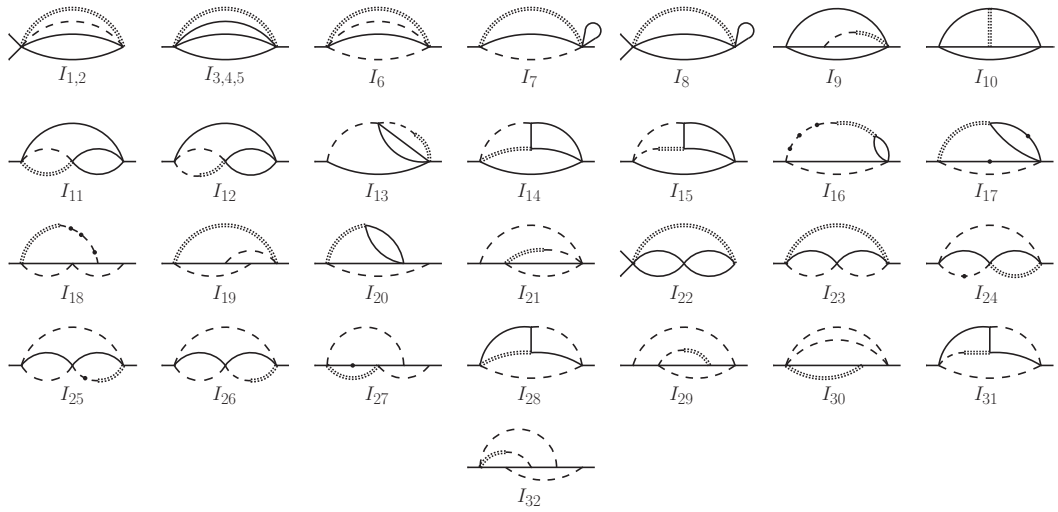


**Figure A.1:** Master integrals for the Lamb shift. Solid lines correspond to massive propagators, dashed lines correspond to massless propagators and the double dotted lines correspond to the ph3D propagator. A dot on a line indicates higher powers of that propagator.

In all of the above results, it should be assumed that an expansion in $\epsilon$ was carried out and that higher order terms exist. The only terms where this does not apply are the results where the full dependence on $\epsilon$ is shown.

$$I_1 = 2e^{3\gamma_E\epsilon}\,\frac{\Gamma(1-\epsilon)\Gamma^2\left(-\frac{3}{2}+2\epsilon\right)\Gamma\left(-\frac{1}{2}+\epsilon\right)\Gamma\left(-\frac{5}{2}+3\epsilon\right)}{\Gamma(-3+4\epsilon)}\,, \tag{A.1}$$

$$I_2 = -2I_1\,, \tag{A.2}$$

$$I_3 = -96.17464240774249 4299(1) - 3003.97283051743374945(1)\epsilon \\ -16370.644886761701890(1)\epsilon^2 - 204040.09217878970569(1)\epsilon^3\,, \tag{A.3}$$

$$
\begin{aligned}
I_4 &= 128.23285654365665907(1) + 4005.2971073565783326(1)\epsilon \\
&\quad +21827.526515682269186(1)\epsilon^2 + 272053.45623838627426(1)\epsilon^3\,, \qquad \text{(A.4)}\\
I_5 &= 213.37528929773859515(1) - 1789.0076495990746772(1)\epsilon\,, \qquad \text{(A.5)}\\
I_6 &= 2\sqrt{\pi}e^{3\gamma_E\epsilon}\,\frac{\Gamma^2(1-\epsilon)\Gamma\left(-\frac{5}{2}+3\epsilon\right)\Gamma\left(-\frac{3}{2}+2\epsilon\right)\Gamma\left(\frac{9}{2}-5\epsilon\right)}{\Gamma(2-2\epsilon)\Gamma(3-3\epsilon)}\,, \qquad \text{(A.6)}\\
I_7 &= 2\sqrt{\pi}e^{3\gamma_E\epsilon}\,\frac{\Gamma(-1+\epsilon)\Gamma\left(-\frac{3}{2}+2\epsilon\right)\Gamma\left(\frac{5}{2}-3\epsilon\right)\Gamma(-\frac{1}{2}+\epsilon)}{\Gamma(2-2\epsilon)}\,, \qquad \text{(A.7)}\\
I_8 &= 2\sqrt{\pi}e^{3\gamma_E\epsilon}\,\frac{\Gamma(-1+\epsilon)\Gamma\left(-\frac{3}{2}+2\epsilon\right)\Gamma^2\left(-\frac{1}{2}+\epsilon\right)}{\Gamma(-1+2\epsilon)}\,, \qquad \text{(A.8)}\\
I_9 &= -\frac{8\pi^2}{\epsilon} - 257.35053226188(1) - 2952.9668342496406(4)\epsilon\,, \qquad \text{(A.9)}\\
I_{10} &= -420.49901(1) + 1860.837(4)\epsilon\,, \qquad \text{(A.10)}\\
I_{11} &= 2^{3-4\epsilon}\pi e^{3\gamma_E\epsilon}\,\frac{\Gamma\left(\epsilon-\frac{1}{2}\right)}{\cos\left(2\pi\epsilon\right)}\left[2\frac{\Gamma\left(\frac{5}{2}-3\epsilon\right)\Gamma\left(\epsilon\right)}{\Gamma\left(4-4\epsilon\right)}\,{}_3F_2\left(1,\frac{5}{2}-3\epsilon,\epsilon;\frac{3}{2},4-4\epsilon;1\right)\right.\\
&\quad \left.-\sqrt{\pi}\frac{\Gamma\left(1-\epsilon\right)\Gamma\left(3\epsilon-\frac{3}{2}\right)}{\Gamma\left(\frac{5}{2}-2\epsilon\right)\Gamma\left(2\epsilon\right)}\,{}_3F_2\left(1,1-\epsilon,3\epsilon-\frac{3}{2};\frac{5}{2}-2\epsilon,2\epsilon;1\right)\right]\,, \qquad \text{(A.11)}\\
I_{12} &= -\frac{4\pi^2}{\epsilon} - 24\pi^2 - \frac{4\pi^4}{3} + \pi^2\left(-116 - \frac{59}{3}\pi^2 + 32\ln(2) + 100\zeta_3\right)\epsilon\,, \qquad \text{(A.12)}\\
I_{13} &= -263.74028719521945979(1) + 1741.1125810306205720(1)\epsilon\,, \qquad \text{(A.13)}\\
I_{14} &= -362.8560(1)\,, \qquad \text{(A.14)}\\
I_{15} &= 36.969282(2)\,, \qquad \text{(A.15)}\\
I_{16} &= \pi^2\left(-\frac{513}{128\epsilon} - \frac{11077}{768} - \frac{571}{16}\ln(2) + 32\sqrt{5}\ln\left(\frac{1+\sqrt{5}}{2}\right)\right)\\
&\quad -1889.3810189605726842(1)\epsilon - 2199.2559561980712031(1)\epsilon^2\,, \qquad \text{(A.16)}\\
I_{17} &= \frac{32\pi^2}{\sqrt{5}}\ln\left(\frac{1+\sqrt{5}}{2}\right) - 683.43054120051764110(1)\epsilon\\
&\quad +5647.2496334930969112(1)\epsilon^2\,, \qquad \text{(A.17)}\\
I_{18} &= \pi^2\left[\frac{343}{512\epsilon} + \frac{125257}{46080} - \frac{2}{3}\pi^2 + \frac{169}{192}\ln(2) + 16\ln^2(2)\right.\\
&\quad \left.-48\ln^2\left(\frac{1+\sqrt{5}}{2}\right)\right]\,, \qquad \text{(A.18)}\\
I_{19} &= -293.4480(2)\,, \qquad \text{(A.19)}\\
I_{20} &= \pi^2\left[-\frac{2}{\epsilon} - 2 - \frac{8}{3}\pi^2 + 16\sqrt{5}\ln\left(\frac{1+\sqrt{5}}{2}\right) + 32\ln^2\left(\frac{1+\sqrt{5}}{2}\right)\right]\\
&\quad +1394.0754186124348755(1)\epsilon\,, \qquad \text{(A.20)}\\
I_{21} &= 2\pi^2 - \frac{4\pi^4}{3} + \pi^2\left(44 - 4\pi^2 + 80\zeta_3\right)\epsilon\,, \qquad \text{(A.21)}\\
I_{22} &= -\frac{128\pi^2}{3} - \pi^2\left(\frac{1792}{3} + \frac{256}{3}\pi - \frac{1024}{3}\ln(2)\right)\epsilon\,, \qquad \text{(A.22)}
\end{aligned}
$$

$$
\begin{aligned}
I_{23} &= \frac{2\pi^3 e^{3\gamma_E\epsilon}}{\Gamma^2(2-2\epsilon)\,\Gamma\left(\frac{3}{2}-\epsilon\right)}\left[2^{2\epsilon-2}\frac{\Gamma(1-\epsilon)\,\Gamma\left(\epsilon-\frac{1}{2}\right)}{\sin(\pi\epsilon)\cos(4\pi\epsilon)}\right.\\
&\left(\frac{\Gamma\left(\frac{7}{2}-5\epsilon\right)\sin(\pi\epsilon)}{\Gamma\left(\frac{5}{2}-3\epsilon\right)\sin(2\pi\epsilon)\cos(3\pi\epsilon)}-\frac{\Gamma\left(3\epsilon-\frac{3}{2}\right)}{\Gamma\left(5\epsilon-\frac{5}{2}\right)\cos(2\pi\epsilon)}\right)\\
&+\frac{\sqrt{\pi}\,\Gamma(2-2\epsilon)\,\Gamma\left(2\epsilon-\frac{1}{2}\right)}{\Gamma(2-\epsilon)\,\Gamma\left(3\epsilon-\frac{1}{2}\right)\sin(\pi\epsilon)\cos(\pi\epsilon)\cos(3\pi\epsilon)}\\
&\times{}_3F_2\left(1,2-2\epsilon,2\epsilon-\frac{1}{2};2-\epsilon,3\epsilon-\frac{1}{2};1\right)\\
&-\frac{2^{1-2\epsilon}\pi\,\Gamma\left(\frac{5}{2}-3\epsilon\right)}{\Gamma\left(\frac{5}{2}-2\epsilon\right)\Gamma\left(\frac{1}{2}+\epsilon\right)\sin(2\pi\epsilon)\cos(\pi\epsilon)\cos(2\pi\epsilon)}\\
&\left.\times\,{}_3F_2\left(1,\frac{5}{2}-3\epsilon,\epsilon;\frac{5}{2}-2\epsilon,2\epsilon;1\right)\right]\,, \qquad \text{(A.23)}\\
I_{24} &= \frac{2\pi^2}{\epsilon}-162.745878930257(1)+640.681562239(2)\epsilon\\
&-9490.745115169417(3)\epsilon^2\,, \qquad \text{(A.24)}\\
I_{25} &= -\frac{4\pi^2}{\epsilon}-192.3546921335253(1)-2297.18352848038(1)\epsilon\\
&-10356.58582995624(1)\epsilon^2\,, \qquad \text{(A.25)}\\
I_{26} &= -\frac{4\pi^2}{\epsilon}-244.4995291143211(3)-2339.54007847666(2)\epsilon\,, \qquad \text{(A.26)}\\
I_{27} &= 136.8086023(2)-907.048(2)\epsilon\,, \qquad \text{(A.27)}\\
I_{28} &= -280.62418(1)+734.494(1)\epsilon\,, \qquad \text{(A.28)}\\
I_{29} &= 118.63826101784(1)\,, \qquad \text{(A.29)}\\
I_{30} &= -10\sqrt{\pi}e^{3\gamma_E\epsilon}\,\frac{\Gamma(\epsilon)\,\Gamma^2(1-\epsilon)\,\Gamma\left(\frac{5}{2}-5\epsilon\right)\Gamma\left(-\frac{3}{2}+3\epsilon\right)}{\Gamma(2-2\epsilon)\,\Gamma\left(\frac{7}{2}-4\epsilon\right)}\\
&\times{}_3F_2\left(\frac{7}{2}-5\epsilon,\frac{3}{2}-\epsilon,-\frac{1}{2}+\epsilon;\frac{7}{2}-4\epsilon,\frac{1}{2}+\epsilon;1\right)\,, \qquad \text{(A.30)}\\
I_{31} &= 49.3616(1)\,, \qquad \text{(A.31)}\\
I_{32} &= 26.272804(6)+291.1097(1)\epsilon\,, \qquad \text{(A.32)}
\end{aligned}
$$

Analytical results for a few of the diagrams were obtained which did not fit in Table 3.1. For completeness, they are presented here.

$$
\begin{aligned}
\text{Diagram } b &= \frac{111}{8}-\pi^2-9\ln(2)+24\ln^2(2)\\
&+\frac{48}{\sqrt{5}}\ln\left(\frac{1+\sqrt{5}}{2}\right)-72\ln^2\left(\frac{1+\sqrt{5}}{2}\right), \qquad \text{(A.33)}\\
\text{Diagram } c &= -\frac{352897}{27000}+\frac{31}{45}\pi^2-\frac{643}{225}\ln(2)-\frac{248}{15}\ln^2(2)\\
&+\frac{104}{9\sqrt{5}}\ln\left(\frac{1+\sqrt{5}}{2}\right)+\frac{248}{5}\ln^2\left(\frac{1+\sqrt{5}}{2}\right). \qquad \text{(A.34)}
\end{aligned}
$$

$$
\text{Set II} = \frac{67282}{6615}-\frac{2}{9}\pi^2+\frac{628}{63}\ln(2)
$$

$$-\frac{872}{63}\sqrt{5}\ln\left(\frac{1+\sqrt{5}}{2}\right)+\frac{8}{3}\ln^2\left(\frac{1+\sqrt{5}}{2}\right), \tag{A.35}$$

$$\text{Set III} \;=\; \frac{15647}{13230}-\frac{25}{63}\pi+\frac{52}{63}\ln(2)\,. \tag{A.36}$$

# Appendix B

# calc3 setup and Use

For the calculation of the Lamb shift and bound $g$-factor corrections a set of packages is used to generate, identify, reduce, and integrate the expressions that appear. The package `qgraf` [76] was used to generate the diagrams. The output was fed to the packages `q2e` and `exp` [77, 78] to express the diagrams in terms of `FORM` [79] readable code. From here, a list of contributing integrals is fed into the Laporta reduction package `FIRE` [29] so that the result can be expressed in terms of a small number of master integrals. The integration of these master integrals is done with custom made routines. The purpose of this appendix is to describe the setup and use of these programs in the context of the Lamb shift and $g$-factor.

## B.1 Setup

The first step in setting up the package is to obtain and install the executables that are needed. `qgraf` can be obtained at `http://cfif.ist.utl.pt/~paulo/qgraf.html` and needs to be compiled with a Fortran compiler. The programs `q2e` and `exp` are private programs that are needed for expansions and `FORM` code generation. These executables should be in a directory that the `$PATH` environment variable points to so that they can be run from any directory.

Next, the `calc3` directories need to be set up. The top directory is `calc3` and can be named as desired. Inside this directory are folders containing `FORM` files for integration. Three of these are the packages `SHELL3, matad` and `mincer`. The other three folders are `common`, `generic`, and `problems`. The `common` folder contains `FORM` routines that are common to all problems such as declarations, averaging routines and one-loop integrals. The `generic` folder contains the `FORM` files that run the calculation and sum the diagrams. Finally, the `problems` folder contains the problems that one wants to calculate using this setup each in separate folders. In order to find the files in all of these folders, the environment variable `FORMPATH` should point to these folders. The folders that are required are `common` and the folder where the topology integration files are kept (these will be discussed in the next section). If the packages `SHELL3, matad` and/or `mincer` are going to be used, `FORMPATH` should also point to these folders. For `matad` and `mincer`, it should point to the `prc` and `inc` folders. A convenient way to implement this is to create a custom exactable that will set the form path before running form.

For the calculation of the Lamb shift and bound $g$-factor, the Mathematica pack-

age FIRE is also used. This can be downloaded from http://www-ttp.particle.uni-karlsruhe.de/~asmirnov/FIRE.htm and also requires the Mathematica program IBP.m found at http://www-ttp.particle.uni-karlsruhe.de/~asmirnov/Tools-IBP.htm. These files should be installed in a directory accessible by the local Mathematica installation or in the directory where FIRE will be run from.

## B.2 Problem Folder

The problems folder contains all of the problems that will be solved using this setup. Inside the problem folder (for convenience, it is named gfactor here), there are several files and directories that need to be created. First, qgraf requires a model, style and qgraf.dat file. Instructions for how to create the model and .dat files are included with qgraf. The style file should be the q2e.sty file that is included with the source code for q2e. This ensures that the output from qgraf is in the proper format for use by q2e. At this point, it should be possible to run qgraf.

The next step is to run q2e with the list of diagrams generated by qgraf. In order to properly run q2e though, a configuration file needs to be created along with a file defining the propagators and vertices in the problem. The configuration file simply points to the propagator and vertex files and gives q2e some specific options. The file used for the $g$-factor calculation looks like

```
* q2e.propagator_file ~/calc3/problems/gfactor/gfactor.prop
* q2e.vertex_file ~/calc3/problems/gfactor/gfactor.vrtx
* q2e.mass fe:M1
* q2e.anti_fermion fe:fE
* q2e.closed_fermion_loop fe:nh
* q2e.expand_naive Q2
```

Here, the qgraf field fe is given a mass M1 and q2e is told that its anti-particle partner is named fE. As well, there are rules saying that any closed fermion loop consisting of the field fe should be multiplied by the factor nh and the variable Q2 will be expanded. The vertex and propagator files (gfactor.vrtx and gfactor.prop) define how q2e should handle the propagators and vertices that appear in the diagrams. This defines the functions for the propagators and vertices used in FORM along with their arguments.

In the vertex file, the basic definition of a vertex is

```
{fe,fE,ph:*FT<spin_line>(<lorentz_index_particle_3>)|||}.
```

This defines the vertex between an electron and photon. The option <spin_line> is substituted with the number corresponding to the fermion spin line so that traces can be taken properly in FORM. The <lorentz_index_particle_3> option gives the Lorentz index of the third particle in the list (in this case the photon) as required by the Feynman rules. After this definition, other arguments can be included (for example a function for colour arguments in QCD). The options for this file can be found in the documentation that comes with the exp and q2e package. The propagators are defined in much the same way.

```
{fe,fE:*FT<spin_line>(<momentum>)|||}
```
With these files defined `q2e` can be run with the command

```
q2e -q qlist. -c gfactor.conf -do gfactor.2.dia -eo gfactor.2.edia.
```

This command specifies the `qgraf` output file that will be read into `q2e` and the configuration file. The program produces two files `gfactor.2.dia` and `gfactor.2.edia` that contain `FORM` folds and a simplified list of each diagram respectively. The 2 refers to the two-loop diagrams and serves as a way to distinguish different orders of the calculation.

Before these files can be run through `exp`, two additional files are needed. The first of these is a file that should be named `GLOBAL` and will be added to every diagram source file. It contains various `FORM` folds that carry out operations specific to the problem being considered. In this set-up, the only required fold is the `GLOBAL` fold. This is where the preprocessor definitions and `exp` variables are set. As an example, the `GLOBAL` fold for the factor calculation is:

```
*--#[ GLOBAL :

#define GAUGE "xi"
#define NUMEXTMOM "3"
#define LOOPS "2"

* exp.loops 2
* exp.problem gfactor
* exp.form_command startform3
* exp.formset_file form.set
* exp.makefile_path ~/home/calc3_cz/problems/gfactor/make
* exp.source_file_path ~/home/calc3_cz/problems/gfactor/src

*--#] GLOBAL :
```

Other possible folds include `TREAT0, TREAT1,..., TREAT4`, `TREATMAIN`, `TREATEXP`, `TREATCOL` and `TREATEXP`. They are called at various times during the calculation and are used to include problem specific procedures like renormalization, special projectors, expansions, etc. The order of most calls to these folds can be found in the file `generic/treat` or `common/treat`. After `q2e` is run, this file, typically named `GLOBAL`, should be combined with the `.dia` file generated by `q2e` such that the `GLOBAL` file appears first.

The second file required is a file that defines the topologies in the problem. This allows `exp` to map each diagram to a topology so that the proper integration routines can be used. For some problems, pre-defined topologies may be able to be used (e.g. the `SHELL3` package comes with a file for this), but it is also possible to create a new list or add to an existing list. Starting with any topology file (even an empty one), `exp` can be run and will assign topologies to the diagrams until it is unable to fit a diagram to a topology. `exp` will print out the information for the diagram it is unable to fit to a topology. The topology file can then be built up by adding new

definitions until all diagrams can be mapped to a topology.

The topologies are defined in the following way:

```
{name; n_lines; n_loops; n_external_mom; n_masses; scale_info;
line_info; mass_distribution}
```

For example, the general two loop self-energy topology corresponding to Figure B.1

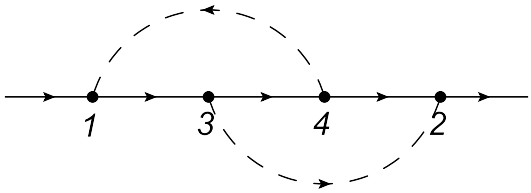


**Figure B.1:** An example two-loop topology. In this appendix it is referred to as twog.

would look like,

```
{twog;5;2;1;1;;(q1:1,2)(p1:1,3)(p2:4,1)(p3:2,3)(p4:4,2)(p5:3,4)
;10011;x0011;100x1}
```

Here, no scale information is required so that part is left blank. The line information is formatted such that the first entry is the external momentum and the following five entries define the internal lines. In general, external momenta should be labeled $q_i$ and internal momenta should be labeled $p_i$. In this example, three mass distributions are given. The first states that the first, fourth and fifth lines have mass $M_1$ and the others are massless. In the next two mass distributions, the `x` means that the corresponding line is not present. Finally, one can run `exp` using the command

```
exp -t topsel.gfactor -ed gfactor.2.edia -dmm gfactor.2.dia -v3
```

where `topsel.gfactor` is the topology file and the other two are the `.edia` and `.dia` files generated by `q2e`. The output is a source file for each diagram containing everything needed for a `FORM` definition of the diagram and a make file that will carry out the calculation. These files are written to the directories defined in the `GLOBAL` fold of the `GLOBAL` file.

The final thing needed to calculate the diagrams is a topology file for each topology defined in the `topsel.gfactor` file. These contain momentum definitions, other expansions that are needed and calls to the integration routines that will be used. In principle, the calculation is ready to go now provided all of the integration routines are in place. The calculation can be run at this point by executing make with the makefile that is created.

## B.3 Lamb Shift and $g$-factor Specific Setup

Some extra steps were needed for the calculation of the Lamb shift and bound $g$-factor. The first of these is the routing of momentum in the $g$-factor diagrams. Occasionally the momentum from the external photon (magnetic field) will be routed through the diagram such that it flows through the photons connecting the electron and nucleus. Since the ph3D propagator is being used for this part of the diagram,

the momentum that flows through it cannot be changed. The solution for this is to re-route the momentum. A short perl script has been created to automatically run through the diagrams and fix the problem. There are only one or two situations in which it is unable to route the momenta properly so the user must go into the files and fix these diagrams manually. The script has been set up to let the user know which diagrams are successful and which need to be changed manually.

Although the program can be successfully run at this point, not much will be done. Files need to be created that tell `FORM` what to do with each topology. These files should have the same name as the topology that they describe. Continuing with the example from the previous section, the file would be named `twog`. This file is called after the setup has finished with the other routines that are automatically run (e.g. Feynman rules, traces, expansions, etc.).

Eventually a reduction routine will be run on the integrals that appear so the topology files are set up to print a list of the integrals required if the preprocessor variable `LAPORTA` is defined. This list can the be used in the Mathematica package `FIRE` to carry out the Laporta reduction. Three different files are used in `FIRE`. One to define the integral, another one to generate the identities and one to write the reduction of each integral in the initial list in a `FORM` compatible format. As an example of how these files are set up, consider the N53d integral from Figure 3.5 that is reproduced here for convenience.

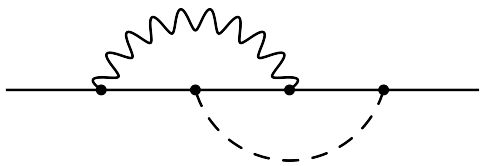

**Figure B.2:** The topology, N53d, required for the $\alpha(Z\alpha)^5$ contribution to the Lamb shift.

First, the integral is defined and the information that `FIRE` needs to carry out the reduction is generated. These steps are put into a single file named `def_N53d` reproduced here.

```
Get["FIRE_3.4.0.m"];
Get["ibp.m"];

Internal = {k1,k2};
External = {p};
Propagators={k1^2,k2^2,k1^2+2*p*k1,k1^2+k2^2+2*(k1+k2)*p+2*k1*k2,
                          2*p*k2};
PrepareIBP[];
reps={p^2->-1};
startinglist={IBP[k1,k1],IBP[k1,k2],IBP[k1,p],IBP[k2,k1],IBP[k2,k2],
                       IBP[k2,p]}/.reps
RESTRICTIONS={{0,0,0,-1,0},{0,0,0,0,-1}};
(* SYMMETRIES={{}}; *)
Prepare[];
SaveStart["N53d"];
```

The first two lines load the routines that will be used into Mathematica. Next, the internal loop momenta and the external momentum is defined. Following this, the propagators are given. The `PrepareIBP[]` command then solves the system of linear equations. Note that for this step to work properly, the terms in the propagators must form a linearly independent system of equations. Occasionally this requires the addition of irreducible numerators to the list. The list of `reps` is composed of rules for replacing certain terms. In this example, the square of the external momentum is set to $-1$. Next, the IBP identities are defined using the function

$$\texttt{IBP[k1,k2]} = \frac{\partial}{\partial k_1^\mu} k_2^\mu. \tag{B.1}$$

The restrictions and symmetries of the integral are then defined and tell `FIRE` when an integral is scaleless or symmetric with respect to a rearrangement of propagators. The restrictions are lists with a zero when a propagator can appear and $-1$ when the propagator is absent or appears in the numerator. They should be defined such that the integral with the allowed propagators is zero. Careful consideration of the restrictions and symmetries can greatly simplify and speed up the reduction. Finally, the system of equations is prepared with `Prepare[]` and the information is saved to a file called `N53d.start`.

Next, the IBP identities are applied to the list of integrals and saved for later use. The file used for this is named `do_N53d` and is reproduced below

```
Get["FIRE_3.4.0.m"];
LoadStart["N53d"];
Burn[];

rnum = 0;
tlist = {};
For[ii = 1,ii < rnum,ii++,tlist=
                Append[tlist,"N53d."<>ToString[ii]<>".tab"]];

If[ 0 =!= Length[tlist],
    LoadTables[tlist];
];

input = OpenRead["./N53d.list"];
expr = Read[input,String];
evlist = {};

While[expr =!= EndOfFile,
      expr = StringReplace[expr,"\n" -> ""];
      expr = ToExpression["{"<>expr<>"}"];
      evlist = Append[evlist,{0,expr}];
      expr = Read[input,String];
  ];
Close[input];

EvaluateAndSave[evlist,"N53d."<>ToString[rnum]<>".tab"];
```

Again, the FIRE routines need to be loaded, but the IBP routines are not required this time because the identities have already been generated. Next, the start file that was created at the end of the previous file is loaded and the reduction is primed using the command Burn[]. This performs some initial setup and optimization for the calculation. The next few arguments look for previously generated tables of identities. This allows new identities to be appended to files that already exist without re-computing the old ones. The final preparation needed before the identities can be evaluated is to read in the list of propagator powers that was created by running FORM. This is accomplished with the lines from "input =" to "Close[input]". The While loop is used to generate the list in the format that is used by FIRE. The file N53d.list had the propagator powers in the form a1,a2,a3,a4,a5 where as FIRE needs them in the form {n,{a1,a2,a3,a4,a5}}. The value n corresponds to the integral number if more than one integral is being evaluated. Only one integral is considered at a time, so this is set to zero. Finally, the IBP identities are evaluated and saved to a table with the command EvaluateAndSave.

This provides the results, but for them to be useful they are needed in a FORM readable format. The table of solutions written at the end of the previous file is not in a format that is useful. As well, the dimension is set to $D = 4 - 2\epsilon$ dimensions so the results need to be expanded in a series in $\epsilon$. This is accomplished with a file named write_N53d.

```
Get["FIRE_3.4.0.m"];

fun = "N53d";
inlist = "N53d.list";
intable = "N53d.0.tab";
outtable = "N53d.inc";
EPLIM = 10;

LoadStart[fun];
Burn[];
LoadTables[intable];

input = OpenRead[inlist];
output = OpenWrite[outtable];

expr = Read[input,String];
cnt = 1;
While[expr =!= EndOfFile,
      expr = StringReplace[expr,"\n" -> ""];
      expr = ToExpression["{"<>expr<>"}"];
      lhs = "id "<>fun<>ToString[expr]<>" = ";
      lhs = StringReplace[lhs,{"{" -> "(", "}" -> ")", ", " -> ","}];

      rhs = F[expr]/.G[a__] :> ToExpression[fun] @@ a;
      rhs = rhs/.d -> 4 - 2*ep;
      rhs = Collect[Normal[Series[rhs,{ep,0,EPLIM}]],ToExpression[fun][___],acc];
      rhs = ToString[InputForm[rhs]];
```

```
      rhs = StringReplace[rhs,{"[" -> "(", "]" -> ")", ", " -> ","}];

      WriteString[output,lhs<>rhs<>";\n"];
      If[0 == Mod[cnt,100],
         WriteString[output,".sort(polyfun=acc);\n"];
     ];
      cnt++;
      expr = Read[input,String];
  ];
Close[input];

If[20 < Mod[cnt,100],
   WriteString[output,".sort(polyfun=acc);\n"];
];
Close[output];
```

For this, the package `FIRE` and access to all of the files that have been created is required. Running `Burn[]` allows the tables of results to be loaded. The `While` loop looks rather complicated and works as follows. First, the list of propagator powers from `N53d.list` is read in and saved to `expr`. This list is written in the form

```
id N53d(a1,a2,a3,a4,a5) =
```

for eventual output to a `FORM` file. Next, the `FIRE` functions $F$ and $G$ are used to solve for the integral in terms of the set of master integrals produced by the IBP reduction. After this, the result is expanded in a series about $\epsilon = 0$ so that `FORM` does not run into any trouble with denominators. Finally, the output is written to a file called `N53d.inc`. Note that `.sort` statements are also included for `FORM` after every 100 replacements. This helps to optimize the evaluation in `FORM`.

In the end, a file called `N53d.inc` is generated that can be used in the topology file. The result of the diagram being calculated can now be expressed in terms of only a few master integrals. From here, the final step is to evaluate the master integrals and plug in the results.

# Appendix C

# Semileptonic $b$-decay

## C.1 Results

The mass expansion for the $\mathcal{O}(\alpha_s^2)$ corrections to the semileptonic decay of a $b$-quark into a $c$-quark is presented here. The parameter $\delta$ is defined by $\delta = 1 - \frac{m_c}{m_b}$. All orders obtained have been included even though the full result is limited to order $\delta^{11}$ because of the non-abelian contribution $X_A$. The notation follows that of Equation 6.40.

$$
\begin{aligned}
X_F \;=\; & \delta^5\left(-\frac{46}{5}+\frac{48}{5}\zeta_3+\frac{32}{5}\pi^2-\frac{32}{5}\pi^2\ln(2)\right)\\
&+\delta^6\left(\frac{69}{5}-\frac{72}{5}\zeta_3-\frac{48}{5}\pi^2+\frac{48}{5}\pi^2\ln(2)\right)\\
&+\delta^7\left(\frac{39329}{3675}+\frac{248}{35}\zeta_3+\frac{3044}{945}\pi^2-\frac{496}{105}\pi^2\ln(2)-\frac{352}{105}\ln(2\delta)\right)\\
&+\delta^8\left(-\frac{34277}{3675}-\frac{8}{7}\zeta_3-\frac{2}{189}\pi^2+\frac{16}{21}\pi^2\ln(2)+\frac{176}{105}\ln(2\delta)\right)\\
&+\delta^9\left(\frac{3860559631}{450084600}+\frac{59}{105}\zeta_3-\frac{77}{486}\pi^2-\frac{118}{315}\pi^2\ln(2)-\frac{821944}{178605}\ln(2\delta)\right.\\
&\qquad\left.+\frac{640}{567}\ln^2(2\delta)\right)\\
&+\delta^{10}\left(\frac{1663522831}{900169200}+\frac{59}{210}\zeta_3-\frac{77}{972}\pi^2-\frac{59}{315}\pi^2\ln(2)-\frac{209372}{178605}\ln(2\delta)\right.\\
&\qquad\left.+\frac{320}{567}\ln^2(2\delta)\right)\\
&+\delta^{11}\left(\frac{1003573027861}{453835305000}+\frac{239}{1155}\zeta_3-\frac{160793}{1871100}\pi^2-\frac{478}{3465}\pi^2\ln(2)\right.\\
&\qquad\left.-\frac{4234786}{3274425}\ln(2\delta)+\frac{512}{945}\ln^2(2\delta)\right)\\
&+\delta^{12}\left(\frac{11734387001723}{5446023660000}+\frac{157}{924}\zeta_3-\frac{167077}{1871100}\pi^2-\frac{157}{1386}\pi^2\ln(2)\right.\\
&\qquad\left.-\frac{12596567}{9823275}\ln(2\delta)+\frac{1504}{2835}\ln^2(2\delta)\right) \qquad \text{(C.1)}
\end{aligned}
$$

$$
\begin{aligned}
X_A &= \delta^5\left(-\frac{286}{15}-\frac{24}{5}\zeta_3-\frac{8}{5}\pi^2+\frac{16}{5}\pi^2\ln(2)\right)\\
&+\delta^6\left(\frac{99}{5}+\frac{36}{5}\zeta_3+\frac{12}{5}\pi^2-\frac{24}{5}\pi^2\ln(2)\right)\\
&+\delta^7\left(-\frac{99547507}{1157625}+\frac{132}{35}\zeta_3+\frac{62206}{33075}\pi^2+\frac{248}{105}\pi^2\ln(2)+\frac{1333376}{33075}\ln(2\delta)\right.\\
&\quad\left.-\frac{256}{315}\pi^2\ln(2\delta)-\frac{1408}{315}\ln^2(2\delta)\right)\\
&+\delta^8\left(\frac{20568622}{385875}-\frac{108}{35}\zeta_3-\frac{57773}{33075}\pi^2-\frac{8}{21}\pi^2\ln(2)-\frac{666688}{33075}\ln(2\delta)\right.\\
&\quad\left.+\frac{128}{315}\pi^2\ln(2\delta)+\frac{704}{315}\ln^2(2\delta)\right)\\
&+\delta^9\left(-\frac{750804877}{83349000}+\frac{23}{70}\zeta_3+\frac{381323}{1190700}\pi^2+\frac{59}{315}\pi^2\ln(2)\right.\\
&\quad\left.+\frac{123248}{33075}\ln(2\delta)-\frac{64}{945}\pi^2\ln(2\delta)-\frac{352}{945}\ln^2(2\delta)\right)\\
&+\delta^{10}\left(-\frac{462489857}{166698000}+\frac{23}{140}\zeta_3+\frac{220043}{2381400}\pi^2+\frac{59}{630}\pi^2\ln(2)\right.\\
&\quad\left.+\frac{61624}{33075}\ln(2\delta)-\frac{32}{945}\pi^2\ln(2\delta)-\frac{176}{945}\ln^2(2\delta)\right)\\
&+\delta^{11}\left(-\frac{21281502607}{9261945000}+\frac{123}{770}\zeta_3+\frac{7361107}{96049800}\pi^2+\frac{239}{3465}\pi^2\ln(2)\right.\\
&\quad\left.+\frac{5498308}{3274425}\ln(2\delta)-\frac{304}{10395}\pi^2\ln(2\delta)-\frac{152}{945}\ln^2(2\delta)\right) \qquad \text{(C.2)}
\end{aligned}
$$

$$
\begin{aligned}
X_l &= \delta^5\left(\frac{56}{15}\right)+\delta^6\left(-\frac{12}{5}\right)\\
&+\delta^7\left(\frac{25577548}{1157625}-\frac{512}{945}\pi^2-\frac{417664}{33075}\ln(2\delta)+\frac{512}{315}\ln^2(2\delta)\right)\\
&+\delta^8\left(-\frac{16877824}{1157625}+\frac{256}{945}\pi^2+\frac{208832}{33075}\ln(2\delta)-\frac{256}{315}\ln^2(2\delta)\right)\\
&+\delta^9\left(\frac{388467053}{187535250}-\frac{128}{2835}\pi^2-\frac{349088}{297675}\ln(2\delta)+\frac{128}{945}\ln^2(2\delta)\right)\\
&+\delta^{10}\left(\frac{218514473}{375070500}-\frac{64}{2835}\pi^2-\frac{174544}{297675}\ln(2\delta)+\frac{64}{945}\ln^2(2\delta)\right)\\
&+\delta^{11}\left(\frac{18247556543}{35658488250}-\frac{608}{31185}\pi^2-\frac{19220056}{36018675}\ln(2\delta)+\frac{608}{10395}\ln^2(2\delta)\right)\\
&+\delta^{12}\left(\frac{491546826713}{998437671000}-\frac{16}{891}\pi^2-\frac{18270172}{36018675}\ln(2\delta)+\frac{16}{297}\ln^2(2\delta)\right)\\
&+\delta^{13}\left(\frac{3361434830933}{7121972607750}-\frac{88}{5265}\pi^2-\frac{1818646}{3764475}\ln(2\delta)+\frac{88}{1755}\ln^2(2\delta)\right)\\
&+\delta^{14}\left(\frac{493896496003601}{1096783781593500}-\frac{6332}{405405}\pi^2-\frac{133364431}{289864575}\ln(2\delta)\right.
\end{aligned}
$$

$$
\begin{aligned}
&+\frac{6332}{135135}\ln^2(2\delta)\Big) \\
&+\delta^{15}\left(\frac{627231045106189}{1462378375458000}-\frac{848}{57915}\pi^2-\frac{5338491967}{12174312150}\ln(2\delta)\right. \\
&\left.+\frac{848}{19305}\ln^2(2\delta)\right) \qquad \text{(C.3)}
\end{aligned}
$$

$$
\begin{aligned}
X_c \;=\;& \delta^5\left(\frac{184}{3}-\frac{32}{5}\pi^2\right)+\delta^6\left(-\frac{828}{5}+\frac{88}{5}\pi^2\right)+\delta^7\left(\frac{108580}{567}-\frac{18968}{945}\pi^2\right) \\
&+\delta^8\left(-\frac{9271088}{99225}+\frac{1922}{189}\pi^2-\frac{1024}{315}\ln(2\delta)\right) \\
&+\delta^9\left(-\frac{124063}{17010}+\frac{1618}{2835}\pi^2\right) \\
&+\delta^{10}\left(\frac{12027229}{396900}-\frac{17147}{5670}\pi^2-\frac{512}{945}\ln(2\delta)\right) \\
&+\delta^{11}\left(-\frac{115761743}{10914750}+\frac{69857}{62370}\pi^2-\frac{512}{945}\ln(2\delta)\right) \\
&+\delta^{12}\left(\frac{8285545}{4939704}-\frac{31873}{249480}\pi^2-\frac{80896}{155925}\ln(2\delta)\right) \\
&+\delta^{13}\left(\frac{284868329}{668918250}-\frac{175}{46332}\pi^2-\frac{77312}{155925}\ln(2\delta)\right) \\
&+\delta^{14}\left(\frac{342856753529}{852201850500}-\frac{25073}{6486480}\pi^2-\frac{6735488}{14189175}\ln(2\delta)\right) \\
&+\delta^{15}\left(\frac{242318342197}{639151387875}-\frac{4813}{1297296}\pi^2-\frac{6461824}{14189175}\ln(2\delta)\right) \qquad \text{(C.4)}
\end{aligned}
$$

$$
\begin{aligned}
X_b \;=\;& \delta^5\left(\frac{184}{3}-\frac{32}{5}\pi^2\right)+\delta^6\left(-12+\frac{8}{5}\pi^2\right)+\delta^7\left(\frac{107444}{2835}-\frac{3848}{945}\pi^2\right) \\
&+\delta^8\left(\frac{37136}{2835}-\frac{1226}{945}\pi^2\right)+\delta^9\left(-\frac{19283}{3402}+\frac{1618}{2835}\pi^2\right) \\
&+\delta^{10}\left(-\frac{6032591}{170100}+\frac{20383}{5670}\pi^2\right)+\delta^{11}\left(-\frac{2500805389}{32744250}+\frac{482687}{62370}\pi^2\right) \\
&+\delta^{12}\left(-\frac{75439453}{582120}+\frac{655189}{49896}\pi^2\right) \\
&+\delta^{13}\left(-\frac{250746622601}{1277025750}+\frac{4608847}{231660}\pi^2\right) \\
&+\delta^{14}\left(-\frac{4967902306483}{17878360500}+\frac{182623657}{6486480}\pi^2\right) \\
&+\delta^{15}\left(-\frac{1230391313243}{3277699425}+\frac{49341749}{1297296}\pi^2\right) \qquad \text{(C.5)}
\end{aligned}
$$

## C.2 Diagrams

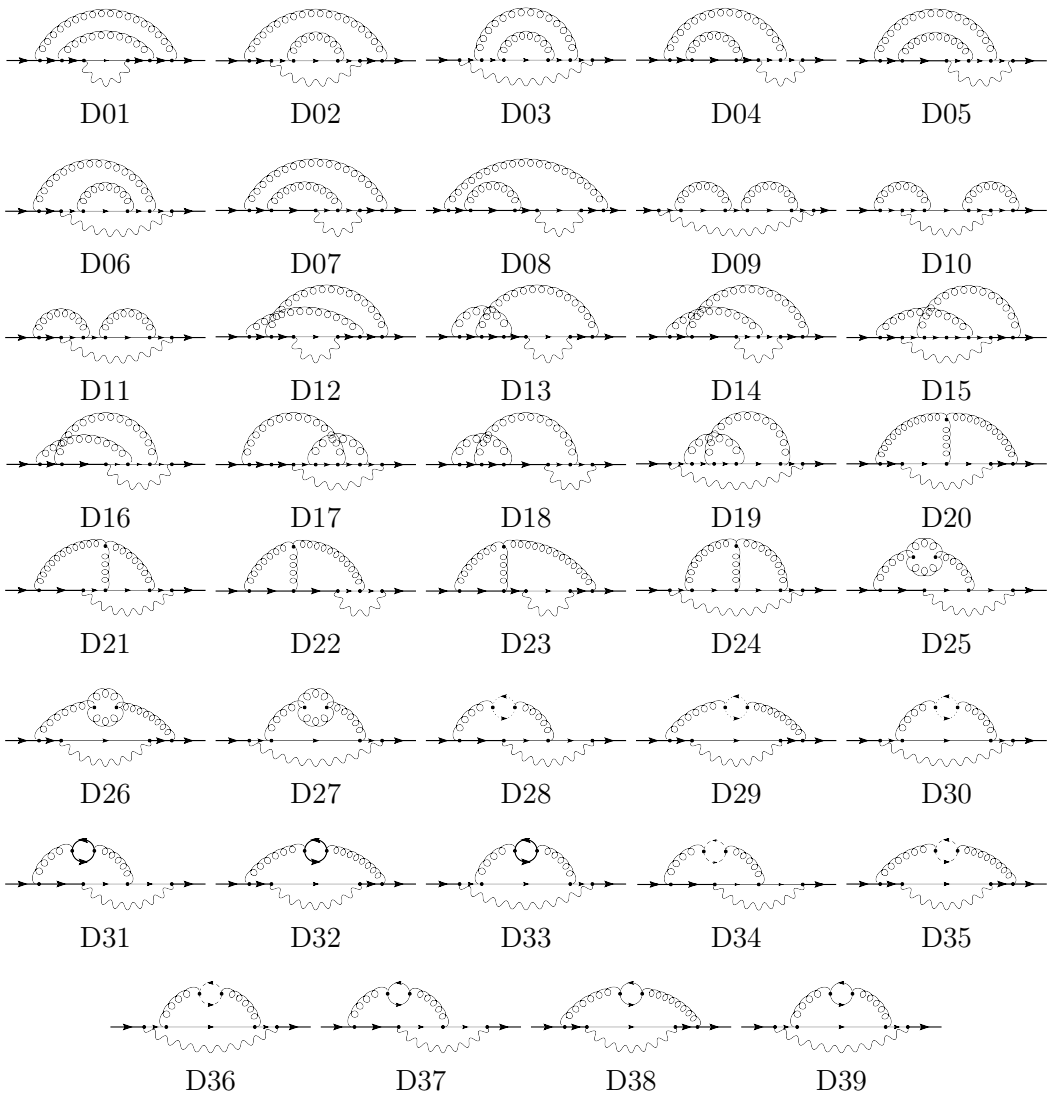


**Figure C.1:** All second order diagrams that needed to be calculated for the semileptonic $b$-decay. The wavy line in each diagram indicates the neutrino loop while the thick lines are $b$-quarks, the thin lines are $c$-quarks, the looped lines are gluons and the dotted lines are ghosts.

# Appendix D

# A Majoron Model

The purpose of this appendix is to introduce a model that results in a Majoron. Models such as this one have been excluded by the invisible $Z^0$ decay width measurements. It is possible, however, to create supersymmetric models that are able to circumvent this limit so that the Majoron is still viable. This theory was developed in [80].

A model with two neutrino states labeled $\nu_L$ and $\nu_R$ is considered. They are arranged such that they are part of a doublet and singlet respectively, $\psi_L = (\nu_L\, e_L^-)$, $\nu_R$. The charge conjugate partners are $\nu_R^C = C(\overline{\nu}_L)^T$ and $\nu_L^C = C(\overline{\nu}_R)^T$, where $C$ is the charge conjugation matrix $i\gamma^2\gamma^0$. A Higgs doublet, $\Phi$, and an additional Higgs singlet, $\varphi$, are introduced and have couplings to the neutrinos given by

$$\mathcal{L}_1 = -h_1 \left( \overline{\psi}_L \Phi \nu_R + \overline{\nu}_R \Phi^\dagger \psi_L \right), \tag{D.1}$$

$$\mathcal{L}_2 = -h_2 \left( \varphi \overline{\nu}_L^C \nu_R + \varphi^\dagger \overline{\nu}_R \nu_L^C \right). \tag{D.2}$$

Note that only the right handed neutrino gets a Majorona mass in this model. When both $\Phi$ and $\varphi$ have non-zero vacuum expectation values the mass terms can be written as

$$\begin{aligned} \mathcal{L}_{mass} &= -\left\{ (\overline{\nu}_L, \overline{\nu}_L^C) \begin{pmatrix} 0 & m \\ m & M \end{pmatrix} \begin{pmatrix} \nu_R^C \\ \nu_R \end{pmatrix} \right. \\ &\quad \left. + (\overline{\nu}_R^C, \overline{\nu}_R) \begin{pmatrix} 0 & m \\ m & M \end{pmatrix} \begin{pmatrix} \nu_L \\ \nu_L^C \end{pmatrix} \right\}, \end{aligned} \tag{D.3}$$

where $m$ is the Dirac mass and $M$ is the Majorana mass. This reconstructs the neutrino parts of $\mathcal{L}_{1,2}$ when multiplied out and the equality $\overline{\nu}_L \nu_R = \overline{\nu}_L^C \nu_R^C$ is used. The equality is realized by explicitly multiplying out the matrices on the right hand side of the equation. Using in the definitions of the conjugate fields, the right hand side becomes

$$\begin{aligned} \overline{\nu}_L^C \nu_R^C &= \left[ \overline{C(\overline{\nu}_R)^T} \right] \left[ C(\overline{\nu}_L)^T \right] && \text{(D.4)} \\ &= (\overline{\nu}_R)^* C^\dagger \gamma^0 C (\overline{\nu}_L)^T && \text{(D.5)} \\ &= (\nu_R)^T \gamma^0 (i\gamma^2\gamma^0)^\dagger \gamma^0 (i\gamma^2\gamma^0) (\overline{\nu}_L)^T && \text{(D.6)} \\ &= -(\nu_R)^T \gamma^0 \gamma^2 \gamma^2 \gamma^0 (\overline{\nu}_L)^T && \text{(D.7)} \\ &= (\nu_R)^T (\overline{\nu}_L)^T && \text{(D.8)} \end{aligned}$$

$$= \quad (\overline{\nu}_L \nu_R)^T = \overline{\nu}_L \nu_R. \tag{D.9}$$

Now, the physical states and their masses have to be found. This is done by diagonalizing the mass Lagrangian to find the mass eigenstates and eigenvalues. Assuming that $M \gg m$, the eigenvalues are approximately $M$ and $\frac{m^2}{M}$. Note that this gives a natural argument as to why the neutrino mass is so much smaller than the Dirac mass $m$. This is known as the seesaw mechanism originally proposed in [81] and is a possible explanation for the observed smallness of the neutrino masses. The physical states are found to be

$$\nu'_L \approx \nu_L - \frac{m}{M}\nu_L^C, \qquad \nu'_R \approx \nu_R^C - \frac{m}{M}\nu_R, \tag{D.10}$$

$$\eta_R \approx \nu_R + \frac{m}{M}\nu_R^C, \qquad \eta_L \approx \nu_L^C + \frac{m}{M}\nu_L. \tag{D.11}$$

The fields $\nu = \nu'_L + \nu'_R = \nu^C$ and $\eta = \eta_R + \eta_L = \eta^C$ are self-conjugate Majorana fields with masses $\frac{m^2}{M}$ and $M$ respectively.

The fields $\nu$ and $\eta$ can be used to determine the couplings to different particles in the SM. The first changes are the $W$ and $Z^0$ couplings to neutrinos.

$$\mathcal{L}_{Z^0-neut} \approx \frac{1}{4}\frac{e}{\sin\theta_W \cos\theta_W} Z^\mu \{\overline{\nu}\gamma_\mu(1-\gamma_5)\nu \tag{D.12}$$

$$+ \frac{m}{M}\left[\overline{\eta}\gamma_\mu(1-\gamma_5)\nu + \overline{\nu}\gamma_\mu(1-\gamma_5)\eta\right] \tag{D.13}$$

$$+ \frac{m}{M^2}\overline{\eta}\gamma_\mu(1-\gamma_5)\eta\Big\}, \tag{D.14}$$

$$\mathcal{L}_{W-neut} \approx \frac{1}{2\sqrt{2}}\frac{e}{\sin\theta_W}\{W^\mu\left[\overline{e}\gamma_\mu(1-\gamma_5)\nu\right. \tag{D.15}$$

$$+ \left.\frac{m}{M}\overline{e}\gamma_\mu(1-\gamma_5)\eta\right] + h.c.\Big\}. \tag{D.16}$$

The scalar Higgs also couples to the neutrinos. Since the Higgs field has a non-zero vacuum expectation value, it can be written as

$$\varphi = \frac{1}{\sqrt{2}}(\langle\varphi\rangle + \rho + iJ). \tag{D.17}$$

This gives the mass $M = \frac{h_2}{\sqrt{2}}\langle\varphi\rangle$ while the fields $\rho$ and $J$ are a massive Higgs and a massless Goldstone boson called the Majoron. Only the Majoron couplings with fermions are used in this thesis, so the massive Higgs field will be ignored in the rest of this discussion. By construction, the Majoron only couples to the neutrinos with the Lagrangian

$$\mathcal{L}_{J-neut} \approx \frac{ih_2}{\sqrt{2}} J\left[\overline{\eta}\gamma_5\eta - \frac{m}{M}(\overline{\eta}\gamma_5\nu + \overline{\nu}\gamma_5\eta) + \left(\frac{m}{M}\right)^2 \overline{\nu}\gamma_5\nu\right]. \tag{D.18}$$

## D.1 Fermion Couplings

The Majoron only couples to the neutrinos, so the only way for it to couple to fermions is through the loop diagrams in Figure D.1. The effective coupling introduced by these two diagrams is needed to calculate decays such as $\mu N \to eNJ$. Note

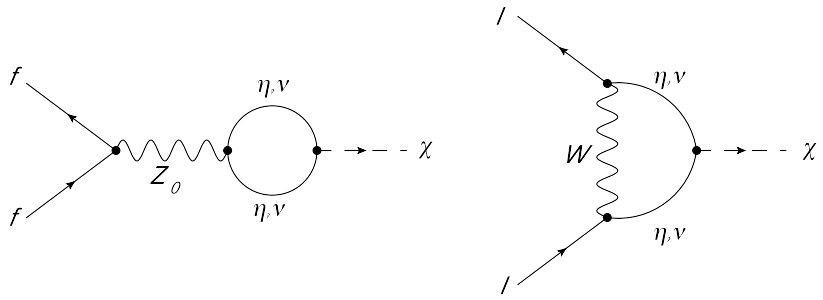


**Figure D.1:** The tree level diagrams for fermion couplings to the $J$ field.

that these are not allowed decays. They are more like extended vertices and will be used to define an effective Feynman rule for a $ffJ$ vertex. Only the lepton couplings will be considered as the quark couplings are not used in this thesis.

Consider first the diagram with the $Z^0$. The amplitude of this diagram is given by

$$\begin{aligned} i\mathcal{M} &= -\overline{u}(\ell)\left[\frac{-ig}{\cos\theta_W}\gamma_\mu\left(c_L\frac{1-\gamma_5}{2}+c_R\frac{1+\gamma_5}{2}\right)\right]u(\ell) \\ &\times \left[\frac{i}{k^2-M_Z^2}\left(-g^{\mu\nu}+\frac{k^\mu k^\nu}{M_Z^2}\right)\right] \\ &\quad \mathrm{Tr}\left[\left(\frac{-ig}{4\cos\theta_W}\left(\sqrt{\frac{m_\nu}{m_\eta}}\right)^m\gamma_\nu(1-\gamma_5)\right)\right. \\ &\times \left.\left(i\frac{\not{p}_1+m_1}{p_1^2-m_1^2}\right)\left[\frac{-h_2}{\sqrt{2}}\left(-\sqrt{\frac{m_\nu}{m_\eta}}\right)^n\gamma_5\right]\left(i\frac{\not{p}_2+m_2}{p_2^2-m_2^2}\right)\right]J, \end{aligned} \tag{D.19}$$

where the exponents $n, m$ are used to include all possible cases of neutrino couplings $(\nu\nu, \nu\eta, \eta\eta)$ to the $Z^0$ and $J$ respectively and $m_1$ and $m_2$ refer to the masses of the neutrinos in the loop. They are left general until the sum over all possible combinations is carried out. The trace is taken to sum over the fermion polarizations in the loop. Looking at the respective couplings, the only possible cases are

$$\begin{cases} m=0 & n=2 \\ m=1 & n=1\,, \\ m=2 & n=0 \end{cases} \tag{D.20}$$

so that $m+n=2$. Collecting like terms and simplifying the matrix element gives

$$\begin{aligned} i\mathcal{M} &= (-1)^n\frac{ig^2h_2}{4\sqrt{2}\cos^2\theta_W}\frac{m_\nu}{m_\eta}\overline{u}(\ell)\left[\gamma_\mu\left(c_L\frac{1-\gamma_5}{2}+c_R\frac{1+\gamma_5}{2}\right)\right]u(\ell) \\ &\times \left[\frac{1}{k^2-M_Z^2}\left(-g^{\mu\nu}+\frac{k^\mu k^\nu}{M_Z^2}\right)\right] \\ &\times \mathrm{Tr}\left[\gamma_\nu(1-\gamma_5)\int\frac{d^dp_1}{(2\pi)^d}\left(\frac{\not{p}_1+m_1}{p_1^2-m_1^2}\right)\gamma_5\left(\frac{\not{p}_2+m_2}{p_2^2-m_2^2}\right)\right]J. \end{aligned} \tag{D.21}$$

The effective coupling wanted is between leptons and and a Majoron. To facilitate this, the limit $k \ll M_Z$ is taken. The $Z^0$ propagator ends up being $g^{\mu\nu}/M_Z^2$, so the

matrix element becomes

$$\begin{aligned} i\mathcal{M} &= (-1)^n \frac{ig^2 h_2}{4\sqrt{2} M_Z^2 \cos^2\theta_W} \frac{m_\nu}{m_\eta} \overline{u}(\ell) \left[\gamma_\mu \left(c_L \frac{1-\gamma_5}{2} + c_R \frac{1+\gamma_5}{2}\right)\right] u(\ell) \\ &\times \int \frac{d^d p_1}{(2\pi)^d} \frac{\mathrm{Tr}\left[\gamma^\mu (1-\gamma_5)\left(\not{p}_1 - m_1\right)\left(\not{p}_1 + \not{k} + m_2\right)\right]}{(p_1^2 - m_1^2)[(p_1+k)^2 - m_2^2]} J. \end{aligned} \tag{D.22}$$

For simplicity, consider just the integral. The trace is given by

$$\begin{aligned} T &= \mathrm{Tr}\left[\gamma^\mu (1-\gamma_5)(p_{1\nu}\gamma^\nu - m_1)\left((p_1+k)_\delta \gamma^\delta + m_2\right)\right] &\text{(D.23)} \\ &= \mathrm{Tr}\left[\gamma^\mu \gamma^\nu p_{1\nu} m_2 - \gamma^\mu \gamma^\delta (p_1+k)_\delta m_1\right] &\text{(D.24)} \\ &= 4\left(p_1^\mu (m_2 - m_1) - k^\mu m_1\right), &\text{(D.25)} \end{aligned}$$

so that the integral becomes

$$I(1,2) = \int \frac{d^d p_1}{(2\pi)^d} \frac{4(p_1^\mu (m_2 - m_1) - k^\mu m_1)}{(p_1^2 - m_1^2)\left[(p_1+k)^2 - m_2^2\right]}. \tag{D.26}$$

The 1 and 2 in $I(1,2)$ refer to the mass terms $m_1$ and $m_2$ respectively. The integral can be computed by introducing a Feynman parameter,

$$\begin{aligned} I(1,2) &= \int \frac{d^d p_1}{(2\pi)^d} \int dx \frac{4[p_1^\mu (m_2 - m_1) - k^\mu m_1]}{[p_1^2 + 2p_1 \cdot kx + k^2 x - m_1^2(1-x) - m_2^2 x]^2} &\text{(D.27)} \\ &= \int dx \int \frac{d^d p}{(2\pi)^d} \frac{4[p^\mu (m_2 - m_1) - k^\mu (m_2 x + m_1(1-x))]}{[p^2 + k^2 x(1-x) - m_1^2(1-x) - m_2^2 x]^2}. &\text{(D.28)} \end{aligned}$$

Now, in dimensional regularization integrals with an odd power of the momentum being integrated appearing in the numerator are zero. This gets rid of the $p^\mu$ term so that the integral becomes

$$\begin{aligned} I(1,2) &= 4\int dx \frac{-ik^\mu}{(4\pi)^{d/2}} \frac{\Gamma(2 - d/2)[m_2 x - m_1(1+x)]}{[m_1^2(1-x) + m_2^2 x]^{d/2-2}} &\text{(D.29)} \\ &= \frac{-4ik^\mu}{(4\pi)^{d/2}} \left[\frac{m_1 + m_2}{2\epsilon}\right. \\ &\quad - \frac{m_1^4 + 4m_1^3 m_2 - 4m_1 m_2^3 - m_2^4 - 4m_1^3(m_1 + 2m_2)\ln(m_1)}{4(m_1 - m_2)(m_1 + m_2)} \\ &\quad \left. + \frac{4m_2^3(2m_1 + m_2)\ln(m_2)}{4(m_1 - m_2)(m_1 + m_2)}\right], &\text{(D.30)} \end{aligned}$$

where $k^2$ has been set to zero as the Majoron is massless. The term that is actually needed is the sum of possible neutrino contributions, and the only part of the matrix element that depends on this is the integral just computed. Summing the different contributions gives $I(\nu,\nu) - I(\nu,\eta) - I(\eta,\nu) + I(\eta,\eta)$, where the $(-1)^n$ term from the matrix element has been taken into account. Carrying out the sum gives

$$I^\mu \equiv \sum I(1,2) = \frac{-ik^\mu}{4\pi^2} \left[\frac{(m_\eta - m_\nu)(m_\eta + m_\nu)(m_\eta + 4m_\eta m_\nu + m_\nu^2)}{2(m_\eta - m_\nu)(m_\eta + m_\nu)^2}\right.$$

$$\left. \frac{-4m_\eta m_\nu (m_\eta^2 + m_\eta m_\nu + m_\nu^2) \ln\left(\frac{m_\eta}{m_\nu}\right)}{2(m_\eta - m_\nu)(m_\eta + m_\nu)^2} \right]. \tag{D.31}$$

Note, as would be expected, there is no $\epsilon$ pole and the result is symmetric with respect to $m_\nu, m_\eta$. Finally, the fact that $m_\eta \gg m_\nu$ is used to let $m_\nu \to 0$ to obtain

$$I^\mu = \frac{-ik^\mu}{8\pi^2} m_\eta. \tag{D.32}$$

Using this in the matrix element from Equation D.22 gives

$$\begin{aligned} i\mathcal{M} &= \frac{G_F h_2}{8\pi^2} m_\nu \overline{u}(\ell) \left[ \gamma_\mu \left( (-1/2 + \sin^2\theta_W) \frac{1-\gamma_5}{2} \right.\right. \\ &\quad \left.\left. + \sin^2\theta_W \frac{1+\gamma_5}{2} \right) \right] u(\ell) k^\mu J \qquad \text{(D.33)} \\ &= \frac{G_F h_2}{8\pi^2} m_\nu \overline{u}(\ell) \left[ \not{k} \left( -\frac{1-\gamma_5}{4} + \sin^2\theta_W \right) \right] u(\ell) J. \qquad \text{(D.34)} \end{aligned}$$

Now, $k = \ell - \ell'$, where $\ell, \ell'$ are the four-momenta of the incoming, outgoing leptons respectively. The Dirac equation can be used to cancel or rewrite some of the momenta in terms of masses so that the matrix element becomes

$$\begin{aligned} i\mathcal{M} &= -\frac{G_F h_2}{8\pi^2} m_\nu \overline{u}(\ell') \left[ (\not{\ell} - \not{\ell}') \left( \frac{1-\gamma_5}{4} - \sin^2\theta_W \right) \right] u(\ell) J \qquad \text{(D.35)} \\ &= -\frac{G_F h_2}{8\pi^2} m_\nu \overline{u}(\ell') \left[ (-m_\ell + \not{\ell}) \left( \frac{1-\gamma_5}{4} - \sin^2\theta_W \right) \right] u(\ell) J \qquad \text{(D.36)} \\ &= -\frac{G_F h_2}{8\pi^2} m_\nu \overline{u}(\ell') \left[ -m_\ell \left( \frac{1-\gamma_5}{4} - \sin^2\theta_W \right) \right. \\ &\quad \left. + \left( \frac{1+\gamma_5}{4} - \sin^2\theta_W \right) \not{\ell} \right] u(\ell) J \qquad \text{(D.37)} \\ &= -\frac{G_F h_2}{8\pi^2} m_\nu \overline{u}(\ell') \left[ -m_\ell \left( \frac{1-\gamma_5}{4} - \sin^2\theta_W \right) \right. \\ &\quad \left. + \left( \frac{1+\gamma_5}{4} - \sin^2\theta_W \right) m_\ell \right] u(\ell) J \qquad \text{(D.38)} \\ &= -\frac{G_F h_2}{16\pi^2} m_\nu m_\ell \overline{u}(\ell') \gamma_5 u(\ell) J. \qquad \text{(D.39)} \end{aligned}$$

This matches the expression found in [80] and defines the $Z^0$ contribution to the coupling between leptons and a Majoron.

The full coupling requires the additional contribution from the diagram with the $W$ in Figure D.1. The matrix element from this diagram is

$$\begin{aligned} i\mathcal{M} &= \overline{u}(\ell) \left[ \frac{-ig}{2\sqrt{2}} \left( \sqrt{\frac{m_\nu}{m_\eta}} \right)^m \gamma_\mu (1-\gamma_5) \right] \int \frac{d^d p_1}{(2\pi)^d} \left( i \frac{\not{p}_1 + m_1}{p_1^2 - m_1^2} \right) \\ &\times \left[ -\frac{h_2}{\sqrt{2}} \left( -\sqrt{\frac{m_\nu}{m_\eta}} \right)^n \gamma_5 \right] \left( i \frac{\not{p}_2 + m_2}{p_2^2 - m_2^2} \right) \\ &\times \left[ \frac{-ig}{2\sqrt{2}} \left( \sqrt{\frac{m_\nu}{m_\eta}} \right)^l \gamma_\nu (1-\gamma_5) \right] u(\ell) \end{aligned}$$

$$\times \quad \left[\frac{i}{k^2 - M_W^2}\left(-g^{\mu\nu} + \frac{k^\mu k^\nu}{M_W^2}\right)\right] J. \tag{D.40}$$

Similar to the previous calculation, the limit $k \ll M_W$ is taken so that the $W$ propagator is essentially a point interaction. This gives

$$\begin{aligned} i\mathcal{M} &= -\frac{(-1)^n i g^2 h_2}{8\sqrt{2}M_W^2}\frac{m_\nu}{m_\eta}\overline{u}(\ell')\left[\gamma_\mu(1-\gamma_5)\right. \\ &\times \left.\int \frac{d^d p_1}{(2\pi)^d}\left(\frac{\not{p}_1 - m_1}{p_1^2 - m_1^2}\right)\left(\frac{\not{p}_2 + m_2}{p_2^2 - m_2^2}\right)(1+\gamma_5)\gamma^\mu\right] u(\ell) J. \end{aligned} \tag{D.41}$$

Here, there is no trace taken, but the $\gamma_5$ structure effectively gives the same result as before. With $(1-\gamma_5)(1+\gamma_5) = 0$ only terms in the integral that have a single gamma matrix need to be evaluated, so the only surviving terms in the integral are

$$I = \int \frac{d^d p_1}{(2\pi)^d}\frac{\not{p}_1 m_2 - \not{p}_2 m_1}{(p_1^2 - m_1^2)(p_2^2 - m_2^2)}. \tag{D.42}$$

This integral is $\gamma_\mu \frac{I^\mu}{4}$ where $I^\mu$ is given in Equation D.32. Substituting the expression for $I^\mu$ and using the Dirac equation to rewrite the factors of $\not{\ell}$ and $\not{\ell}'$ gives

$$i\mathcal{M} = -\frac{G_F h_2}{64\pi^2} m_\nu \overline{u}(\ell')\left[\gamma_\mu(1-\gamma_5)\not{k}(1+\gamma_5)\gamma^\mu\right] u(\ell) J \tag{D.43}$$

$$= -\frac{G_F h_2}{64\pi^2} m_\nu \overline{u}(\ell')\left[(1+\gamma_5)\gamma_\mu(2k^\mu - \gamma^\mu\not{k})(1-\gamma_5)\right] u(\ell) J \tag{D.44}$$

$$= \frac{G_F h_2}{64\pi^2} m_\nu \overline{u}(\ell')\left[(1+\gamma_5)2\not{k}(1-\gamma_5)\right] u(\ell) J \tag{D.45}$$

$$= \frac{G_F h_2}{32\pi^2} m_\nu \overline{u}(\ell')\left[(1+\gamma_5)(\not{\ell} - \not{\ell}')(1-\gamma_5)\right] u(\ell) J \tag{D.46}$$

$$= \frac{G_F h_2}{32\pi^2} m_\nu \overline{u}(\ell')\left[-m_\ell 2(1-\gamma_5) + m_\ell 2(1+\gamma_5)\right] u(\ell) J \tag{D.47}$$

$$= \frac{G_F h_2}{8\pi^2} m_\nu m_\ell \overline{u}(\ell')\gamma_5 u(\ell) J. \tag{D.48}$$

Finally, combining the results from Equations D.39 and D.48 gives the effective vertex between leptons and the Majoron,

$$\mathcal{L} = \frac{G_F h_2}{16\pi^2} m_\nu m_f \overline{u}\gamma_5 u J. \tag{D.49}$$

## D.2 The Model With $n$ Flavours

The process that will be computed using this model is the decay of a muon into an electron and Majoron in the field of a nucleus. Thus, a decay channel must be found that allows a muon to decay into an electron and Majoron. In order to provide a channel like this, the model needs to have at least two flavours of leptons. The addition of extra flavours causes the mass matrix elements in Equation D.3 to become $n \times n$ matrices, where $n$ is the number of flavours. An arbitrary number of flavours is considered here instead of generalizing to just two or three.

With more than one flavour of neutrino, the see-saw mechanism is more complex. The mass matrix that must be diagonalized is

$$M^\nu = \begin{pmatrix} 0 & m_D \\ m_D^T & M_M \end{pmatrix}, \tag{D.50}$$

where $m_D, M_M$ are $n \times n$ matrices with $n$ being the number of flavours.

This matrix can be diagonalized by a unitary transformation $U$ via $U^T M^\nu U$. The transformation matrix then gives the relation between the mass and weak eigenstates of the neutrinos in the theory via

$$\begin{pmatrix} \nu_L^0 \\ \nu_R^{0C} \end{pmatrix}_i = U_{ij}^* n_{L_j}, \qquad \begin{pmatrix} \nu_L^{0C} \\ \nu_R^0 \end{pmatrix}_i = U_{ij} n_{R_j}, \tag{D.51}$$

where $\nu_{L,R_i}$ are the weak eigenstates. Not much is known experimentally about the elements of the neutrino mass matrix, so it is best to consider the elements to be general and complex with the only condition being that the matrix is symmetric. The elements of the matrix can likely be further constrained using neutrino oscillation data, but these effects won't be considered here. The interaction Lagrangians with the $J$ and $W^\mp$ are given by

$$\begin{aligned} \mathcal{L}_{int}^J &= -\frac{ig_W t_\beta}{4M_W} J\overline{n}_i \left[\gamma_5 \left(m_{n_i} + m_{n_j}\right)\left(\frac{1}{2}\delta_{ij} - \mathrm{Re}C_{ij}\right)\right. \\ &\quad \left. + i\left(m_{n_i} - m_{n_j}\right)\mathrm{Im}C_{ij}\right] n_j \qquad \text{(D.52)} \\ \mathcal{L}_{int}^{W^\mp} &= -\frac{g_W}{2\sqrt{2}} W^\mu \overline{\ell}_i B_{\ell_{ij}} \gamma_\mu (1-\gamma_5) n_j + \text{h.c.}, \qquad \text{(D.53)} \end{aligned}$$

where $C_{ij} = \sum_{k=1}^n U_{ki} U_{kj}^*$ and $B_{\ell ij} = \sum_{k=1}^n V_{\ell ij}^\ell U_{kj}^*$ are introduced, with $V^\ell$ the unitary matrix responsible for diagonalizing the lepton $(e, \mu, \tau)$ mass matrix and $t_\beta = \tan\frac{\langle\Phi\rangle}{\langle\varphi\rangle}$. It is interesting to note that, if $C_{ij}$ is diagonal, there is no mixing between the lepton flavours.

Of interest is the Majoron coupling to leptons, so the matrix element of the diagram in Figure D.2 is what is required.

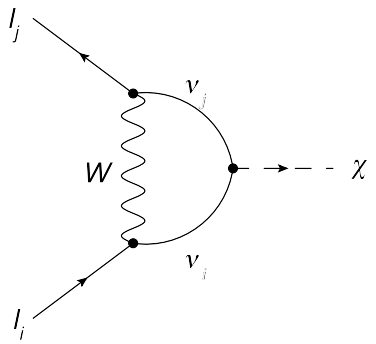


**Figure D.2:** The only (first order) diagram contributing to the lepton coupling to the Majoron.

Following a procedure similar to the previous section, the coupling its found to be

$$\mathcal{L}_{int}^{\ell_1\ell_2} = \overline{\ell}_1 \left[g_1(1-\gamma_5) + g_2(1+\gamma_5)\right] \ell_2 J. \tag{D.54}$$

Since the actual couplings are not known, all dependence on mass, $g_W$, $t_\beta$, etc., is grouped into the two distinct coupling constants $g_1$ and $g_2$.

This model provides an effective coupling between fermions and a Majoron. Although this particular model has been ruled out by experiments, the same coupling appears in supersymmetry models that include Majorons. For this reason, the coupling can be used to compute the Majoron decay rate in Chapter 5.

# Appendix E

# $\mathcal{O}(\alpha^3)$ Renormalization

In order to compute the (N)$^3$LO corrections to muon decay, the corresponding $\mathcal{O}(\alpha^3)$ renormalization constants are required. These have been computed in [82] and expansions were given in the limit $\frac{m}{M} = 0$. Unfortunately, in this limit, the integrals are difficult and needed to be computed numerically. As well, it would be quite a challenge to re-expand the results in the limit that is needed, $\delta = (1 - \frac{m}{M}) = 0$. For this purpose, the required renormalization constants are computed here. The method followed is the same as in [82] with the exception that the expansion is carried out in the limit $\delta = 0$.

## E.1 Method

The calculation of the wave function and mass renormalization constants relies on a relation between self-energy diagrams and the constant of interest. These formulas have been derived in [83, 84] and are given by

$$Z_m^{OS} = 1 + \Sigma_1(M_q^2, M_q), \tag{E.1}$$

$$\left(Z_2^{OS}\right)^{-1} = 1 + 2M_q^2 \frac{\partial}{\partial q^2}\Sigma_1(q^2, M_q)\Big|_{q^2=M_q^2} + \Sigma_2(M_q^2, M_q), \tag{E.2}$$

where $Z_m^{OS}$ and $Z_2^{OS}$ are defined by

$$m_{q,0} = Z_m^{OS} M_q, \tag{E.3}$$

$$\psi_0 = \sqrt{Z_2^{OS}}\psi, \tag{E.4}$$

and the $OS$ refers to the on-shell scheme. In these expressions, $\Sigma_1$ and $\Sigma_2$ are components of the self-energy contributions of the particle $q$ with momentum and mass $q, M_q$ respectively. They are given by the decomposition

$$\Sigma(q, m_q) = m_q\Sigma_1(q^2, m_q) + (\not{q} - m_q)\Sigma_2(q^2, m_q). \tag{E.5}$$

This decomposition of the self-energy of $q$ can be used to directly calculate the renormalization constants. This is done by multiplying Equation E.5 on the left by the projector $\frac{\not{Q}+m_q}{4m_q^2}$, where $q = Q(1 + t)$ and $t$ is a small parameter, and taking the trace

$$\mathrm{Tr}\left[\frac{\not{Q} + m_q}{4m_q^2}\right]\Sigma(q^2, m_q) = \mathrm{Tr}\left[\frac{\not{Q} + m_q}{4m_q}\Sigma_1(q^2, m_q)\right.$$

$$+\frac{(\not{Q}+m_q)\,(\not{Q}(1+t)-m_q)}{4m_q^2}\Sigma_2(q^2,m_q)\Big] \quad \text{(E.6)}$$

$$= \Sigma_1(q^2,m_q)+t\Sigma_2(q^2,m_q). \quad \text{(E.7)}$$

Here, $Q^2=m_q^2$ has been used. Expanding to first order in $t$ gives

$$\begin{aligned}\mathrm{Tr}\left[\frac{\not{Q}+m_q}{4m_q^2}\right]\Sigma(q^2,m_q) &= \Sigma_1(m_q^2,m_q)\\ &+ t\left(2m_q^2\frac{\partial}{\partial q^2}\,\Sigma_1(q^2,m_q)\big|_{q^2=m_q^2}+\Sigma_2(m_q^2,m_q)\right) \quad \text{(E.8)}\\ &= \left(Z_m^{OS}-1\right)+t\left(\left(Z_2^{OS}\right)^{-1}-1\right). \quad \text{(E.9)}\end{aligned}$$

This shows that it is possible to compute the renormalization constants from self-energy diagrams by expanding the external momentum $q$ to first order in $t$. The leading order term is then equal to $Z_m^{OS}$ and the term linear in $t$ is equal to $\left(Z_2^{OS}\right)^{-1}$.

The main purpose of carrying out this calculation is to obtain the terms in the renormalization constants that depend on the expansion parameter $\delta=\left(1-\frac{m_e}{m_\mu}\right)$. These terms appear in diagrams that have an electron loop. The only treatment required, differing from other diagrams in the calculation, is expanding the electron mass in the propagators using $m_e=m_\mu(1-\delta)$. With this expansion, the calculation can be reduced using IBP to 15 three loop master integrals.

## E.2 Results

The full results for the $\mathcal{O}(\alpha^3)$ corrections to $Z_m^{OS}$ and $Z_2^{OS}$ are presented here. The leading orders in the $\delta$ expansion have been checked with known results [82] and the $\mathcal{O}(\alpha)$ and $\mathcal{O}(\alpha^2)$ results have been reproduced. All results agree well with the known expansions.

To facilitate the parameterization of the muon decay results, contributions from a diagram with an electron loop or muon loop are indicated with factors of $n_e$ or $n_\mu$ respectively. In the following expressions, the $^{(3)}$ denotes the third order corrections ,$a_4$ is the multiple polylogarithm $\mathrm{Li}_4\left(\frac{1}{2}\right)$, and $\zeta_n$ is the Riemann Zeta function evaluated at $n$.

$$\begin{aligned}Z_M^{OS(3)} &= i(M^2)^{-3\epsilon}\left[-\frac{9}{128\epsilon^3}-\frac{63}{256\epsilon^2}+\frac{1}{\epsilon}\left(-\frac{457}{512}+\frac{9}{16}\zeta_3-\frac{3}{8}\pi^2\ln(2)+\frac{15}{64}\pi^2\right)\right.\\ &\quad -\frac{14225}{3072}-\frac{1}{16}\zeta_3\pi^2+\frac{9}{8}\zeta_3+\frac{5}{8}\zeta_5+5\pi^2\ln(2)+\frac{5}{4}\pi^2\ln^2(2)-\frac{731}{384}\pi^2\\ &\quad \left.-\frac{73}{480}\pi^4-\frac{\ln^4(2)}{8}-3a_4\right]\\ &+ n_\mu^2\left[-\frac{1}{36\epsilon^3}-\frac{17}{108\epsilon^2}+\frac{1}{\epsilon}\left(-\frac{385}{324}+\frac{\pi^2}{9}\right)-\frac{5441}{972}+\frac{79}{135}\pi^2-\frac{2}{3}\pi^2\ln(2)\right.\\ &\quad \left.+\frac{53}{18}\zeta_3\right]\\ &+ n_e^2\left[-\frac{5441}{972}-\frac{1}{36\epsilon^3}+\frac{1}{\epsilon}\left(-\frac{385}{324}+\frac{\pi^2}{9}\right)-\frac{17}{108\epsilon^2}+\frac{79}{135}\pi^2-\frac{2}{3}\pi^2\ln(2)\right.\end{aligned}$$

$$
\begin{aligned}
&+\frac{53}{18}\zeta_3 \\
&+ \delta\left(\frac{1}{\epsilon}\left(\frac{4}{3}-\frac{2}{9}\pi^2\right)+\frac{52}{9}-\frac{79}{135}\pi^2+\frac{4}{3}\pi^2\ln(2)-\frac{22}{3}\zeta_3\right) \\
&+ \delta^2\left(\frac{1}{\epsilon}\left(-1+\frac{\pi^2}{12}\right)-\frac{5}{3}-\frac{7}{18}\pi^2-\frac{\pi^2\ln(2)}{2}+\frac{23}{4}\zeta_3\right) \\
&+ \delta^3\left(\frac{1}{\epsilon}\left(-\frac{1}{3}+\frac{\pi^2}{36}\right)-\frac{22}{9}+\frac{53}{108}\pi^2-\frac{\pi^2\ln(2)}{6}-\frac{25}{12}\zeta_3\right) \\
&+ \delta^4\left(\frac{1}{\epsilon}\left(\frac{1}{4}-\frac{\pi^2}{36}\right)+\frac{5}{8}-\frac{77}{288}\pi^2+\frac{\pi^2\ln(2)}{6}+\frac{\zeta_3}{12}\right) \\
&+ \delta^5\left(-\frac{407}{540}-\frac{1}{90\epsilon}+\frac{\pi^2}{40}\right)+\delta^6\left(\frac{29}{540}-\frac{1}{180\epsilon}-\frac{707}{17280}\pi^2\right) \\
&+ \delta^7\left(-\frac{56543}{567000}-\frac{2}{675\epsilon}-\frac{1877}{120960}\pi^2\right) \\
&+ \delta^8\left(-\frac{127777}{1512000}-\frac{1}{600\epsilon}-\frac{491}{46080}\pi^2\right)\Bigg] \\
&+ n_\mu n_e\left[-\frac{1}{18\epsilon^3}-\frac{17}{54\epsilon^2}+\frac{1}{\epsilon}\left(-\frac{385}{162}+\frac{2}{9}\pi^2\right)-\frac{5441}{486}+\frac{158}{135}\pi^2-\frac{4}{3}\pi^2\ln(2)\right. \\
&\quad +\frac{53}{9}\zeta_3 \\
&+ \delta\left(\frac{1}{\epsilon}\left(\frac{4}{3}-\frac{2}{9}\pi^2\right)+\frac{52}{9}-\frac{79}{135}\pi^2+\frac{4}{3}\pi^2\ln(2)-\frac{22}{3}\zeta_3\right) \\
&+ \delta^2\left(\frac{1}{\epsilon}\left(-1+\frac{\pi^2}{12}\right)-3+\frac{7}{30}\pi^2-\frac{\pi^2\ln(2)}{2}+\frac{9}{4}\zeta_3\right) \\
&+ \delta^3\left(\frac{1}{\epsilon}\left(-\frac{1}{3}+\frac{\pi^2}{36}\right)-\frac{10}{9}-\frac{17}{540}\pi^2-\frac{\pi^2\ln(2)}{6}+\frac{17}{12}\zeta_3\right) \\
&+ \delta^4\left(\frac{1}{\epsilon}\left(\frac{1}{4}-\frac{\pi^2}{36}\right)-\frac{185}{72}+\frac{193}{864}\pi^2+\frac{\pi^2\ln(2)}{6}-\frac{13}{12}\zeta_3\right) \\
&+ \delta^5\left(-\frac{1}{90\epsilon}-\frac{407}{540}+\frac{\pi^2}{24}\right)+\delta^6\left(-\frac{1}{180\epsilon}-\frac{166}{135}+\frac{1741}{17280}\pi^2\right) \\
&+ \delta^7\left(-\frac{2}{675\epsilon}-\frac{784193}{567000}+\frac{425}{3456}\pi^2\right) \\
&+ \delta^8\left(-\frac{1}{600\epsilon}-\frac{2277007}{1512000}+\frac{3005}{21504}\pi^2\right)\Bigg] \\
&+ n_\mu\left[-\frac{3}{32\epsilon^3}-\frac{77}{192\epsilon^2}+\frac{1}{\epsilon}\left(-\frac{631}{384}+\frac{\pi^2}{3}-\frac{\pi^2\ln(2)}{3}+\frac{\zeta_3}{4}\right)-\frac{8743}{2304}+\frac{32}{3}a_4\right. \\
&\quad +\frac{4}{9}\ln^4(2)+\frac{425}{432}\pi^2-\frac{67}{36}\pi^2\ln(2)+\frac{5}{9}\pi^2\ln^2(2)-\frac{161}{2160}\pi^4+\frac{71}{12}\zeta_3\Bigg] \\
&+ n_e\left[-\frac{3}{32\epsilon^3}-\frac{77}{192\epsilon^2}+\frac{1}{\epsilon}\left(-\frac{631}{384}+\frac{\pi^2}{3}-\frac{\pi^2\ln(2)}{3}+\frac{\zeta_3}{4}\right)-\frac{8743}{2304}+\frac{32}{3}a_4\right. \\
&\quad +\frac{4}{9}\ln^4(2)+\frac{425}{432}\pi^2-\frac{67}{36}\pi^2\ln(2)+\frac{5}{9}\pi^2\ln^2(2)-\frac{161}{2160}\pi^4+\frac{71}{12}\zeta_3
\end{aligned}
$$

$$
\begin{aligned}
&+ \quad \delta\left(\frac{1}{\epsilon}\left(\frac{3}{2}-\frac{\pi^2}{4}\right)\frac{823}{108}-\frac{32}{3}a_4-\frac{4}{9}\ln^4(2)+\frac{575}{648}\pi^2-\frac{17}{18}\pi^2\ln(2)\right.\\
&\quad \left.+\frac{4}{9}\pi^2\ln^2(2)-\frac{11}{270}\pi^4-\frac{323}{72}\zeta_3\right)\\
&+ \quad \delta^2\left(\frac{1}{\epsilon}\left(-\frac{9}{8}+\frac{3}{32}\pi^2\right)-\frac{59}{9}+16a_4+\frac{2}{3}\ln^4(2)-\frac{433}{216}\pi^2+\frac{7}{16}\pi^2\ln(2)\right.\\
&\quad \left.-\frac{2}{3}\pi^2\ln^2(2)+\frac{11}{180}\pi^4+\frac{835}{96}\zeta_3\right)\\
&+ \quad \delta^3\left(\frac{1}{\epsilon}\left(-\frac{3}{8}+\frac{\pi^2}{32}\right)-\frac{581}{216}-\frac{32}{3}a_4-\frac{4}{9}\ln^4(2)+\frac{6295}{2592}\pi^2-\frac{41}{48}\pi^2\ln(2)\right.\\
&\quad \left.+\frac{4}{9}\pi^2\ln^2(2)-\frac{11}{270}\pi^4-\frac{2089}{288}\zeta_3\right)\\
&+ \quad \delta^4\left(\frac{1}{\epsilon}\left(\frac{9}{32}-\frac{\pi^2}{32}\right)\frac{161}{64}+\frac{8}{3}a_4+\frac{\ln^4(2)}{9}-\frac{10129}{11520}\pi^2+\frac{3}{16}\pi^2\ln(2)\right.\\
&\quad \left.-\frac{\pi^2\ln^2(2)}{9}+\frac{11}{1080}\pi^4+\frac{209}{96}\zeta_3\right)\\
&+ \quad \delta^5\left(-\frac{1}{80\epsilon}-\frac{413}{1440}+\frac{9179}{60480}\pi^2-\frac{2}{15}\pi^2\ln(2)-\frac{13}{30}\zeta_3\right)\\
&+ \quad \delta^6\left(-\frac{1}{160\epsilon}-\frac{121}{1440}+\frac{133157\pi^2}{1612800}-\frac{4}{45}\pi^2\ln(2)-\frac{13}{60}\zeta_3\right)\\
&+ \quad \delta^7\left(\frac{1}{300\epsilon}+\frac{1024301}{13608000}+\frac{34284317}{372556800}\pi^2-\frac{23}{315}\pi^2\ln(2)-\frac{52}{315}\zeta_3\right)\\
&+ \quad \delta^8\left(\frac{3}{1600\epsilon}+\frac{2400299}{36288000}+\frac{981989681}{12915302400}\pi^2-\frac{53}{840}\pi^2\ln(2)\right.\\
&\quad \left.\left.-\frac{39}{280}\zeta_3\right)\right]\Bigg], \qquad \text{(E.10)}
\end{aligned}
$$

$$
\begin{aligned}
Z_2^{OS(3)} &= -\frac{9}{128\epsilon^3}-\frac{81}{256\epsilon^2}+\frac{1}{\epsilon}\left(-\frac{1039}{512}+\frac{9}{8}\zeta_3-\frac{3}{4}\pi^2\ln(2)+\frac{39}{64}\pi^2\right)\\
&\quad -\frac{10823}{3072}+\frac{\zeta_3\pi^2}{8}-\frac{187}{32}\zeta_3-\frac{5}{16}\zeta_5+\frac{685}{48}\pi^2\ln(2)\\
&\quad +3\pi^2\ln^2(2)-\frac{7199}{1152}\pi^2-\frac{41}{120}\pi^4-\frac{5}{12}\ln^4(2)-10a_4+\frac{71}{12}\zeta_3\\
&+ \quad n_\mu^2\left[-\frac{1}{36\epsilon^3}-\frac{17}{108\epsilon^2}+\frac{1}{\epsilon}\left(-\frac{385}{324}+\frac{\pi^2}{9}\right)-\frac{5441}{972}+\frac{79}{135}\pi^2\right.\\
&\quad \left.-\frac{2}{3}\pi^2\ln(2)+\frac{53}{18}\zeta_3\right]\\
&+ \quad n_e^2\left[-\frac{1}{36\epsilon^3}-\frac{17}{108\epsilon^2}+\frac{1}{\epsilon}\left(-\frac{385}{324}+\frac{\pi^2}{9}\right)-\frac{5441}{972}+\frac{79}{135}\pi^2\right.\\
&\quad \left.-\frac{2}{3}\pi^2\ln(2)+\frac{53}{18}\zeta_3\right.\\
&+ \quad \delta\left(\frac{1}{\epsilon}\left(\frac{4}{3}-\frac{2}{9}\pi^2\right)+\frac{52}{9}-\frac{79}{135}\pi^2+\frac{4}{3}\pi^2\ln(2)-\frac{22}{3}\zeta_3\right)
\end{aligned}
$$

$$
\begin{aligned}
&+ \quad \delta^2 \left( \frac{1}{\epsilon} \left( -1 + \frac{\pi^2}{12} \right) - \frac{5}{3} - \frac{7}{18}\pi^2 - \frac{\pi^2 \ln(2)}{2} + \frac{23}{4}\zeta_3 \right) \\
&+ \quad \delta^3 \left( \frac{1}{\epsilon} \left( -\frac{1}{3} + \frac{\pi^2}{36} \right) - \frac{22}{9} + \frac{53}{108}\pi^2 - \frac{\pi^2 \ln(2)}{6} - \frac{25}{12}\zeta_3 \right) \\
&+ \quad \delta^4 \left( \frac{1}{\epsilon} \left( \frac{1}{4} - \frac{\pi^2}{36} \right) + \frac{5}{8} - \frac{77}{288}\pi^2 + \frac{\pi^2 \ln(2)}{6} + \frac{\zeta_3}{12} \right) \\
&+ \quad \delta^5 \left( -\frac{1}{90\epsilon} - \frac{407}{540} + \frac{\pi^2}{40} \right) + \delta^6 \left( -\frac{1}{180\epsilon} + \frac{29}{540} - \frac{707}{17280}\pi^2 \right) \\
&+ \quad \delta^7 \left( -\frac{2}{675\epsilon} - \frac{56543}{567000} - \frac{1877}{120960}\pi^2 \right) \\
&+ \quad \delta^8 \left( -\frac{1}{600\epsilon} - \frac{127777}{1512000} - \frac{491}{46080}\pi^2 \right) \Bigg] \\
&+ \quad n_\mu n_e \left[ -\frac{1}{18\epsilon^3} - \frac{17}{54\epsilon^2} + \frac{1}{\epsilon} \left( -\frac{385}{162} + \frac{2}{9}\pi^2 \right) - \frac{5441}{486} + \frac{158}{135}\pi^2 \right. \\
&\qquad \left. - \frac{4}{3}\pi^2 \ln(2) + \frac{53}{9}\zeta_3 \right. \\
&+ \quad \delta \left( \frac{1}{\epsilon} \left( 43 - \frac{2}{9}\pi^2 \right) + \frac{52}{9} - \frac{79}{135}\pi^2 + \frac{4}{3}\pi^2 \ln(2) - \frac{22}{3}\zeta_3 \right) \\
&+ \quad \delta^2 \left( \frac{1}{\epsilon} \left( -1 + \frac{\pi^2}{12} \right) - 3 + \frac{7}{30}\pi^2 - \frac{\pi^2 \ln(2)}{2} + \frac{9}{4}\zeta_3 \right) \\
&+ \quad \delta^3 \left( \frac{1}{\epsilon} \left( -\frac{1}{3} + \frac{\pi^2}{36} \right) - \frac{10}{9} - \frac{17}{540}\pi^2 - \frac{\pi^2 \ln(2)}{6} + \frac{17}{12}\zeta_3 \right) \\
&+ \quad \delta^4 \left( \frac{1}{\epsilon} \left( \frac{1}{4} - \frac{\pi^2}{36} \right) - \frac{185}{72} + \frac{193}{864}\pi^2 + \frac{\pi^2 \ln(2)}{6} - \frac{13}{12}\zeta_3 \right) \\
&+ \quad \delta^5 \left( -\frac{1}{90\epsilon} - \frac{407}{540} + \frac{\pi^2}{24} \right) + \delta^6 \left( -\frac{1}{180\epsilon} - \frac{166}{135} + \frac{1741}{17280}\pi^2 \right) \\
&+ \quad \delta^7 \left( -\frac{2}{675\epsilon} - \frac{784193}{567000} + \frac{425}{3456}\pi^2 \right) \\
&+ \quad \delta^8 \left( -\frac{1}{600\epsilon} - \frac{2277007}{1512000} + \frac{3005}{21504}\pi^2 \right) \Bigg] \\
&+ \quad n_\mu \left[ -\frac{3}{32\epsilon^3} - \frac{77}{192\epsilon^2} + \frac{1}{\epsilon} \left( -\frac{631}{384} + \frac{\pi^2}{3} - \frac{\pi^2 \ln(2)}{3} + \frac{\zeta_3}{4} \right) - \frac{8743}{2304} + \frac{71}{12}\zeta_3 \right. \\
&\qquad \left. + \frac{32}{3}a_4 + \frac{4}{9}\ln^4(2) + \frac{425}{432}\pi^2 - \frac{67}{36}\pi^2 \ln(2) + \frac{5}{9}\pi^2 \ln^2(2) - \frac{161}{2160}\pi^4 \right] \\
&+ \quad n_e \left[ -\frac{3}{32\epsilon^3} - \frac{77}{192\epsilon^2} + \frac{1}{\epsilon} \left( -\frac{631}{384} + \frac{\pi^2}{3} - \frac{\pi^2 \ln(2)}{3} + \frac{\zeta_3}{4} \right) - \frac{8743}{2304} + \frac{71}{12}\zeta_3 \right. \\
&\qquad \left. + \frac{32}{3}a_4 + \frac{4}{9}\ln^4(2) + \frac{425}{432}\pi^2 - \frac{67}{36}\pi^2 \ln(2) + \frac{5}{9}\pi^2 \ln^2(2) - \frac{161}{2160}\pi^4 \right. \\
&+ \quad \delta \left( \frac{1}{\epsilon} \left( \frac{3}{2} - \frac{\pi^2}{4} \right) + \frac{823}{108} - \frac{32}{3}a_4 - \frac{4}{9}\ln^4(2) + \frac{575}{648}\pi^2 - \frac{17}{18}\pi^2 \ln(2) \right. \\
&\qquad \left. + \frac{4}{9}\pi^2 \ln^2(2) - \frac{11}{270}\pi^4 - \frac{323}{72}\zeta_3 \right)
\end{aligned}
$$

$$
\begin{aligned}
&+ \quad \delta^2 \left( \frac{1}{\epsilon} \left( -\frac{9}{8} + \frac{3}{32}\pi^2 \right) - \frac{59}{9} + 16a_4 + \frac{2}{3}\ln^4(2) - \frac{433}{216}\pi^2 + \frac{7}{16}\pi^2 \ln(2) \right. \\
&\qquad \left. -\frac{2}{3}\pi^2 \ln^2(2) + \frac{11}{180}\pi^4 + \frac{835}{96}\zeta_3 \right) \\
&+ \quad \delta^3 \left( \frac{1}{\epsilon} \left( -\frac{3}{8} + \frac{\pi^2}{32} \right) - \frac{581}{216} - \frac{32}{3}a_4 - \frac{4}{9}\ln^4(2) + \frac{6295}{2592}\pi^2 - \frac{41}{48}\pi^2 \ln(2) \right. \\
&\qquad \left. +\frac{4}{9}\pi^2 \ln^2(2) - \frac{11}{270}\pi^4 - \frac{2089}{288}\zeta_3 \right) \\
&+ \quad \delta^4 \left( \frac{1}{\epsilon} \left( \frac{9}{32} - \frac{\pi^2}{32} \right) + \frac{161}{64} + \frac{8}{3}a_4 + \frac{\ln^4(2)}{9} - \frac{10129}{11520}\pi^2 + \frac{3}{16}\pi^2 \ln(2) \right. \\
&\qquad \left. -\frac{\pi^2 \ln^2(2)}{9} + \frac{11}{1080}\pi^4 + \frac{209}{96}\zeta_3 \right) \\
&+ \quad \delta^5 \left( -\frac{1}{80\epsilon} - \frac{413}{1440} + \frac{9179}{60480}\pi^2 - \frac{2}{15}\pi^2 \ln(2) - \frac{13}{30}\zeta_3 \right) \\
&+ \quad \delta^6 \left( -\frac{1}{160\epsilon} - \frac{121}{1440} + \frac{133157}{1612800}\pi^2 - \frac{4}{45}\pi^2 \ln(2) - \frac{13}{60}\zeta_3 \right) \\
&+ \quad \delta^7 \left( \frac{1}{300\epsilon} + \frac{1024301}{13608000} + \frac{34284317}{372556800}\pi^2 - \frac{23}{315}\pi^2 \ln(2) - \frac{52}{315}\zeta_3 \right) \\
&+ \quad \delta^8 \left( \frac{3}{1600\epsilon} + \frac{2400299}{36288000} + \frac{981989681}{12915302400}\pi^2 - \frac{53}{840}\pi^2 \ln(2) \right. \\
&\qquad \left. -\frac{39}{280}\zeta_3 \right) \Bigg] . \qquad \text{(E.11)}
\end{aligned}
$$

# Appendix F

# Full Muon Results

The full known $\mathcal{O}(\alpha^3)$ corrections to the muon decay rate are presented here. The decay rate is given by

$$\Gamma(\mu \to e\overline{\nu}_e\nu_\mu) = \Gamma_0 \left[ X_0 + \frac{\alpha}{\pi} C_F X_1 + \left(\frac{\alpha}{\pi}\right)^2 C_F X_2 + \left(\frac{\alpha}{\pi}\right)^3 C_F X_3 + \ldots \right], \quad \text{(F.1)}$$

where

$$\Gamma_0 = \frac{G_F^2 m_\mu^5}{192\pi^3}, \quad \text{(F.2)}$$

$X_0$, $X_1$ are given in Chapter 6 and $X_2$ can be obtained from the results in Chapter 6 by setting $C_A$ and $n_l$ to zero. The factor $X_3$ is further parametrized by,

$$X_3 = C_F^2 X_F + C_F T_F (X_\mu + X_e) + T_F^2 (X_{\mu\mu} + X_{\mu e} + X_{ee}), \quad \text{(F.3)}$$

where $X_F$ refers to contributions from diagrams with no muon or electron loops, and the other $X_i$'s refer to contributions from diagrams with one or two muon and electron loops.

The full known results are

$$\begin{aligned} X_{\mu\mu} &= \delta^5 \left(-\frac{1688}{27} + \frac{256}{5}\zeta_3\right) + \delta^6 \left(-\frac{4}{9} - \frac{128}{45}\pi^2 + \frac{128}{5}\zeta_3\right) \\ &\quad + \delta^7 \left(-\frac{621668}{25515} - \frac{2656}{189}\pi^2 + \frac{126848}{945}\zeta_3\right) \\ &\quad + \delta^8 \left(\frac{2651296}{25515} - \frac{95584}{2835}\pi^2 + \frac{180224}{945}\zeta_3\right) \quad \text{(F.4)} \\ X_{\mu e} &= \delta^5 \left(-\frac{3376}{27} + \frac{512}{5}\zeta_3\right) + \delta^6 \left(\frac{952}{9} + \frac{128}{15}\pi^2 - \frac{768}{5}\zeta_3\right) \\ &\quad + \delta^7 \left(-\frac{4781416}{25515} - \frac{13792}{945}\pi^2 + \frac{51344}{189}\zeta_3\right) \\ &\quad + \delta^8 \left(-\frac{14432}{729} + \frac{44144}{2835}\pi^2 - \frac{104168}{945}\zeta_3\right) \quad \text{(F.5)} \\ X_{ee} &= \delta^5 \left(-\frac{1688}{27} + \frac{256}{5}\zeta_3\right) + \delta^6 \left(\frac{956}{9} + \frac{512}{45}\pi^2 - \frac{896}{5}\zeta_3\right) \\ &\quad + \delta^7 \left(-\frac{730532}{25515} - \frac{7360}{189}\pi^2 + \frac{320384}{189}\zeta_3\right) \end{aligned}$$

$$+\delta^8\left(-\frac{14432}{729}+\frac{44144}{2835}\pi^2-\frac{104168}{945}\zeta_3\right) \tag{F.6}$$

$$\begin{aligned} X_e &= \delta^5\left(\frac{3539}{135}-\frac{5632}{405}\pi^2+\frac{16}{25}\pi^4+\frac{512}{45}\pi^2\ln(2)-\frac{128}{15}\pi^2\ln^2(2)\right. \\ &\quad \left.+\frac{128}{15}\ln^4(2)+\frac{1024}{5}a_4-\frac{568}{9}\zeta_3\right) \end{aligned} \tag{F.7}$$

$$\begin{aligned} X_\mu &= \delta^5\left(\frac{3539}{135}-\frac{5632}{405}\pi^2+\frac{16}{25}\pi^4+\frac{512}{45}\pi^2\ln(2)-\frac{128}{15}\pi^2\ln^2(2)\right. \\ &\quad \left.+\frac{128}{15}\ln^4(2)+\frac{1024}{5}a_4-\frac{568}{9}\zeta_3\right) \end{aligned} \tag{F.8}$$

$$\tag{F.9}$$

## F.1 Results From $\eta_A$

In Chapter 7 the extraction of the first two orders of the mass expansion for corrections to the muon decay rate is discussed. For completeness, the results are presented here. Note that the calculation is done with $m_e = m_\mu$, so the $X_{\mu,e}$ terms are combined into a single result.

$$\begin{aligned} X_{\mu\mu}+X_{\mu e}+X_{ee} &= \delta^5\left(-\frac{6752}{27}+\frac{1024}{5}\zeta_3\right) \\ &\quad +\delta^6\left(\frac{1904}{9}+\frac{256}{45}\pi^2-\frac{1536}{5}\zeta_3\right) \end{aligned} \tag{F.10}$$

$$\begin{aligned} X_e+X_\mu &= \delta^5\left(\frac{7078}{135}-\frac{11264}{405}\pi^2+\frac{32}{25}\pi^4+\frac{1024}{45}\pi^2\ln(2)\right. \\ &\quad \left.-\frac{256}{15}\pi^2\ln^2(2)+\frac{256}{15}\ln^4(2)+\frac{2048}{5}a_4-\frac{1136}{9}\zeta_3\right) \\ &\quad +\delta^6\left(-\frac{8801}{45}-\frac{3072}{5}a_4+\frac{6784}{135}\pi^2-\frac{48}{25}\pi^4-\frac{448}{15}\pi^2\ln(2)\right. \\ &\quad \left.+\frac{128}{5}\pi^2\ln^2(2)-\frac{128}{5}\ln^4(2)+\frac{2744}{15}\zeta_3\right) \end{aligned} \tag{F.11}$$

$$\begin{aligned} X_F &= \delta^5\left(-\frac{967}{30}-\frac{256}{3}a_4+\frac{476}{45}\pi^2-\frac{28}{45}\pi^4-\frac{96}{5}\pi^2\ln(2)\right. \\ &\quad \left.+\frac{32}{9}\pi^2\ln^2(2)-\frac{32}{9}\ln^4(2)+\frac{1208}{5}\zeta_3+\frac{56}{5}\pi^2\zeta_3-128\zeta_5\right) \\ &\quad +\delta^6\left(\frac{967}{20}+128a_4-\frac{238}{15}\pi^2+\frac{14}{15}\pi^4+\frac{144}{5}\pi^2\ln(2)\right. \\ &\quad -\frac{16}{3}\pi^2\ln^2(2)+\frac{16}{3}\ln^4(2)-\frac{604}{5}\zeta_3 \\ &\quad \left.-\frac{84}{5}\pi^2\zeta_3+192\zeta_5\right) \end{aligned} \tag{F.12}$$